

**LOADING DEFORMATION ON VARIOUS TIMESCALES USING GPS AND
GRACE MEASUREMENTS**

**A
THESIS**

**Presented to the Faculty
of the University of Alaska Fairbanks**

**in Partial Fulfillment of the Requirements
for the Degree of**

DOCTOR OF PHILOSOPHY

By

Yuning Fu

Fairbanks, Alaska

December 2012

UMI Number: 3537844

All rights reserved

INFORMATION TO ALL USERS

The quality of this reproduction is dependent upon the quality of the copy submitted.

In the unlikely event that the author did not send a complete manuscript and there are missing pages, these will be noted. Also, if material had to be removed, a note will indicate the deletion.



UMI 3537844

Published by ProQuest LLC 2013. Copyright in the Dissertation held by the Author.

Microform Edition © ProQuest LLC.

All rights reserved. This work is protected against unauthorized copying under Title 17, United States Code.



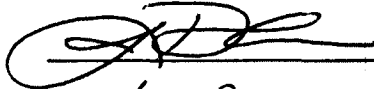
ProQuest LLC
789 East Eisenhower Parkway
P.O. Box 1346
Ann Arbor, MI 48106-1346

LOADING DEFORMATION ON VARIOUS TIMESCALES USING GPS AND
GRACE MEASUREMENTS

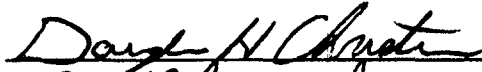
By

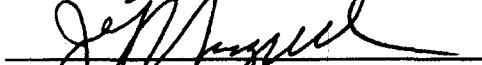
Yuning Fu

RECOMMENDED:








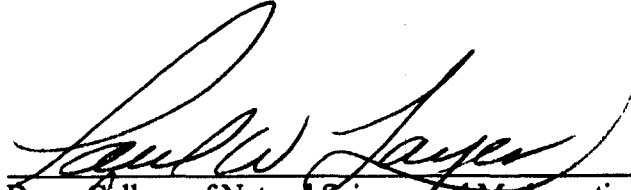


Advisory Committee Chair



Chair, Department of Geology and Geophysics

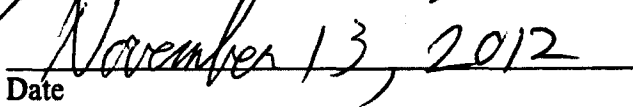
APPROVED:



Dean, College of Natural Science and Mathematics



Dean of the Graduate School



Date

Abstract

Tidal, seasonal and long-term surface mass movements cause the earth to deform and the gravity field to change. Current geodetic satellites, GPS and GRACE, accurately measure these geophysical signals. I examine the effect on GPS solutions of using inconsistent reference frames to model ocean tidal loading (OTL). For seasonal loading, I choose two study areas, Nepal Himalaya and southern Alaska, and compare GPS-measured and GRACE-modeled seasonal hydrological ground loading deformation.

Globally distributed stations are employed to compare GPS coordinate solutions with OTL corrections computed in different reference frames: center of mass of the solid Earth (CE), and center of mass of the Earth system (CM). A strong spectral peak at a period of ~14 days appears when inconsistent OTL models are applied along with smaller peaks at ~annual and ~semi-annual periods. Users of orbit/clock products must ensure to use OTL coefficients computed in the same frame as the OTL coefficients used by the analysis centers; otherwise, systematic errors will be introduced into position solutions.

Continuous GPS measurements of seasonal deformation in Nepal Himalaya are compared with load model predictions derived from GRACE observations. The GPS seasonal height variation and GRACE-modeled seasonal vertical displacement due to the changing hydrologic load exhibit consistent results, for both amplitude and phase. GRACE indicates a long-term mass loss in the Himalaya region, which leads to crustal uplift since the earth behaves as an elastic body. We model this effect and remove it from GPS observed vertical rates. Then most GPS vertical rates can be explained by interseismic strain from the Main Himalayan Thrust.

In southern Alaska, vertical seasonal loading deformation observed by GPS stations and modeled displacements due to seasonal hydrological loading inferred from GRACE are highly correlated. The effects of atmosphere and non-tidal ocean loading are important. Adding the AOD1B de-aliasing model to the GRACE solutions improves the correlation between these two geodetic measurements, because the displacements due to

these loads are present in the GPS data. Weak correlations are found for some stations located in areas where the magnitude of the load changes over a short distance, due to GRACE's limited spatial resolution.

Table of Contents

| | Page |
|--|----------|
| Signature Page | i |
| Title Page | ii |
| Abstract | iii |
| Table of Contents | v |
| List of Figures | viii |
| List of Tables | x |
| Acknowledgements | xi |
| | |
| Chapter 1 Introduction | 1 |
| References | 4 |
| | |
| Chapter 2 The Effect of Using Inconsistent Ocean Tidal Loading Models on GPS Coordinate Solutions | 5 |
| Abstract | 5 |
| 2.1 Introduction | 6 |
| 2.2 GPS data and processing strategy..... | 9 |
| 2.3 Comparison results | 10 |
| 2.3.1 Comparison between solutions using different frames during point positioning | 10 |
| 2.3.2 Testing the importance of consistency in OTL coefficients | 13 |
| 2.3.3 Network solutions with clocks estimated | 15 |
| 2.3.4 Ambiguity Resolution | 17 |
| 2.4 Discussion | 18 |
| 2.4.1 Theoretical Interpretation | 18 |
| 2.4.2 Effect of frame transformations | 20 |
| 2.5 Conclusions | 21 |

| | |
|------------------------|----|
| Acknowledgements | 22 |
| References | 23 |

Chapter 3 Seasonal and Long-term Vertical Deformation in the Nepal Himalaya Constrained by GPS and GRACE Measurements

| | |
|---|----|
| Abstract | 39 |
| 3.1 Introduction | 39 |
| 3.2 Geodetic Measurements | 41 |
| 3.2.1 Continuous GPS observations and data analysis | 41 |
| 3.2.2 GRACE models | 42 |
| 3.2.3 Displacements due to the changing load | 43 |
| 3.3 Comparison between GPS and GRACE-derived seasonal height variations | 43 |
| 3.4 Long-term uplift due to the mass loss | 47 |
| 3.5 Discussion | 48 |
| 3.5.1 Tectonic interpretation for the corrected vertical rates, assuming no GIA effect | 48 |
| 3.5.2 GIA and other effects | 49 |
| 3.5.3 Seasonal variations in horizontal displacements | 50 |
| 3.5.4 Removing hydrological loading deformation from GPS measurements using GRACE data..... | 51 |
| 3.6 Conclusions | 52 |
| Acknowledgements | 53 |
| References | 54 |

Chapter 4 Seasonal Hydrological Loading in Southern Alaska Observed by GPS and GRACE

| | |
|------------------------|----|
| Abstract | 72 |
| 4.1 Introduction | 72 |
| 4.2 Data | 73 |

| | |
|------------------------------------|-----------|
| 4.2.1 GPS data | 73 |
| 4.2.2 GRACE data | 74 |
| 4.3 Results | 75 |
| 4.4 Discussion | 77 |
| 4.5 Conclusion | 78 |
| Acknowledgements | 78 |
| References | 80 |
| Chapter 5 Conclusions | 91 |
| References | 94 |

List of Figures

| | Page |
|---|------|
| 2.1 Globally distributed continuous GPS stations adopted in this study | 27 |
| 2.2 Differences between GPS solutions determined using OTL-CM and OTL-CE coefficients, for the station TIDB | 28 |
| 2.3 Power spectrum of vertical coordinate differences from the 6-year timeseries computed using OTL-CM and OTL-CE corrections, for the station TIDB | 29 |
| 2.4 Amplitude of the ~14 day periodic variation in the difference between solutions using OTL-CM and OTL-CE coefficients, as a function of latitude | 30 |
| 2.5 Stacked power spectrum for the vertical coordinate timeseries | 31 |
| 2.6 Stacked power spectrum showing the ~14-day period component of 1-year detrended vertical coordinate timeseries for GPS solutions derived using two different orbit products | 32 |
| 2.7 Histograms of WRMS (mm) of vertical coordinate differences after application of a 7-parameter transformation between solutions with OTL modeled in two different frames | 33 |
| 2.8 Stacked power spectra showing the ~14-day period component from 1-year detrended vertical coordinate timeseries | 34 |
| 2.9 Time series of frame parameters over a half-year period determined from a 7-parameter transformation between solutions using OTL-CM and OTL-CE models | 35 |
| 2.10 Comparison between ambiguity-fix and ambiguity-free solutions | 36 |
| 2.11 Predicted OTL displacement of station TIDB for the first 5 days of 2005 .. | 37 |
| 2.12 Comparison between solutions before and after aligning to ITRF..... | 38 |
| | |
| 3.1 Locations of continuous GPS stations in Nepal | 59 |
| 3.2 GRACE-derived vertical displacement time series due to the changing load calculated for four GPS stations, CHLM, GUMB, DRCL, TIMP | 60 |

| | | |
|------|---|----|
| 3.3 | Comparison between 10-day averaged GPS detrended heights and GRACE-derived detrended seasonal vertical displacements | 61 |
| 3.4 | Stacked 10-day averaged GPS seasonal (detrended) vertical timeseries and GRACE-derived seasonal vertical timeseries | 62 |
| 3.5 | WRMS reductions for GPS detrended heights after removing GRACE-derived detrended displacements | 63 |
| 3.6 | Short-term WRMS of station CHLM | 64 |
| 3.7 | Comparison of annual amplitude between GPS observed heights and GRACE-derived vertical displacements | 65 |
| 3.8 | Vertical velocity field in Nepal Himalaya | 66 |
| 3.9 | Comparison between GPS observed and modeled vertical rates in Nepal | 67 |
| 3.10 | Comparison between GPS-observed and GRACE-derived horizontal seasonal displacements | 68 |
| 3.11 | Comparison of linear fit between actual GPS observed timeseries (blue) and corrected timeseries (red) with seasonal effects removed, based on GRACE-derived seasonal variations | 69 |
| 4.1 | Distribution of Continuous GPS station and example timeseries | 83 |
| 4.2 | Four examples (AC06, POT3, ELDC and LEVC) for GRACE-modeled vertical seasonal displacements | 84 |
| 4.3 | Selected examples of the WRMS reduction when removing GPS seasonal variation using GRACE-modeled seasonal displacements | 85 |
| 4.4 | The WRMS Reduction Ratios for all continuous GPS stations in southern Alaska | 86 |
| 4.5 | Seasonal variations for three example stations | 87 |
| 4.6 | Timeseries of campaign GPS site FS32 | 88 |

List of Tables

| | |
|--|-----------|
| 3.1 Information of continuous GPS stations in Nepal Himalaya | 70 |
| 3.2 Parameters of the Main Himalayan Thrust fault model adopted based on previous studies | 71 |
| 4.1 Information of continuous GPS stations analyzed in this study for southern Alaska | 89 |

Acknowledgements

After spending five years pursuing my Ph.D degree at the Geophysical Institute and the Department of Geology and Geophysics of UAF, I have reached the point of summarizing my work, and transforming from a student to a researcher. I appreciate all the help and support I received from my academic advisors, family and friends. It has been most fortunate to have all of you around.

I still remember how excited I was five years ago when I got the reply from Jeff Freymueller that there would be a student opportunity for me. It has been a pleasant and memorable journey to work with Jeff, whose support, encouragement and advice are the foundations of my dissertation. Jeff is always open-minded about science and gives me enough freedom about my research. I tried a lot of things before I found my study interests. No matter what kinds of studies I did and how poor the results I got, Jeff could always be patient, provide insightful guidance and share independent new ideas. His wide range of scientific knowledge impressed me all the time. When I expressed my willingness of doing field work in Tibet, which hopefully may benefit my projects, Jeff supported my trips although they were expensive.

Discussion and cooperation with many outstanding geoscience scholars significantly improved my dissertation. I am sincerely thankful to my committee members, Doug Christensen, Chris Larsen and Jon Dehn, for their academic directions and the life tips of “surviving” in a subarctic university. Besides, Doug led me my first seismometer field trip; Chris’ scripts and programs always inspired me and made my projects much easier; Jon’s passionate course broadened my knowledge for volcanology and remote sensing.

I greatly appreciate Tonie van Dam (University of Luxembourg) for her help and suggestions on my studies. She gave me strong encouragement for my study of the effect of using inconsistent reference frame to model ocean tidal loading on GPS positioning (Chapter 2), and generously provided the Green’s Function in different reference frames. I also express my gratitude to Anthony Arendt. My work of comparing GPS and GRACE

has benefited a lot from the discussion with Anthony. I want to thank my Chinese collaborators, Qi Wang, Caijun Xu, Shaomin Yang, Gang Chen and Rong Zou for our cooperative projects on the Tibetan Plateau.

I am thankful to the Caltech Tectonic Observatory for maintaining continuous GPS measurements in Nepal, and sharing the data with the scientific community. Those data are essential for the study of Chapter 3 of my dissertation. A Global Change Student Grant from the Center for Global Change and Arctic System Research provided financial support for the final stages of my research.

Our Geodesy Group members are always enjoyable to work with, both outside in the field and in the office. Ronni Grapenthin, Max Kaufman, Julie Elliott, Summer Miller, Lissy Hennig, Yan Hu and Tim Jensen, you all made my research go smoothly and with lots of fun. All of my friends here in Fairbanks fill my life with many more smiles.

I am mostly grateful to my family. My parents are always supporting my scientific interests and desires of studying abroad. My grandmother always concerns my life and study at the other side of telephone. This dissertation is for you!

Chapter 1 Introduction

The earth, behaving as an elastic body, deforms due to large surface mass variations. The Global Positioning System (GPS) has been extensively applied to monitor the crustal deformation due to tectonic, cryospheric and hydrological phenomena. The Gravity Recovery and Climate Experiment (GRACE) mission observes Earth's time-variable gravity field, which has been used to measure the Earth's mass variation both on the surface and interior of Earth.

Due to global climate change, the cryosphere is experiencing considerable mass loss globally. Large surface mass movements cause the elastic earth to deform and the gravity field to change. This current climate-driven ice and snow loss is superposed with other phenomena, mainly tectonics in locations like the Tibetan Plateau and southeast Alaska.

The central idea of this dissertation is to model the hydrological or/and cryospheric induced crustal deformation based on GRACE measured gravity data, and remove it from GPS measurements so as to derive tectonic-only deformation. Ground displacement due to the changing mass load can be expressed in terms of load Love numbers and GRACE-derived spherical harmonic coefficients for the gravity field (Wahr et al., 1998; Kusche and Schrama, 2005).

van Dam et al. (2007) compared GPS observed seasonal heights variations over Europe with GRACE modeled heights variations, and found that the annual signals for those two measurements did not show very good agreement. They attributed it to GPS data processing flaws, especially the spurious annual signals propagated into daily solutions during GPS data processing. Since that time, there have been a number of improvements to standard GPS processing, so it is a good time to reassess this question.

In order to reduce the aliased ocean tidal errors in GPS processing, I examine the effect of using inconsistent ocean tidal loading models on GPS coordinates in Chapter 2. With refined GPS data analysis, I present two case studies to correlate GPS and GRACE to analyze the hydrological and tectonic deformation in the Nepal Himalaya (Chapter 3), and seasonal hydrological loading in southern Alaska (Chapter 4).

Chapter 2 has been published in the *Journal of Geodesy*. I used a 6-year span of GPS data from 85 globally distributed stations to compare solutions using ocean tidal loading (OTL) corrections computed in different reference frames: center of mass of the solid Earth (CE), and center of mass of the Earth system (CM). Results show that significant biases can be introduced into GPS solutions when a user solution uses OTL coefficients computed in a different reference frame to those used by the analysis center in their product generation solution. To avoid this aliased periodic errors, researchers should ensure they adopt OTL coefficients computed in the same reference frame as those used by the analysis center that provides the orbit and clock products.

Chapter 3 has been published in the *Journal of Geophysical Research*. In this study, I use two kinds of geodetic techniques, continuous GPS and GRACE, to study seasonal mass change and its resulting vertical displacement in Nepal and southern Tibet. Quantitative comparisons between the observed GPS seasonal vertical deformation and GRACE-modeled seasonal deformation demonstrate that a consistent physical mechanism is responsible for the correlation between these two kinds of geodetic measurements. We also discuss the long-term mass loss revealed by GRACE measurements and its impacts on tectonic vertical rate evaluations. GRACE indicates a long-term mass loss (melting ice and snow) in this region. I model the consequent uplift caused by the load decrease, and remove this effect from observed GPS vertical rates. The residual vertical rates are mainly dominated by tectonic deformation due to the earthquake cycle in the thrusting. Comparison between observed and modeled (2D dislocation model) vertical rates show the interseismic slip of the Main Himalayan Thrust can explain the most of the vertical motion of most GPS stations.

Chapter 4 has been published in the *Geophysical Research Letters*. The seasonal hydrological mass cycle in southern Alaska is significant. Both GPS and GRACE detect this seasonal variation. Seasonal vertical deformation of GPS timeseries in southern Alaska was reported by Freymueller et al. (2008), and published GRACE time series indicated strong seasonal gravity changes in southeast Alaska caused by seasonal hydrologic mass variations (e.g., Tamisiea et al., 2005; Luthcke et al., 2008). In this

chapter, I compare the seasonal variation measured by GPS and GRACE across southern Alaska, and analyze the correlation between these two geodetic observations using an elastic loading model.

Chapter 5 summarizes the results and conclusions of this dissertation, and also indicates some potential follow-on work of combining GPS and GRACE to investigate cryospheric, hydrology and tectonic phenomena.

References

- Freymueller, J. T., H. Woodard, S. Cohen, R. Cross, J. Elliott, C. Larsen, S. Hreinsdottir, and C. Zweck (2008), Active deformation processes in Alaska, based on 15 years of GPS measurements, in *Active Tectonics and Seismic Potential of Alaska*, Geophys. Monogr. Ser., vol. 179, edited by J. T. Freymueller et al., pp. 1–42, AGU, Washington, D.C.
- Kusche, J., and E. J. O. Schrama (2005), Surface mass redistribution inversion from global GPS deformation and Gravity Recovery and Climate Experiment (GRACE) gravity data, *J. Geophys. Res.*, 110, B09409, doi:10.1029/2004JB003556.
- Luthcke, S. B., A. A. Arendt, D. D. Rowlands, J. J. McCarthy, and C. F. Larsen (2008), Recent glacier mass changes in the Gulf of Alaska region from GRACE mascon solutions, *J. Glaciol.*, 54, 767–777, doi:10.3189/002214308787779933.
- Tamisiea, M. E., E. W. Leuliette, J. L. Davis, and J. X. Mitrovica (2005), Constraining hydrological and cryospheric mass flux in southeastern Alaska using space-based gravity measurements, *Geophys. Res. Lett.*, 32, L20501, doi:10.1029/2005GL023961.
- van Dam, T., J. Wahr, and D. Lavallée (2007), A comparison of annual vertical crustal displacements from GPS and Gravity Recovery and Climate Experiment (GRACE) over Europe, *J. Geophys. Res.*, 112, B03404, doi:10.1029/2006JB004335.
- Wahr, J., M. Molenaar, and F. Bryan (1998), Time variability of the Earth's gravity field: Hydrological and oceanic effects and their possible detection using GRACE, *J. Geophys. Res.*, 103, 30,205–30,229.

Chapter 2 The Effect of Using Inconsistent Ocean Tidal Loading Models on GPS Coordinate Solutions¹

Abstract

We use up to a 6-year span of GPS data from 85 globally distributed stations to compare solutions using ocean tidal loading (OTL) corrections computed in different reference frames: center of mass of the solid Earth (CE), and center of mass of the Earth system (CM). We compare solution sets that differ only in the frame used for the OTL model computations, for three types of GPS solutions. In global solutions with all parameters including orbits estimated simultaneously, we find coordinate differences of ~ 0.3 mm between solutions using OTL computed in CM and OTL computed in CE. When orbits or orbits and clocks are fixed, larger biases appear if the user applies an OTL model inconsistent with that used to derive the orbit and clock products. Network solutions (orbits fixed, satellite clocks estimated) show differences smaller than 0.5 mm due to model inconsistency, but precise point positioning (PPP) solutions show distortions at the ~ 1.3 mm level. The much larger effect on PPP solutions indicates that satellite clock estimates are sensitive to the OTL model applied. The time series of coordinate differences shows a strong spectral peak at a period of ~ 14 days when inconsistent OTL models are applied and smaller peaks at \sim annual and \sim semi-annual periods, for both ambiguity-free and ambiguity-fixed solutions. These spurious coordinate variations disappear in solutions using consistent OTL models. Users of orbit and clock products must ensure that they use OTL coefficients computed in the same reference frame as the OTL coefficients used by the analysis centers that produced the products they use; otherwise, systematic errors will be introduced into position solutions. All modern products should use loading models computed in the CM frame, but legacy products may require loading models computed in the CE frame. Analysts and authors

¹Fu, Y., J. T. Freymueller, and T. van Dam (2012), The effect of using inconsistent ocean tidal loading models on GPS coordinate solutions, *J. Geod.*, 86(6), 409-421, doi:10.1007/s00190-011-0528-1.

need to document the frame used for all loading computations in product descriptions and papers.

2.1 Introduction

Ocean tidal loading (OTL) is the periodic crustal displacement caused by the load of the ocean tides. OTL surface displacements can reach several cm in magnitude in the vertical component for coastal areas, and are smaller but still detectable in the horizontal components (Vey et al., 2002; Urschl et al., 2005). Additionally, any mismodeling of diurnal and semidiurnal tidal constituents can be propagated to longer-period signals in the GPS coordinate time series (Penna and Stewart, 2003; Penna et al., 2007; Yuan et al., 2009), which results in spurious periodic variations. The magnitude of the OTL deformations makes correcting for them important during precise geodetic data analysis (e.g., van Dam et al., 1997; Dragert et al., 2000; King et al., 2008), especially because the measurement and modeling of variations in time series is becoming more important. Corrections for OTL deformation are usually made by computing a set of coefficients (amplitudes and phases of the loading deformation for each tidal component), and subsequently removing this model from the GPS observations in the solution for coordinates and other parameters.

Isomorphic terrestrial reference frames can be defined with differing origins, including the center of mass of the solid Earth (CE), or the center of mass of the whole Earth system (CM), which includes the ocean and other surface loads, such as atmosphere and continental water storage (Blewitt, 2003). The International Terrestrial Reference Frame (ITRF) is a CM frame in the sense of long-term secular motions, but does not account for short-term variations, such as seasonal variations or sub-daily variations (Dong et al., 2003). The Center of Figure (CF) frame, defined based on the center of figure of the solid Earth surface, can be well approximated by a no-net-translation condition on a global geodetic network. The CF frame is very nearly equivalent to CE, with the difference between CE and CF being only about 2% of the difference between CE and CM (Dong et al., 2003; Blewitt, 2003).

Ocean loading corrections can be computed by convolving Green's Functions with tidal variations over the global ocean domain (Goad, 1980). Green's Functions are derived from load Love numbers in a specific reference frame, and describe the deformation of the Earth due to a point surface load. The most widely used Green's Functions were obtained by Farrell (1972) in the CE frame. Load Love numbers and the resulting Green's Functions can be transformed between the CE and CM frames based on the individual physical definition of geocenter (Dong et al., 1997; Blewitt, 2003). The Green's functions differ in that the computed loading differs for the degree 1 deformation. In the CM frame, movement of fluid mass is accompanied by an opposite motion of the center of mass of the solid Earth, while in the CE frame the center of mass of the solid Earth is fixed (by definition). The geocentric component of the frame difference can be on the order of several millimeters in size, depending on how the tidal components add up (Scherneck et al., 2000). (H.-G. Scherneck provides tabulated coefficients for this "center of mass correction" for various tidal models and tidal components at <http://froste.oso.chalmers.se/loading/cmc.html>). In this paper we will use OTL-CM to refer to an OTL model computed in the CM frame, and OTL-CE for a model computed in the CE frame.

The current IERS Conventions and the International GNSS Service (IGS) recommendations both suggest using OTL corrections computed in the CM frame (IERS Conventions, 2010; Kouba, 2009). However, older conventions were different. Many if not most papers do not specify in which frame their loading computations were calculated, even when OTL and other sub-daily variations are the focus of the paper. For a typical example, King et al. (2008) did not report which frame was used for their OTL computations. But we know they must have used the CE frame Greens functions. This conclusion can only be deduced by a reader who knows that only the CE frame Greens functions were available for the SPOTL (Some Programs for Ocean-Tide Loading) code (Agnew, 1997) at that time. Few studies have examined the difference between loading computations in the CM vs. CE frame. Scherneck et al. (2000) compared sets of precise point positioning (PPP) solutions using both OTL-CE and OTL-CM models, and found

that the solutions using OTL-CE provided a better match for the tidal variations observed in the solutions. They suggested that this resulted from the fact that the orbit and clock products held fixed in their PPP solutions were generated using OTL-CE models, and that consistency between the solutions that generated the products and the user's solution is important. In this paper, we use PPP and other solutions to evaluate the effects of the frame used for OTL model computations, using an extensive global data set.

The frame used for OTL model computations needs to be kept distinct in the mind from the frame used for orbit integration, or any corrections applied to the orbits in preparing specific file formats. GPS satellites are gravitationally attracted by the mass of the whole Earth system, so their trajectories are physically relative to CM. GPS orbit files in the SP3 format are supposed to be in a crust-fixed reference frame, so the center of mass correction (difference between CM and CE) is removed in preparing these files, at least in the IGS reprocessed products (IERS Conventions, 2010). In this paper we do not discuss frame issues of the orbits themselves, but only the frame used to compute the OTL models. For consistency, all loading computations should be done in a CM frame, but when the frame for the loading computations is commonly not specified, it may be easy for inconsistency to arise, or for an incorrect theory to be applied.

In this study, we reprocessed a multi-year set of GPS data that included 85 globally distributed continuous stations with OTL modeled in both CE and CM, in order to examine the differences when using precise point positioning (Zumberge et al., 1997). We used shorter subsets of this data set for additional, more in-depth comparisons of different types of GPS solutions. In particular, we investigated solution strategies in which 1) the user computes a regional solution using fixed orbit products but estimates satellite clocks; and 2) the user estimates coordinates, orbits and all other parameters in a single solution, rather than using products derived by an external analysis center. We repeated our analysis for two different ocean tidal models and two different OTL computation programs to eliminate the possibility that the observed differences are due to the ocean tide models or to the software used to estimate the corrections.

2.2 GPS data and processing strategy

We analyzed a set of 85 globally distributed continuous GPS stations in this study (Figure 2.1). We use a global distribution of sites because using a regional network may introduce considerable errors during frame alignment (Tregoning and van Dam, 2005). We reprocessed all data for these sites from the beginning of 2002 through the end of 2007, 6 years in total, using the GIPSY/OASIS-II (Version 5.0) software in point positioning mode (satellite clocks and orbits fixed) to obtain daily coordinates and covariances. We then analyzed subsets of this data in network positioning mode (satellite clocks estimated, but orbits fixed) and using solutions in which we estimated all parameters simultaneously, including orbits. In point positioning, the user estimates site coordinates using fixed orbit and clock products that were derived by a separate global solution and that are usually provided by an external analysis center. Multiple sites can be analyzed together or one by one, giving the same result either way (Zumberge et al., 1997). We used JPL's reanalysis set of orbit and clock products, which were determined using a consistent set of models over the entire time span, including absolute antenna phase center models for both GPS receiver and satellite antennas (Schmid et al., 2007). We included antenna plus radome specific phase center models where they were available. We used the GMF tropospheric mapping function (Boehm et al., 2006), and adopted a priori dry tropospheric delay estimates from the Global Pressure and Temperature (GPT) model (Boehm et al., 2007). The solutions shown here do not include ambiguity resolution, although we test the impact of ambiguity resolution later in the paper. All solution series used exactly the same data, and in a variety of tests we vary the orbits, clocks, and OTL model used.

For our base set of solutions, we used JPL's fiducial free orbit and clock products (in the native GIPSY format). We transformed each daily solution into the ITRF2005 reference frame, estimating our own frame alignment transformation. Because we transform each solution into ITRF using a global set of reference sites, these comparisons highlight distortions of the network rather than differences in the solutions that can be removed by a 7-parameter transformation. A comparison of solutions that used the

fiducial products that are already in ITRF, would be very similar except that any frame-like bias between the solutions would remain as normally no frame alignment transformation is applied to those solutions. In other comparisons, we aligned the OTL-CE solution to the OTL-CM solution using a standard 7-parameter transformation so that we could directly evaluate both distortions and frame-like biases between the solutions.

We used the ocean tide models FES2004 and TPXO7.0 to calculate OTL corrections for all GPS stations, in both the CE and the CM frames, using two different software packages. The OTL model amplitudes and phases from the FES2004 tide model (including the tidal components M2, S2, N2, K2, K1, O1, P1, Q1, MF, MM and SSA) were computed using Hans-Georg Scherneck's web tool (<http://www.oso.chalmers.se/~loading/>). The OTL model amplitudes and phases using TPXO7.0 (Egbert and Erofeeva, 2002) (components M2, S2, N2, K2, K1, O1, P1, Q1, MF, MM) were computed using the SPOTL software (Agnew, 1997). The Green's functions provided with SPOTL are in the CE frame. We developed our own set of CM Green's functions to use with this program. We compared the SPOTL calculations for TPXO7.0 to those using Scherneck's online tool. The results agreed very closely for both the CE and CM frames (e.g. the difference in amplitude for the M2 component between SPOTL and Scherneck's online tool is less than 1.5% of its amplitude). This result is consistent with the work of Penna et al. (2008) that also assessed different algorithms for computing OTL.

2.3 Comparison results

2.3.1 Comparison between solutions using different frames during point positioning

Using JPL's reanalysis orbit/clock products, Figure 2.2 depicts the differences between solutions for station TIDB (Canberra, Australia) using OTL derived in the CE frame and the CM frame. The only difference between these solutions is the OTL coefficients used. All the GPS stations investigated in this study, independent of their

proximity to the ocean, show very similar patterns. The patterns are similar because the OTL displacements computed in CM and CE differ only by a degree 1 deformation. While all the stations show similar patterns, the phase of peaks of the difference varies over the globe. This result holds for solutions derived using either the FES2004 or TPXO7.0 models, consistent with the conclusion of Thomas et al. (2007) that the present ocean tide models give very similar results at the global scale.

The most obvious periodic component in Figure 2.2 has a period of about 14-days, appearing consistently in East, North and Height. The vertical component has larger peak-to-peak amplitudes, but differences in the horizontal components can reach about one third of that observed in the height. The power spectrum (Figure 2.3) for the difference (Figure 2.2) shows a spectral peak at 26.71 cycles per year (period of 13.67 days), and also reveals \sim annual and \sim semiannual components. Penna and Stewart (2003), Stewart et al. (2005) and Penna et al. (2007) demonstrated that, with a discrete 24-hour GPS data processing strategy, mismodeled diurnal and semidiurnal tidal constituents could be aliased into errors in longer periods in the timeseries. They predicted that propagated tidal deformation would appear at about 14-days (due to the aliasing of M2 and O1), semiannual (due to the aliasing of S2, K2 and P1) and annual periods (due to the aliasing of S2 and K1). These are the peaks that we observe in the vertical coordinate differences between the two solution sets (Figure 2.3). Other studies (Amiri-Simkooei et al. 2007; Ray et al. 2008; Tregoning and Watson, 2009) have shown that the observed \sim annual and \sim semiannual peaks in power spectra of GPS timeseries are really GPS draconitic annual (\sim 351.4 days) and semiannual (\sim 175.7 days) periods. A GPS draconitic year is the period for the GPS constellation to repeat its orientation relative to the Sun (Ray et al., 2008). For simplicity, we will refer to these peaks as \sim annual, \sim semi-annual, and \sim 14-day or \sim bi-weekly.

Figure 2.4 depicts the amplitudes of the \sim 14-day periodic variation in differences between solutions using OTL-CE and OTL-CM, as a function of latitude. GPS stations located at lower latitudes show larger amplitudes. Similar latitude-dependence of the

effects of mismodeling signals at tidal frequencies was found by Penna et al. (2007) and Tregoning and Watson (2011).

Solutions using OTL-CE and OTL-CM models differ by periodic variations, but which solution contains this spurious periodic variation? The stacked power spectrum for the detrended station timeseries is shown in Figure 2.5. The 48 GPS stations used for the stack (solid diamonds in Figure 2.1) were chosen based on the criteria that their timeseries should be continuous without obvious gaps or sudden offsets of coordinates due to strong earthquakes or receiver antenna changes. The stacked power spectrum (Figure 2.5) clearly illustrates that the ~14-days periodic variation is present only in solutions using OTL-CE frame. There is no spectral peak around this period in the solutions from the solutions using OTL-CM. This obvious difference between solutions using OTL-CE and OTL-CM does not depend on the tidal model, with similar results using both FES2004 and TPXO7.0 (Figure 2.5). The amplitude of the ~14-day peak in the power spectrum is reduced by 41% from OTL-CE solutions to OTL-CM solutions for FES2004, and by 40% from for TPXO7.0. Therefore, the difference between frames is much larger than the difference between ocean load models in the same frame. This result means that the choice of frame for OTL computations is more significant than the choice of ocean tide model. JPL uses the FES2004 ocean tide model and OTL-CM coefficients in the solutions it uses to generate its current and reanalysis orbit and clock products (S. Desai, personal communication, 2010). JPL's use of OTL-CM coefficients is consistent with current conventions. Our results show that point positioning users introduce systematic errors into their solutions if they do not use the same OTL coefficients used in the solution that generated the orbit and clock products.

For other periodic components, the amplitudes of the stacked power spectrum for the detrended timeseries derived using OTL-CM are also smaller than those derived using OTL-CE. For the annual component, the amplitude is decreased by 1.13% by changing from OTL-CE to OTL-CM for FES2004, and by 1.06% for TPXO7.0. The semiannual is reduced by 3.25% by changing from OTL-CE to OTL-CM for FES2004, and by 3.44% for TPXO7.0.

2.3.2 Testing the importance of consistency in OTL coefficients

JPL currently uses OTL-CM coefficients in the solutions that generate its products, but the older JPL legacy orbit products employed OTL-CE coefficients (S. Desai, personal communication, 2010). We use this difference to test the hypothesis that the differences we observe result from inconsistencies between the user solution and the solution that generated the orbit and clock products. We reprocessed data for all of 2002 using two different orbit/clock products: JPL's legacy products (eci orbit) determined using OTL-CE, and JPL's reanalysis products (pos orbit) determined using OTL-CM. For each set of orbit and clock products, we compared solutions using OTL coefficients modeled in the CE and CM frames, giving us 4 different combinations of OTL coefficients used for the user and product solutions (Figure 2.6). The ocean tide model FES2004 is adopted here. We label the solution sets based on the tide model, frame for OTL computations, and the orbit set used, for example FES04CM_POS means the FES2004 tide model, OTL computed in CM, and the reprocessed orbits (pos format).

Figure 2.6 displays the stacked power spectrum of the ~14-day period component for the four different combinations. It is clear that the amplitude of the position variations at this period is smaller for the solutions in which the same OTL coefficients were used in the product solution and the user solution, FES04CM_POS and FES04CE_ECI. This confirms that significant spurious periodic signal will be introduced into the GPS position solutions if the user solution employs OTL coefficients that differ from those used in the product solution. The solutions using the reanalysis products, FES04CM_POS, display markedly lower noise compared to the solutions using the legacy products, FES04CE_ECI. Indeed, there are many differences between the two sets of orbit products. Thus, from this comparison alone we cannot be sure how much of the observed scatter is due to the use of any particular frame for computing the OTL coefficients. However, it is clear that a user's solution in point positioning mode needs to use OTL coefficients that are consistent with those used in the solution that generated the

orbit and clock products. This confirms the suggestion of Scherneck et al. (2000) that such consistency should be very important.

We generated a 1-year (2006) set of solutions with orbits, clocks and positions estimated to test whether using one frame for OTL computations gives an intrinsically better result, using ocean tide model TPXO7.0. In a single-step global solution, there is no possibility of having an inconsistency in OTL coefficients as all parameters are estimated simultaneously in the solutions. We integrated orbits for each day based on the IGS reprocessed orbits (ig1), and estimated global solutions including adjustment to the orbits, using the same global stations as before. All processing models were the same as in the point positioning case, except that the solution was done in network mode with satellite clocks, orbit initial conditions and solar radiation pressure models estimated, along with all station parameters. We did not estimate Earth orientation parameters, but instead used IERS final values. One set of solutions used OTL-CM coefficients and the other set used OTL-CE, with no other differences.

We compared solutions by aligning each daily OTL-CE solution to the OTL-CM solution with a 7-parameter transformation and examining the residual differences after alignment. This comparison elucidates the distortion of the two solutions relative to each other, removing any differences that are described purely by translation, rotation or scaling of the network. The coordinate differences after transformation are very small, mostly 0.1-0.4 mm with a mean WRMS difference of ~ 0.25 mm (Figure 2.7, green bars). These differences are much smaller than the differences between the point positioning solutions (Figure 2.7, red bars). Analysis of the stacked power spectrum (Figure 2.8, top) indicates that the biases at ~ 14 -day period shown in Figure 2.6 clearly disappear. The magnitudes of the power for the global solutions, TPXO_CE and TPXO_CM differ at the level of 0.01 mm^2 or less, so they are indistinguishable, and both are, in fact, very close to the best result in point positioning mode, FES04CM_POS. All these results suggest that the use of consistent OTL coefficients is more important than using one particular frame or the other; that is, an inconsistency between the product solution and user solution introduces larger errors than does using the wrong theory consistently. Our time

series of global solutions is too short to demonstrate that using the correct theory (OTL-CM coefficients) produces a superior result than consistently using OTL-CE coefficients, but we assume this to be the case.

2.3.3 Network solutions with clocks estimated

Many users do not employ point positioning mode, but rather fix orbits based on external products, and either estimate satellite clock errors or remove them by double-differencing. If the choice of frame for the OTL model computations affects only the orbit product and not the satellite clocks, then this type of solution will exhibit the same biases as PPP solutions if the user solution uses OTL coefficients computed in a different frame. However, if the choice of OTL model coefficients mainly affects the clock parameters, the impact of inconsistency in this type of solution would be much smaller. To test the effects on this type of solution, we ran a 1-year (2006) series of network solutions with both clocks and positions estimated. JPL's reanalysis orbits were held fixed, but satellite clock parameters were estimated. We fixed a single reference clock, usually that at the site ALGO. The solutions were repeated using each of the OTL-CM and OTL-CE model coefficients.

We used a 7-parameter transformation to compare the coordinate differences of the two different solution sets. The residual coordinate differences after transformation (Figure 2.7, blue bars) have a mean WRMS of ~ 0.3 mm, very similar to what we observed for the global solutions with orbits estimated and much smaller than the differences we find for PPP solutions. The network solutions and PPP solutions differ only in that the satellite clocks are fixed to the values from the product solution in the PPP solution, but are estimated in the network solution. This result shows that the satellite clock estimates must be significantly different in solutions that use OTL-CM and OTL-CE, and that the difference is large enough to cause ~ 1.3 mm distortions of the network when inconsistent OTL models are used in the user and product solutions.

Figure 2.9 compares the frame parameters determined from transforming solutions using OTL-CE into alignment with solutions using OTL-CM (Figure 2.7 compares the

coordinate residuals after this transformation). The transformation parameters for network solutions with orbits, clocks and coordinates estimated (green line, Figure 2.9) are smaller than other two solutions, being much less than 0.1 mm. For the solutions that use fixed orbits (network solutions or PPP), the translation parameters are on the order of 0.3 mm or smaller, and the rotation parameters are equivalent to surface displacements of the same order. There is a small systematic bias of the z-axis rotation parameter for the PPP equivalent to a ~ 0.3 mm displacement at the equator. The cause of this bias is unknown, but presumably it reflects a mean time bias that could impact time transfer. We do not observe any systematic geocenter offset between the two solution sets of a size equivalent to the magnitude of the center of mass correction (several mm), because the geocenter translation of the daily frame is the geocenter offset averaged over the 24 hour solution period, not the instantaneous offset at one epoch.

When all parameters are estimated simultaneously in a single solution, the differences between solutions using OTL-CM and OTL-CE are of the order of ~ 0.3 mm, which are small, yet much larger than the GGOS (Global Geodetic Observing System) goal, 0.1 mm accuracy at the global scale (Gross et al., 2009). The same level of network distortion is found for network solutions that used fixed orbits, although these also include frame biases equivalent to ~ 0.3 mm displacements. PPP solutions have frame biases of the same order as the network solutions, but a much greater level of network distortion (~ 1.3 mm). While the satellite orbit parameters must be different between solutions using OTL-CM and OTL-CE models, this difference is small enough that biases remain at the sub-millimeter level when inconsistent OTL models are used in the product and user solutions. The much larger degree of distortion in the PPP solutions means that the effect on the satellite clock parameters must be substantially larger than the effect on the orbits. This result seems counter-intuitive, but we suggest that it is because the bias introduced by inconsistent OTL models is similar for most stations that observe a given satellite at a given epoch. Each satellite is visible to stations only within a $\sim 66^\circ$ - 76° radius about the nadir point, depending on the elevation cutoff angle (10° - 0°). Stations on the opposite side of the Earth would have an opposite bias but do not observe

the satellite. The common-mode part of the bias at each epoch (defined by the stations actually observing the satellite) will bias the satellite clock estimate for that epoch. In the limit of a sufficiently small regional network solution, the bias from inconsistent OTL models would be completely common mode, and would be removed by double-differencing or be indistinguishable from the satellite clock error.

2.3.4 Ambiguity Resolution

Tregoning and Watson (2009, 2011) found that ambiguity resolution affected the propagation of periodic modeling errors into station coordinates. Specifically, ambiguity-free solutions showed higher power than ambiguity-fixed solutions at the periods characteristic of tidal aliasing variations. To test the effect of ambiguity resolution on GPS coordinates with OTL corrections computed in inconsistent reference frames, we used the Ambizap algorithm to implement GPS carrier phase ambiguity resolution together with PPP (Blewitt, 2008). Ambizap carries out ambiguity resolution on a baseline-by-baseline basis and applies the resulting coordinate changes to the combined PPP solution; the result is equivalent to a network-based ambiguity resolution. We ran a 1-year-long solution series (calendar year 2006) using JPL's reanalysis orbit/clock products, but with OTL corrections computed in CM and CE, respectively. We then compared solutions before and after ambiguity resolution with Ambizap.

We computed the vertical coordinate differences between OTL-CM and OTL-CE ambiguity-fixed solutions. A typical example (station TIDB) is given in Figure 2.10 (top, blue line). Compared with the result of ambiguity-free solution (red line), the difference at 14-day period is still in the ambiguity-fixed result (blue line), although the amplitude is reduced slightly. However, for about 1/4 of the stations the amplitude of the periodic difference was slightly increased. Overall, the ambiguity-fixed solutions show smaller differences at all frequencies, consistent with a lower overall noise level, but the reduction in power due to ambiguity resolution at the ~14 day period was smaller than at other periods (Figure 2.10, bottom).

The stacked power spectra (Figure 2.10, bottom) indicate that significant systematic errors are still introduced in ambiguity-fixed solutions if inconsistent OTL models are applied (red solid line). The smaller effect in ambiguity-fixed solutions is similar to that seen by Tregoning and Watson (2009, 2011) for atmospheric loading effects. However, the ambiguity-fixed solutions show the same essential characteristics as the ambiguity-free solutions, in that the use of inconsistent OTL models introduces significant systematic errors.

2.4 Discussion

2.4.1 Theoretical Interpretation

GPS satellites are gravitationally attracted by the mass of the whole Earth system that includes the ocean, the atmosphere and other external and internal mass redistributions. The satellite trajectories are intrinsically determined with respect to the CM. Therefore, for consistency all corrections applied in the coordinate model (especially loading corrections) ought to utilize the CM reference frame. Current IERS conventions require IGS Analysis Centers to use OTL-CM corrections when generating orbit/clock solutions (IERS Conventions, 2010; Kouba, 2009). Our study indicates that users need to use OTL coefficients that are consistent with those used by the analysis center that generated the orbit and clock products, especially when using point positioning. Using inconsistent OTL coefficients will introduce periodic systematic errors at the periods characteristic of aliased ocean tidal loading, mainly ~14-days, ~semi-annual and ~annual periods. The GPS solutions themselves are biased at specific periods because, during the 24-hour positioning process, the frame bias does not exactly average to zero over the course of the time period of the GPS solution (Penna and Stewart, 2003; Stewart et al., 2005; Penna et al., 2007). This bias is over and above any errors that result from limitations of the tidal models themselves, which do not depend on the frame. Several recent studies have demonstrated that modern tidal models and OTL computation software produce very similar results (Thomas et al., 2007; Penna et al.,

2008; Fok et al., 2010). The difference between solutions using OTL-CM and OTL-CE coefficients is much larger than the difference that results from using different tidal models.

Figure 2.11 shows predicted OTL displacements of station TIDB for the first five days of 2005. The displacements predicted by the OTL-CM and OTL-CE models are clearly different, and the differences are shown with a green curve. The difference curve (green) is the geocenter difference between the two frames, also termed the “center of mass correction” or “frame origin tides” (Scherneck et al., 2000), expressed in the local east-north-up coordinate system at this site. Because this difference results from a degree-1 deformation, OTL models for all sites around the world show a similar magnitude variation (in terms of the 3D vector). If one correction is applied in the solution that generated the orbit and clock products, and the other is applied in a user solution making use of those products, biases related to the green curve will be introduced into the GPS observation model, which will distort the estimated parameters in that solution. With a 24-hour processing period, mismodeled tidal signals are propagated to longer-period noise in the GPS daily solutions (Penna and Stewart 2003; Penna et al. 2007), as revealed by the spectral analysis in Figure 2.3 and Figure 2.5. These biases distort the network (Figure 2.7) and induce spurious variations in frame parameters (Figure 2.9).

Scherneck et al. (2000) examined a set of point positioning solutions and compared observed tidal variations to models using OTL coefficients computed in both CM and CE. They expected to find the geocentric component in their solutions, but instead found that the observed variations agreed better with the OTL-CE model. They believed the reason for this to be that they used orbit and clock products generated from a solution generated using OTL-CE coefficients; thus the OTL-CM model was not consistent with the product solution. Our results show that their reasoning was correct. The orbit and clock products generated from a global solution essentially “lock in” the OTL model used in that product solution. Any user solution must use OTL coefficients consistent with the product solution. The choice of frame for the OTL model computations is much

more important than the choice of tidal model. We find that the satellite clock parameters show larger differences than the orbit parameters, so the impact of inconsistencies between the product and user solutions is much larger for PPP solutions than for network solutions in which satellite clocks are estimated or removed by double-differencing.

2.4.2 Effect of frame transformations

The observed coordinate differences shown in Figure 2.2 and analyzed in this paper demonstrate that introducing biases through inconsistency in OTL models causes distortions of the network that cannot be removed by a 7-parameter frame transformation (Figure 2.7). Figure 2.12 shows vertical coordinate differences for TIDB from point positioning solutions, both before and after aligning the fiducial-free solution to ITRF2005. Before the frame alignment, each day's fiducial-free solution is in no particular frame, depending on the loose constraints applied in the solution that generated the orbit and clock products. Because we are comparing two solutions that are identical except for the OTL model applied, the two solutions being compared each day are nominally in the same frame. The patterns for the timeseries of the differences are very similar, and the amplitudes diminish slightly after the frame alignment. This confirms that most of the solution differences result from distortions in the network introduced by inconsistency in the OTL models. However, a portion of the bias from the OTL model frame error is absorbed into the frame transformation, and therefore into estimates of geocenter variation.

Tregoning and van Dam (2005) demonstrated that 80% of the geocenter motion can be recovered with a standard seven-parameter transformation for a global network, and the distribution of transformation sites can have a major impact on the transformation results. Thus, the globally distributed GPS sites used in this study improve our ability to distinguish surface displacements due to OTL from geocenter motion, during the process of transforming a non-fiducial solution into ITRF2005. If a small regional solution is used instead of a global solution, the coherence of the loading effect over long spatial wavelengths would not be preserved during the process of transformation. Subsequently,

most of the coherent loading signals would be absorbed into the estimate of geocenter motion (Tregoning and van Dam 2005). This would impair the estimates for both the loading deformation and the geocenter.

2.5 Conclusions

Our study has shown that significant biases can be introduced into GPS solutions when a user solution uses OTL coefficients computed in a different reference frame to those used by the analysis center in their product generation solution. The choice of frame for the OTL model computations has a substantial effect on estimated satellite clock parameters, and a smaller effect on the estimated satellite orbits. For global solutions in which orbits, clocks and coordinates are estimated simultaneously, there are coordinate differences of ~ 0.3 mm between solutions using OTL-CM and OTL-CE coefficients. When orbits and/or clocks determined from an external product solution are fixed, biases will be introduced into the user solutions if an OTL model is applied that is not consistent with the model used in the product solution. For network solutions the overall frame biases and distortion of the network remains at the sub-mm level, but for PPP solutions we find distortions of the network at the ~ 1.3 mm level because the fixed satellite clocks are now inconsistent with the applied observation model.

Solutions in which inconsistent OTL coefficients are used display significant differences at several periodic components that are characteristic of aliasing of OTL errors. Power spectrum analysis for our 6-year detrended timeseries of continuous GPS positions shows that the most distinguishable difference occurs at a period of about ~ 14 days. Using JPL's current and reanalysis orbits products, which use OTL coefficients computed in the CM frame in accordance with IERS Conventions, we find a significant spectral peak at ~ 14 -day period in the solution with OTL coefficients computed in the CE frame, but no peak at this period in the solutions using OTL computed in the CM frame. This result stands true for both ambiguity-free and ambiguity-fixed solutions. In addition, there are small differences at \sim annual and \sim semiannual periods. This phenomenon has been confirmed using both ocean tide models FES2004 and TPXO7.0,

calculated using independent software. All of these improvements coincide well with the predicted periods of aliasing signals from OTL errors.

In any solution that uses fixed orbits or fixed orbits and satellite clocks, it is the analyst's responsibility to maintain consistency with the analysis center that generated the products. The need for consistency makes it critical both for analysis centers that generate orbit and clock products and researchers using these products to report which frame was used to compute the OTL coefficients in their analysis. Authors should also make clear which frame they used. The same is true for any other loading model applied at the observation level, such as the tidal component of atmospheric loading (Tregoning and Watson, 2009, 2011). Both users and analysis centers that produce precise orbits and clocks should use OTL-CM coefficients for theoretical consistency and adherence to current IERS conventions. However, users of legacy products in which OTL-CE coefficients were used in the product generation will induce significant errors in their solutions if they do not maintain consistency and also use OTL-CE coefficients. This need for consistency may limit the degree to which PPP solutions can be used to assess other changes or improvements in observation models, such as the 2nd or higher order ionospheric effects (e.g., Kedar et al., 2003; Fritsche et al., 2005).

Acknowledgements

We gratefully acknowledge Matt King and two anonymous reviewers for helpful suggestions that significantly improve this paper. We also thank Duncan Agnew for providing the SPOTL software, and Hans-Georg Scherneck for maintaining the web tool to compute OTL, both of which were critical for this study. Our CM Greens functions for SPOTL will be distributed with future SPOTL releases and are also available from the authors. This work was supported by NSF grants EAR-0911764 and EAR-0911677.

References

- Agnew, D. C. (1997), NLOADF: a program for computing ocean-tide loading. *J. Geophys. Res.*, 102, 5109-5110.
- Amiri-Simkooei, A. R., C. C. J. M. Tiberius, and P. J. G. Teunissen (2007), Assessment of noise in GPS coordinate time series: Methodology and results. *J. Geophys. Res.*, 112, B07413, doi:10.1029/2006JB004913.
- Blewitt, G. (2003), Self-consistency in reference frames, geocenter definition, and surface loading of the solid Earth. *J. Geophys. Res.*, 108(B2), doi:10.1029/2002JB002082.
- Blewitt, G. (2008), Fixed point theorems of GPS carrier phase ambiguity resolution and their application to massive network processing: Ambizap. *J. Geophys. Res.*, 113, B12410, doi:10.1029/2008JB005736.
- Boehm, J., A. Niell, P. Tregoning, and H. Schuh (2006), Global Mapping Function (GMF): A new empirical mapping function based on numerical weather model data. *Geophys. Res. Lett.*, 33, L07304, doi:10.1029/2005GL025546.
- Boehm, J., R. Heinkelmann, and H. Schuh (2007), Short Note: A global model of pressure and temperature for geodetic applications. *J. Geod.*, doi:10.1007/s00190-007-0135-3.
- Dong, D., J. O. Dickey, Y. Chao, and M. K. Cheng (1997), Geocenter variations caused by atmosphere, ocean and surface ground water. *Geophys. Res. Lett.*, 24, 1867-1870.
- Dong, D., T. Yunck, and M. Heflin (2003), Origin of the International Terrestrial Reference Frame. *J. Geophys. Res.*, 108(B4), 2200, doi:10.1029/2002JB002035.
- Dragert, H., T. S. James, and A. Lambert (2000), Ocean loading corrections for continuous GPS: A Case study at the Canadian Coastal Site Holberg. *Geophys. Res. Lett.*, 27(14), 2045-2048.
- Egbert, G. D. and L. Erofeeva (2002), Efficient inverse modeling of barotropic ocean tides. *J. Atmos. Oceanic Technol.*, 19, 183-204.

- Farrell, W. E. (1972), Deformation of the Earth by surface loads. *Rev. Geophys.*, 10, 761–797.
- Fok, H. S. , H. B. Iz, CK Shum, Y. Yi, O. Andersen, A. Braun, Y. Chao, G. Han, CY Kuo, K. Matsumoto, and Y. T. Song (2010), Evaluation of Ocean Tide Models Used for Jason-2 Altimetry Corrections. *Marine Geodesy*, 33(1 supp 1): 285-303.
- Fritsche, M., R. Dietrich, C. Knöfel, A. Rülke, S. Vey, M. Rothacher, and P. Steigenberger (2005), Impact of higher-order ionospheric terms on GPS estimates. *Geophys. Res. Lett.*, 32, L23311, doi:10.1029/2005GL024342.
- Goad, C. C. (1980), Gravimetric tidal loading computed from integrated Green's functions. *J. Geophys. Res.*, 85: 2679-2683.
- Gross, R., G. Beutler, and H. P. Plag (2009), Integrated scientific and societal user requirements and functional specifications for the GGOS. *Global Geodetic Observing System*, 209-224.
- IERS Conventions (2010), Gérard Petit and Brian Luzum (eds.). (IERS Technical Note ; 36) Frankfurt am Main: Verlag des Bundesamts für Kartographie und Geodäsie, 2010. 179 pp., paperback, in print.
- Kedar, S., G. A. Hajj, B. D. Wilson, and M. B. Heflin (2003), The effect of the second order GPS ionospheric correction on receiver positions. *Geophys. Res. Lett.*, 30(16), 1829, doi:10.1029/2003GL017639.
- King, M. A., C. S. Watson, N. T. Penna and P. J. Clarke (2008), Subdaily signals in GPS observations and their effect at semiannual and annual periods. *Geophys. Res. Lett.*, 35, L03302, doi: 10.1029/2007GL032252.
- Kouba, J. (2009), A Guide to Using International GNSS Service (IGS) Products. <http://igs.cb.jpl.nasa.gov/components/usage.html>.
- Penna, N. T. and M. P. Stewart (2003), Aliased tidal signatures in continuous GPS height time series. *Geophys. Res. Lett.*, 30(23), 2184, doi:10.1029/2003GL018828.
- Penna, N. T., M. A. King, and M. P. Stewart (2007), GPS height time series: Short-period origins of spurious long-period signals. *J. Geophys. Res.* 112, B02402, doi:10.1029/2005JB004047.

- Penna, N. T., M. S. Bos, T. F. Baker, and H. G. Scherneck (2008), Assessing the accuracy of predicted ocean tide loading displacement values. *J. Geod.*, 82: 893-907, DOI: 10.1007/s00190-008-0220-2.
- Ray, J., Z. Altamimi, X. Collilieux and T. van Dam (2008), Anomalous harmonics in the spectra of GPS position estimates. *GPS Solut.*, 12: 55-64, DOI 10.1007/s10291-007-0067-7.
- Scherneck, H. G., J. M. Johansson and F. H. Webb (2000), Ocean loading tides in GPS and rapid variations of the frame origin. *Geodesy Beyond 2000 - The Challenges in the First Decade Vol. 121*, Schwarz, Springer - Verlag Berlin Heidelberg 2000.
- Schmid, R., P. Steigenberger, G. Gendt, M. Ge, and M. Rothacher (2007), Generation of a consistent absolute phase center correction model for GPS receiver and satellite antennas. *J. Geod.*, 81(12), 781-798, DOI: 10.1007/s00190-007-0418-y.
- Stewart, M. P., N. T. Penna, and D. D. Lichti (2005), Investigating the propagation mechanism of unmodelled systematic errors on coordinate time series estimated using least squares. *J. Geod.*, 79(8), 479– 489.
- Thomas, I. D., M. A. King, and P. J. Clarke (2007), A comparison of GPS, VLBI and model estimates of ocean tide loading displacements. *J. Geod.*, 81, 359-368. DOI 10.1007/s00190-006-0118-9.
- Tregoning, P. and T. van Dam (2005), Effects of atmospheric pressure loading and seven-parameter transformations on estimates of geocenter motion and station heights from space geodetic observations. *J. Geophys. Res.*, 110, B03408, doi:10.1029/2004JB003334.
- Tregoning, P. and C. Watson (2009), Atmospheric effects and spurious signals in GPS analyses. *J. Geophys. Res.*, 114, B09403, doi:10.1029/2009JB006344.
- Tregoning, P. and C. Watson (2011), Correction to “Atmospheric effects and spurious signals in GPS analyses”. *J. Geophys. Res.*, 116, B02412, doi:10.1029/2010JB008157.
- Urschl, C., R. Dach, U. Hugentobler, S. Schaer, and G. Beutler (2005), Validating ocean tide loading models using GPS. *J. Geod.*, 78: 616-625.

- Vey, S., E. Calais, M. Llubes, N. Florsch, G. Woppelmann, J. Hinderer, M. Amalvict, M. F. Lalancette, B. Simon, F. Duquenne, and J. S. Haase (2002), GPS measurement of ocean loading and its impact on zenith tropospheric delay estimates: a case study in Brittany, France. *J. Geod.*, 76(8): 419-427, DOI 10.1007/s00190-002-0272-7.
- van Dam, T., J. Wahr, Y. Chao, and E. Leuliette (1997), Predictions of crustal deformation and of geoid and sea-level variability caused by oceanic and atmospheric loading. *Geophys. J. Int.*, 129, 507-517.
- Yuan, L. G., X. L. Ding, P. Zhong, W. Chen, and D. F. Huang (2009), Estimates of ocean tide loading displacements and its impact on position time series in Hong Kong using a dense continuous GPS network. *J. Geod.*, 83: 999-1015.
- Zumberge, J. F., M. B. Heflin, D. C. Jefferson, M. M. Watkins and F. H. Webb (1997), Precise point positioning for the efficient and robust analysis of GPS data from large networks. *J. Geophys. Res.*, 102(B3):5005-5017.

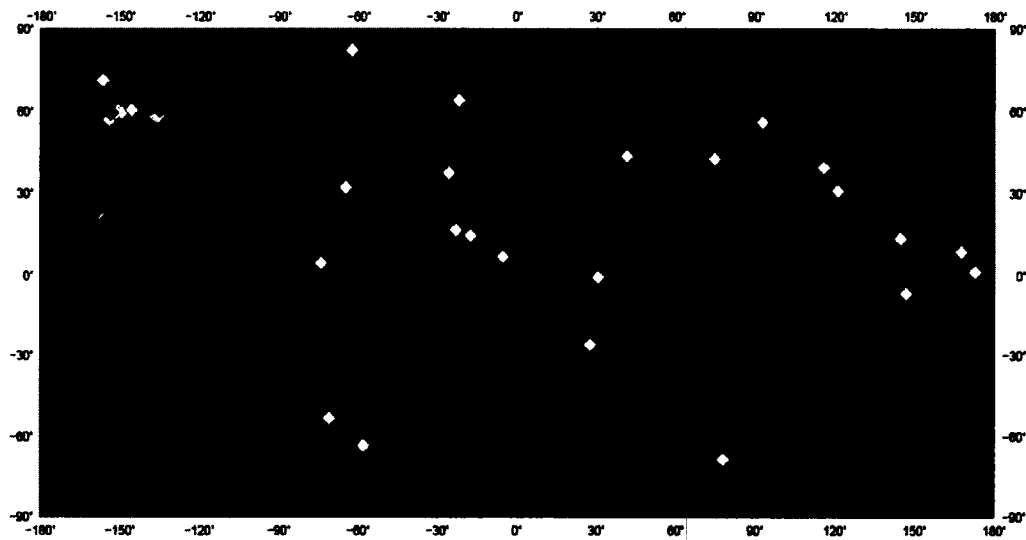


Figure 2.1: Globally distributed continuous GPS stations adopted in this study. We processed 6-years of GPS data using OTL coefficients obtained in different frames. Solid diamonds denote sites used in the stacked power spectral analysis (~48 sites). White diamonds depict stations with nonnegligible temporal gaps or sudden coordinate offsets in the timeseries that were not used in the stack.

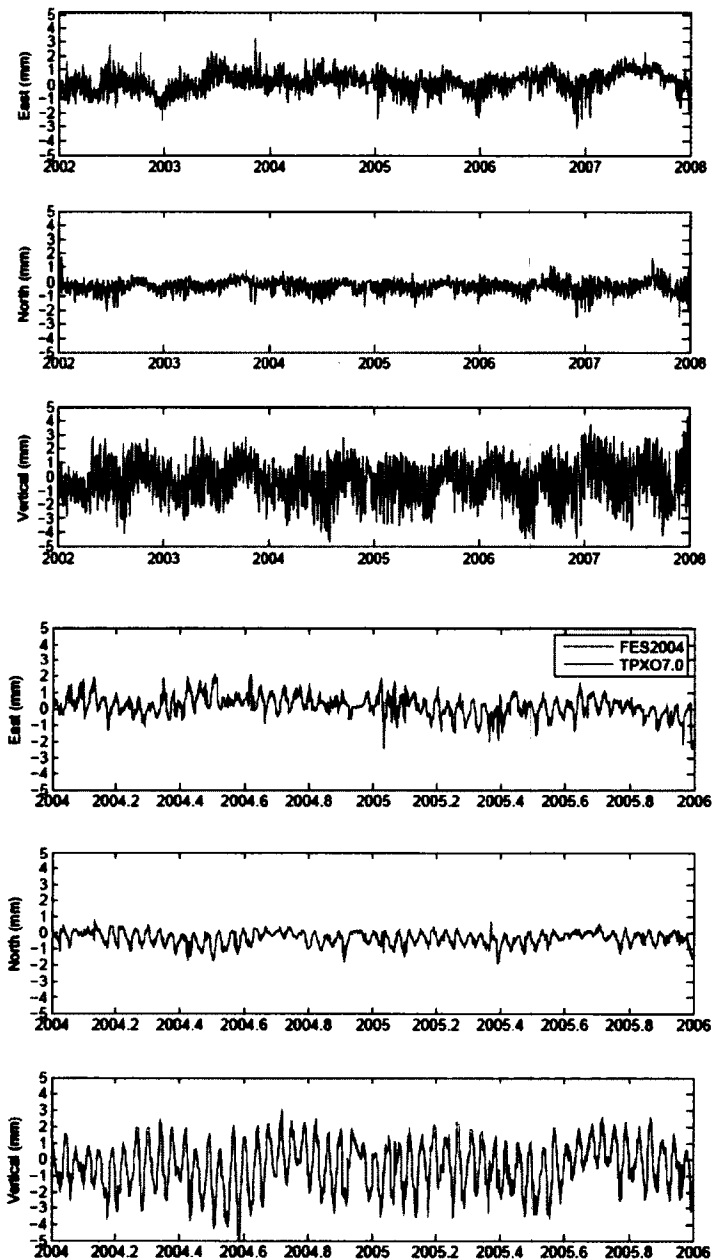


Figure 2.2: Differences between GPS solutions determined using OTL-CM and OTL-CE coefficients, for the station TIDB. Top: 6-year time series of differences using the ocean tide model FES2004. Bottom: A 2-year time series comparing the FES2004 (blue) and TPXO7.0 (red) models; at this scale, the two models give nearly identical results.

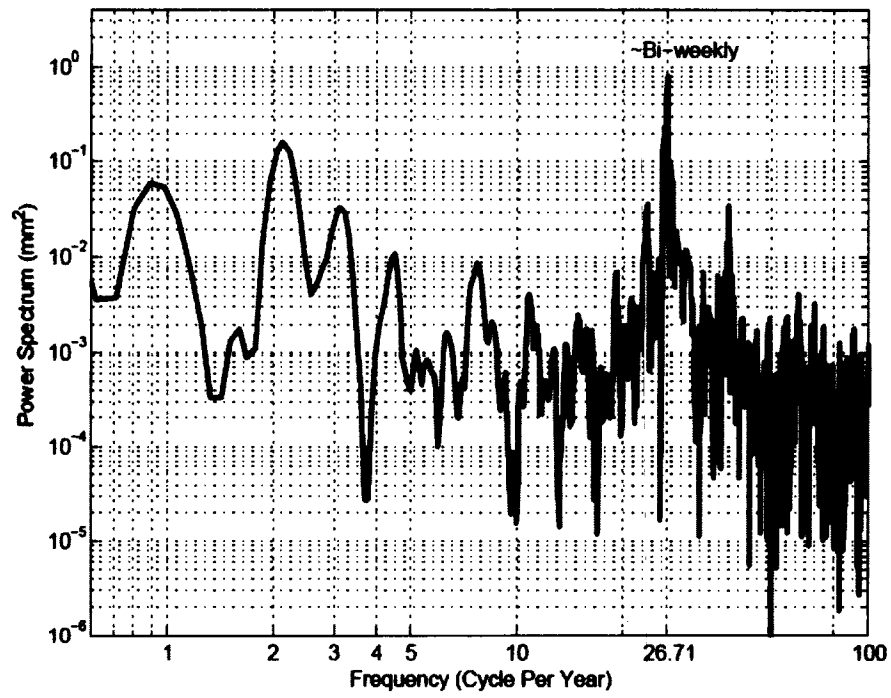


Figure 2.3: Power spectrum of vertical coordinate differences from the 6-year timeseries computed using OTL-CM and OTL-CE corrections, for the station TIDB. A sharp peak appears at a frequency of about 26.71 cycles per year. This represents a period of about 13.67 days.

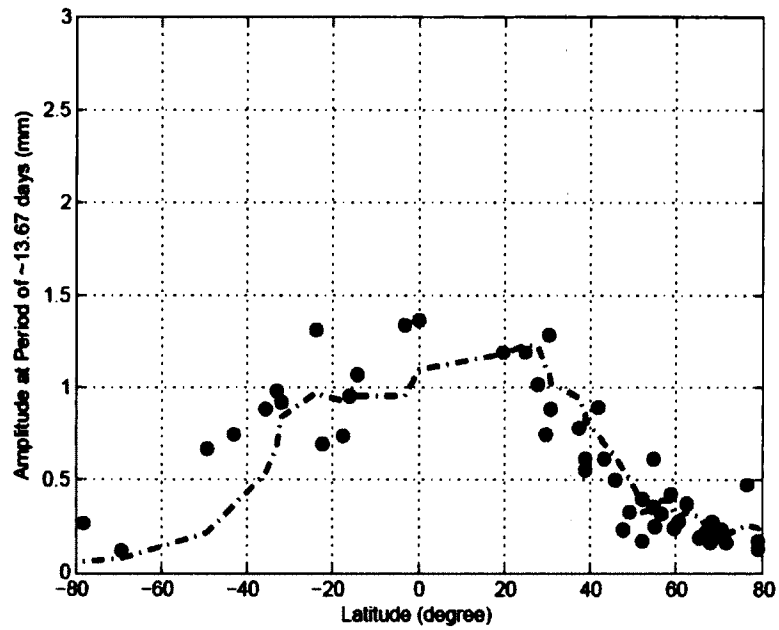


Figure 2.4: Amplitude of the ~14 day periodic variation in the difference between solutions using OTL-CM and OTL-CE coefficients, as a function of latitude. Blue dash-dot line is a five-point moving average.

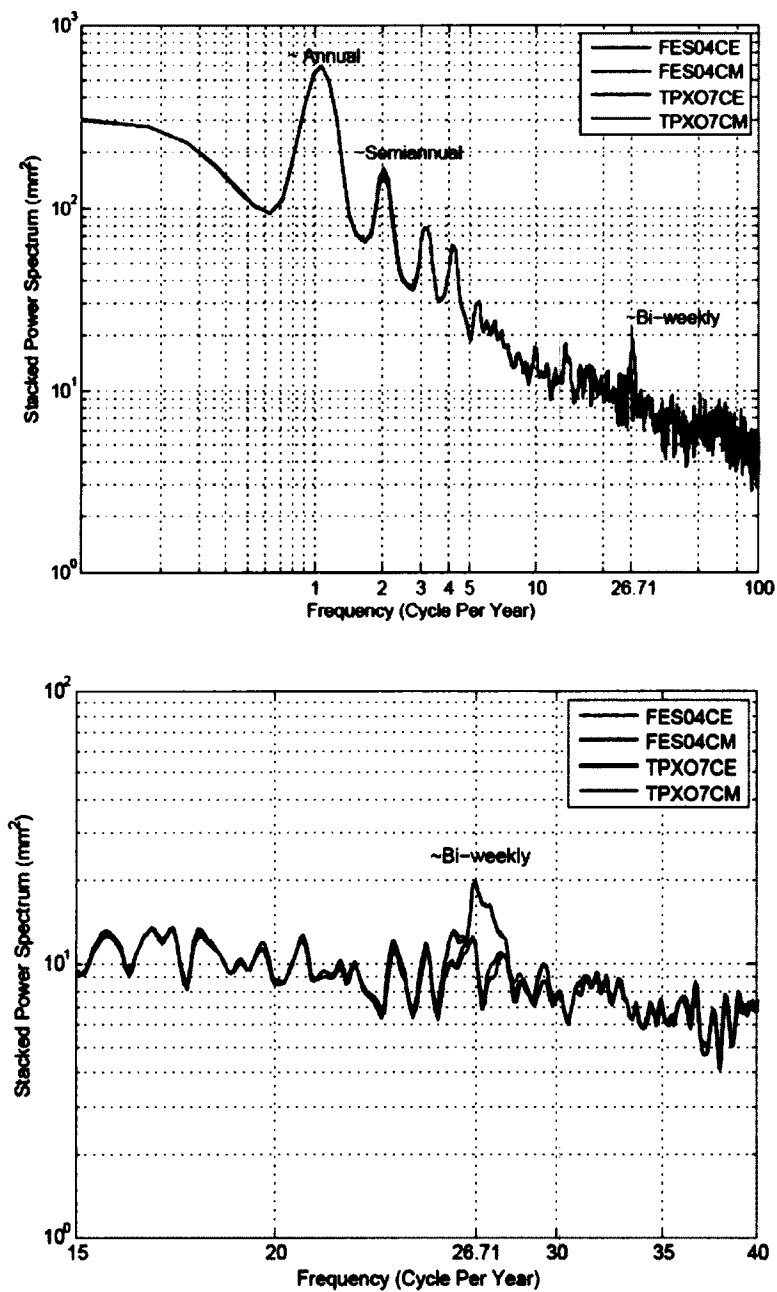


Figure 2.5: Stacked power spectrum for the vertical coordinate timeseries. (Top) Stacked power spectrum for the vertical coordinate timeseries, using all stations in the stack. (Bottom) A detailed of the top panel highlighting the ~14-day period. GPS stations used for stack are marked with solid diamonds in Figure 2.1.

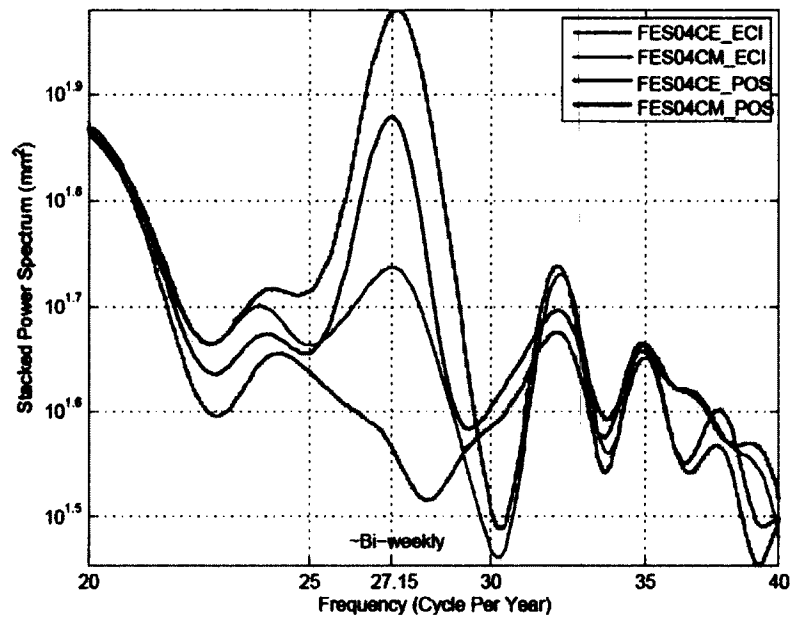


Figure 2.6: Stacked power spectrum showing the ~14-day period component of 1-year detrended vertical coordinate timeseries for GPS solutions derived using two different orbit products: JPL's legacy products (eci), derived using OTL-CE coefficients, and JPL's reanalysis products (pos), derived using OTL-CM coefficients. For each set of orbits, we compare the noise spectra for solutions using OTL-CM and OTL-CE coefficients, giving four sets of solutions. The two solution sets with inconsistency in the OTL coefficients show significant noise peaks at ~14-day period, while the solutions using consistent OTL coefficients do not.

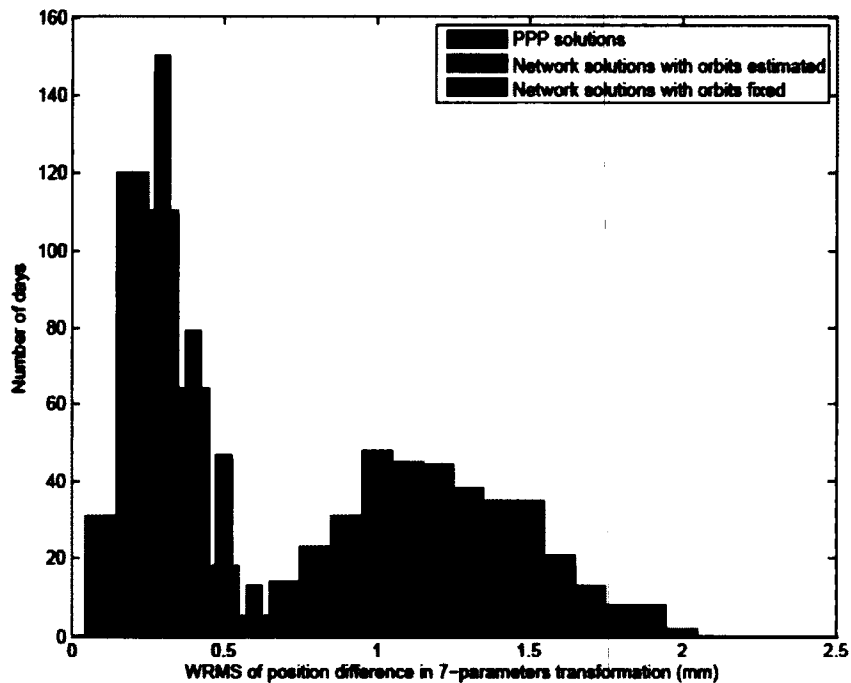


Figure 2.7: Histograms of WRMS (mm) of vertical coordinate differences after application of a 7-parameter transformation between solutions with OTL modeled in two different frames. All the data are from the same year: 2006. Red bars represents the WRMS distortions for PPP solutions between FES04CE_POS and FES04CM_POS; green bars show WRMS distortions for network solutions with orbits, clocks and coordinates estimated, and blue bars for network solution with clocks and coordinates estimated.

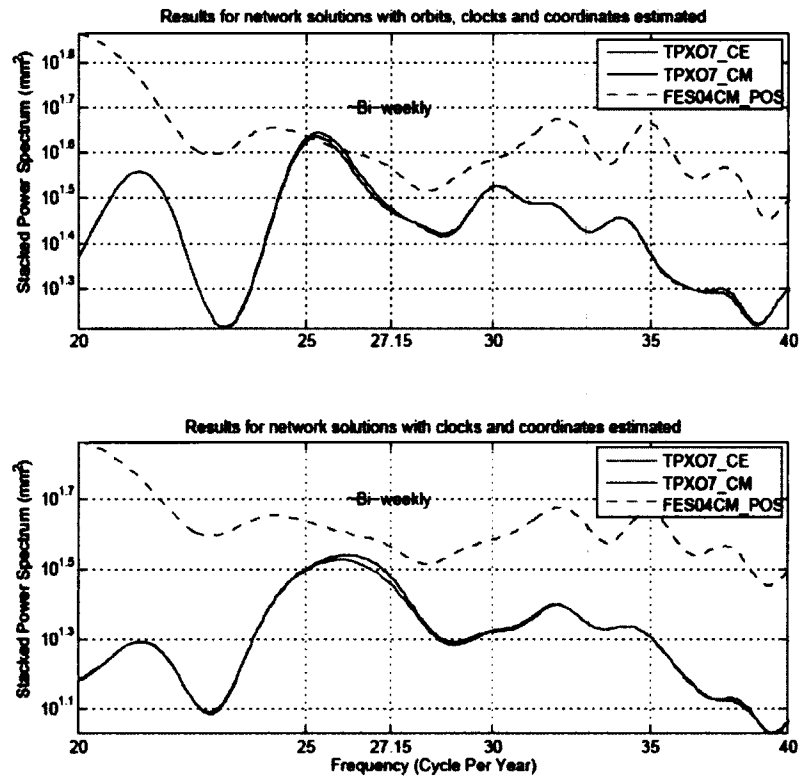


Figure 2.8: Stacked power spectra showing the ~ 14 -day period component from 1-year detrended vertical coordinate timeseries, for global solutions with orbits, clocks and coordinates estimated (upper), and network solutions with clocks and coordinates estimated (bottom). FES04CM_POS (dashed line) is the same as that shown in Figure 2.6 and is plotted here for comparison; it depicts the result in point positioning using JPL's reanalysis products (pos) and the OTL-CM model.

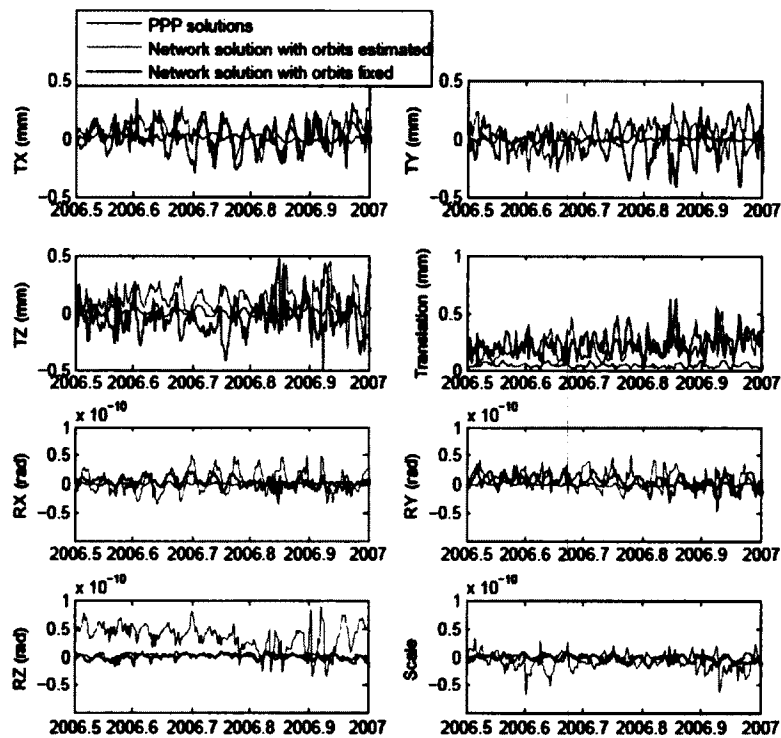


Figure 2.9: Time series of frame parameters over a half-year period determined from a 7-parameter transformation between solutions using OTL-CM and OTL-CE models. [TX TY TZ] are translation parameters (in mm); [RX RY RZ] represent rotation parameters (in 10^{-10} rad). The panel in (row 2, column 2) depicts the magnitude of the 3D translation vector (square root of $(TX^2 + TY^2 + TZ^2)$). The red line is for transformation between FES04CE_POS and FESCM_POS, the green line is for transformation of network solutions (orbits, clocks and coordinates estimated), and the blue line shows the results for network solutions (orbits fixed, satellite clocks and coordinates estimated).

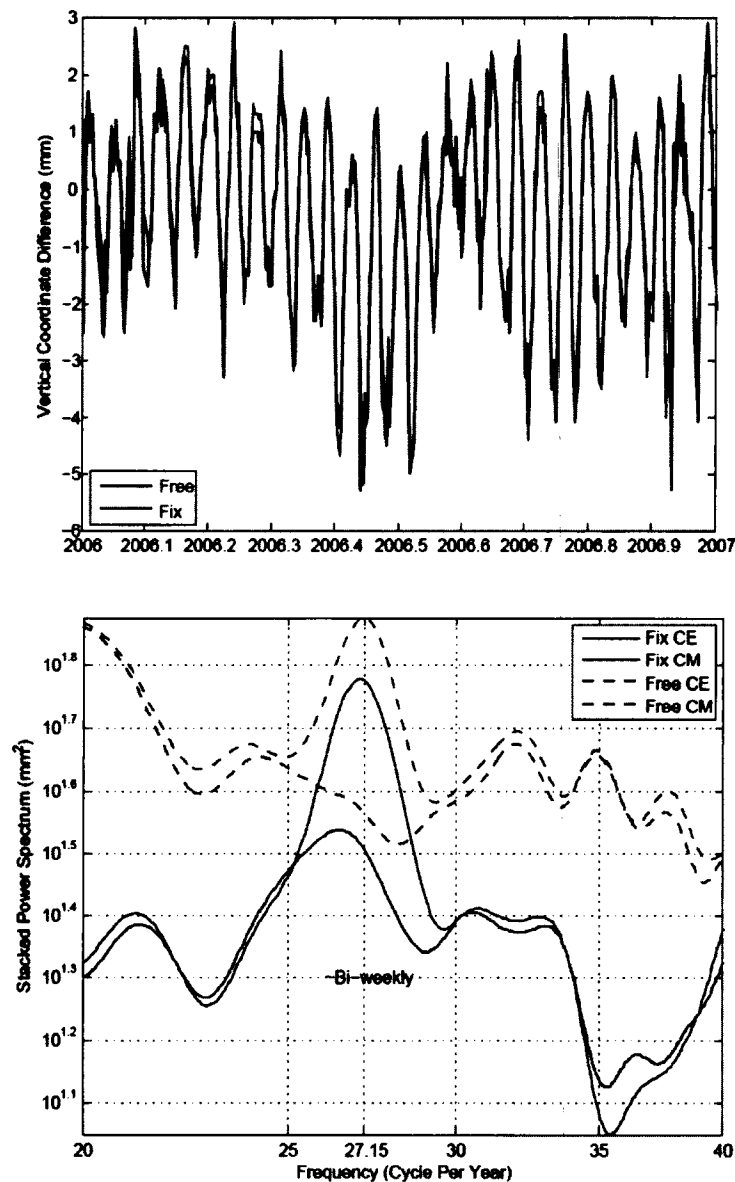


Figure 2.10: Comparison between ambiguity-fix and ambiguity-free solutions. Top: Vertical coordinate difference between solutions using OTL-CM and OTL-CE, for ambiguity-fix solutions (blue), and ambiguity-free solutions (red). Bottom: Stacked power spectra showing the ~ 14 -day period component from 1-year detrended vertical coordinate timeseries; Solid lines are ambiguity-fixed result; dash lines are the same as FES04CE_POS and FES04CM_POS in Figure 2.6, and for ambiguity-free solutions.

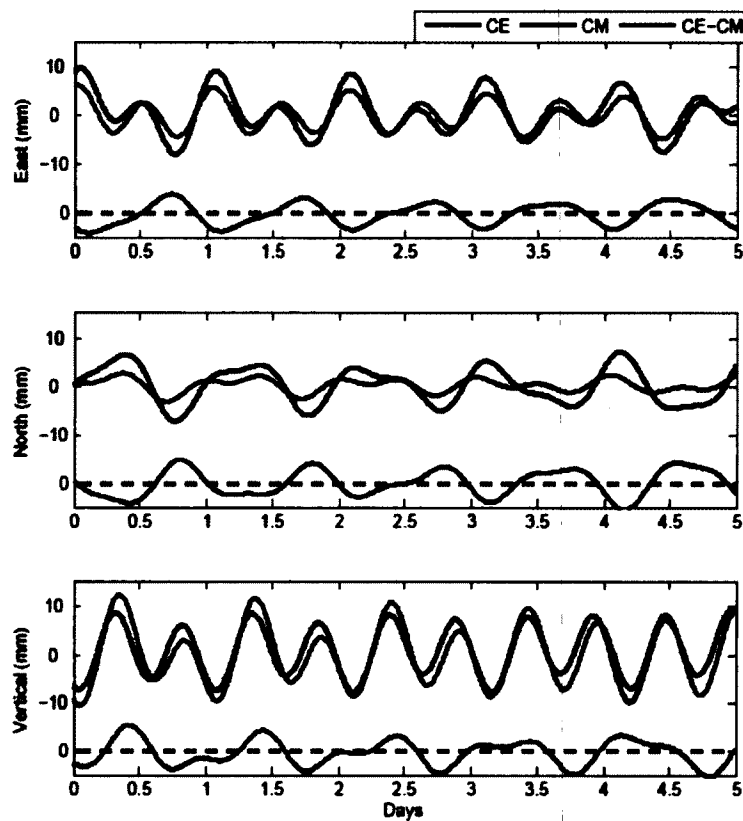


Figure 2.11: Predicted OTL displacement of station TIDB for the first 5 days of 2005. Displacements for OTL-CE (red) and OTL-CM (blue) were calculated from ocean tide model TPXO7.0 using the SPOTL program, using the appropriate CE or CM Green's functions. The difference (CE-CM) is also plotted with a green line at the bottom of figures for each component, and illustrates the time-dependent bias introduced into the GPS observation model when inconsistent OTL coefficients are used in a processing strategy with orbits and clocks fixed to values estimated in a separate solution.

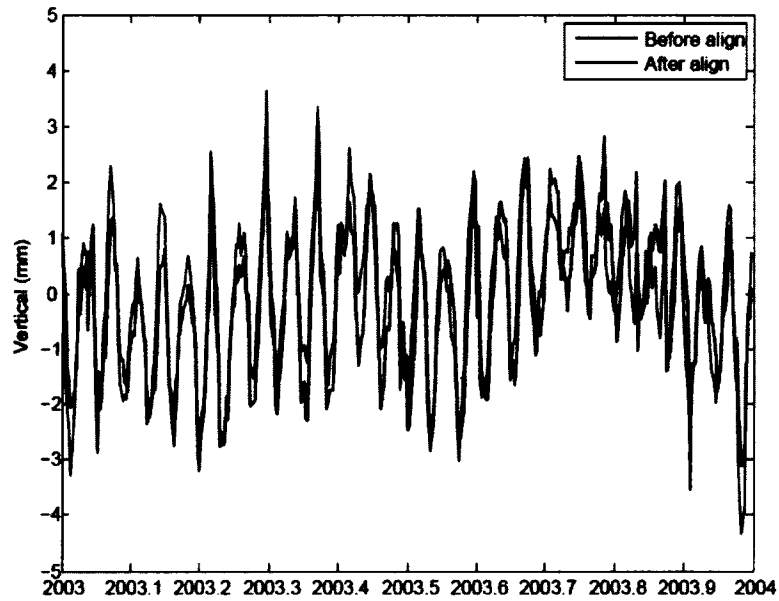


Figure 2.12: Comparison between solutions before and after aligning to ITRF. Vertical coordinate differences between solutions using OTL-CM and OTL-CE before aligning to ITRF2005 (red line), and after transforming to ITRF2005 (blue line), for station TIDB, for 2003. Most of the solution differences represent distortions of the network.

Chapter 3 Seasonal and Long-term Vertical Deformation in the Nepal Himalaya Constrained by GPS and GRACE Measurements¹

Abstract

We analyze continuous GPS measurements in Nepal, southern side of the Himalaya, and compare GPS results with GRACE observations in this area. We find both GPS and GRACE show significant seasonal variations. Further comparison indicates that the observed seasonal GPS height variation and GRACE-derived seasonal vertical displacement due to the changing hydrologic load exhibit very consistent results, for both amplitude and phase. For continuous GPS stations whose observation time span are longer than 3 years, the average WRMS reduction is ~45% when we subtract GRACE-derived vertical displacements from GPS observed timeseries. The comparison for annual amplitudes between GPS observed and GRACE-derived seasonal displacements also shows consistent correlation. The good seasonal correlation between GPS and GRACE is due to the improved GPS processing strategies and also because of the strong seasonal hydrological variations in Nepal. Besides the seasonal signal, GRACE also indicates a long-term mass loss in the Himalaya region, assuming no GIA effect. This mass loss therefore will lead to crustal uplift since the earth behaves as an elastic body. We model this effect and remove it from GPS observed vertical rates. With a 2D dislocation model, most GPS vertical rates, especially in the central part of Nepal, can be interpreted by interseismic strain from the Main Himalayan Thrust, and several exceptions may indicate the complexity of vertical motion in this region and some potential local effects.

3.1 Introduction

Seasonal hydrospheric mass movements cause periodic displacements of the lithosphere. Global Positioning System (GPS) coordinate variations, principally for the

¹Fu, Y., and J. T. Freymueller (2012), Seasonal and long-term vertical deformation in the Nepal Himalaya constrained by GPS and GRACE measurements, *J. Geophys. Res.*, 117, B03407, doi:10.1029/2011JB008925.

vertical component, have been used to investigate global (Blewitt et al., 2001; Dong et al., 2002; Wu et al., 2003) and local (Grapenthin et al., 2006) seasonal deformation modes, and the relationship between seasonal load and strain within active tectonic areas (Heki, 2001; Bettinelli et al., 2008). With the development of satellite gravimetry, especially the Gravity Recovery and Climate Experiment (GRACE), the time-variable gravity field and mass variation from the surface water and ice, can be quantitatively estimated (Chen et al., 2006; Luthcke et al., 2008; Bruinsma et al., 2010).

The GRACE-derived time-variable gravity field coefficients can be converted to harmonic coefficients for crustal deformation in three components, E, N, H (Kusche and Schrama, 2005; van Dam et al., 2007), which provides a way to quantitatively compare and correlate GRACE and GPS measurements. Van Dam et al., (2007) compared GPS observed heights over Europe with GRACE predicted heights, and found the annual signals for those two measurements did not show good agreement; this was thought to be due to spurious annual signals propagated during GPS processing. Khan et al., (2010) realized that the GRACE measurements in Greenland underestimated the uplifts for GPS stations, and attributed this difference to the varied spatial sensitivity of GPS and GRACE for changing loads. With better GPS processing strategies and improved correction models (atmosphere delay, atmosphere loading, etc) applied, considerable global agreement between GPS and GRACE has been observed in the regions where hydrologic seasonal effects are significant and local effects are small (Tregoning et al., 2009; Tesmer et al., 2011).

The Himalaya, as the planet's highest mountain range, was created by the collision between the Indian and Eurasian plates during the last 40 million years (Molnar and Tapponnier, 1975). It also contains one of the largest collections of glaciers outside the Arctic and Antarctic, with glacier coverage area of 34,600 km² (Thomas and Rai, 2005). Glaciers and snowpack in the Himalaya and Tibet feed the great Asian rivers and supply water to millions of people for living. Therefore the Himalaya and Tibet are called the "Water Tower of Asia" (Thomas and Rai, 2005). In addition, the seasonal hydrological cycle around the high mountains of the Himalaya is significant: during the summer

season from June through September, the high Himalaya range blocks the northward moisture-rich monsoon winds, so that moist air is raised in altitude and cooled down in temperature; this results in strong precipitation, especially on the southern side of the range. Additionally, the annual cycle of accumulation and melt of mountain snow and ice contributes to the seasonal hydrological variations.

In this study, we use two kinds of geodetic techniques, continuous GPS and GRACE, to study the seasonal mass change and its resulting vertical displacement in Nepal and southern Tibet. We also discuss the long-term mass loss revealed by GRACE measurements and its impacts on tectonic vertical rates evaluations.

3.2 Geodetic Measurements

3.2.1 Continuous GPS observations and data analysis

Caltech and other groups have installed ~30 continuous GPS stations in Nepal (Table 3.1), and some of them have continuous observations for more than one decade. These GPS data are publicly available through Caltech's Tectonics Observatory website and the UNAVCO archive. We used the GIPSY/OASIS II software (Version 5.0) to process the GPS data and estimate station coordinates for these stations and others in the surrounding area in point positioning mode. We adopted JPL's reanalysis orbit and clock products, which were determined using a consistent set of models over the entire time span, including absolute antenna phase center models for both GPS receiver and satellite antennas (Schmid et al., 2007). We used the GMF tropospheric mapping function (Boehm et al., 2006), and adopted a priori dry tropospheric delay estimates from the Global Pressure and Temperature (GPT) model (Boehm et al., 2007). Ocean tide loading effects were corrected using ocean tide model TPXO7.0 with Greens Functions modeled in the reference frame of CM (center of the mass of the whole Earth system) to maintain consistency with JPL's orbit/clock products and therefore avoid systematic errors (Fu et al., 2012). Non-tidal ocean variations and atmospheric loading are not removed in the

daily GPS analysis, and their effects remain in the GPS time series along with deformation due to other load variations that have periods > 1 day.

In order to remove the effects of atmospheric loading on the GPS coordinates, we computed the displacements due to atmospheric loading using data and programs developed by the GGFC (Global Geophysical Fluid Center) (van Dam 2010, <http://geophy.uni.lu/ncep-loading.html>), which utilized the NCEP (National Center of Environmental Protection) reanalysis surface pressure data set. The GRACE solutions adopted in this study have two different temporal resolutions: 10 days (GRGS) and a month (CSR, GFZ and JPL). We first derive the daily-averaged atmospheric loading, and then average those daily results into 10-day and monthly corrections and remove them from 10-day and monthly averaged GPS solutions.

3.2.2 GRACE models

We employed the second release of 10-day gravity fields models (RL02) derived by the Space Geodesy Research Group (GRGS), in France. Spherical harmonic coefficients up to degree and order 50 for the gravity field are provided every 10 days. The details of the GRACE data processing can be found in Bruinsma et al. (2010). No further smoothing or filtering is required for GRGS products, because they have been stabilized during their data analysis. Because LAGEOS observations are incorporated in the GRGS's gravity solutions, lower degrees, especially C20, are well constrained (Bruinsma et al., 2010). We replace the degree-1 components with results obtained by Swenson et al. (2008).

We also compared GRACE Level-2 RL-04 solutions from several other groups: CSR (Center for Space Research, Austin, USA), GFZ (GeoForschungsZentrum, Potsdam, Germany), and JPL (Jet Propulsion Laboratory, USA). For those monthly products, we replace C20 terms with the results from observations of Satellite Laser Ranging (Cheng and Tapley, 2004), and Degree-1 terms using Stokes coefficients derived by Swenson et al. (2008). For GRACE monthly solutions from CSR, GFZ and

JPL, we adopted 400 km as the averaging radius to implement Gaussian smoothing, which suppresses errors at high degrees (Wahr et al., 1998; van Dam et al., 2007).

3.2.3 Displacements due to the changing load

Displacement in height due to the changing mass load can be expressed in terms of spherical harmonic coefficients for the gravity field and load Love numbers (Kusche and Schrama, 2005; van Dam et al., 2007).

$$\Delta h(\theta, \phi) = R \sum_{l=1}^{\infty} \sum_{m=0}^l \bar{P}_{lm}(\cos \theta) \cdot [C_{lm} \cos(m\phi) + S_{lm} \sin(m\phi)] \frac{h'_l}{1 + k'_l} \quad (1)$$

in which R is the Earth radius; \bar{P}_{lm} are fully normalized Legendre functions for degree l and order m ; C_{lm} and S_{lm} are spherical harmonic coefficients of the gravity field, and h'_l and k'_l are Load Love numbers at degree l ; we adopt Load Love numbers provided by Farrell (1972), which are computed in the center of mass of solid earth frame. Similar equations can be used to compute the horizontal displacements (e.g., Kusche and Schrama (2005)).

We also tested loading computations with half space models, and spherical earth models using cylindrical loads, with a load history based on GRACE mascon solutions. We found both of these computational methods to be problematic. The spatial extent of the load was too large for a half space model, although the data could be fit well if the Young's modulus was increased as more distant loads were included in the computation. Using disk loads proved to be less computationally efficient than the Love number approach given that loads over a large region had to be considered.

3.3 Comparison between GPS and GRACE-derived seasonal height variations

Figure 3.1 shows the locations of continuous GPS stations in the Nepal Himalaya, and four example time series of daily solutions for GPS sites CHLM, GUMB, KKN4, DAMA. Besides the long-term linear trends, which are mainly dominated by tectonic processes, all GPS timeseries show significant seasonal variations. The peak-to-peak seasonal amplitude can be more than two centimeters, which reflects the strong seasonal

hydrological fluctuations in Nepal. Steckler et al. (2010) studied similar seasonal phenomenon in Bangladesh with hydrographic, GPS and GRACE data. The average peak-to-peak vertical seasonal displacement in Bangladesh (5~6 cm) are larger than those in Nepal (2~4 cm), due to the very large seasonal river loading in Bangladesh.

The vertical displacements are computed at the GPS sites from the GRACE-derived gravity field coefficients using equation (1), and four selected stations (CHLM, GUMB, DRCL, TIMP) are shown in Figure 3.2. CHLM and GUMB are the same sites whose GPS timeseries are shown in Fig. 1. DRCL and TIMP are two more distant sites selected for comparison. Solutions from GRGS, CSR, GFZ and JPL exhibit very similar and consistent results, although there are several obvious outliers in 2004 for the GFZ solutions. In addition to the remarkable seasonal oscillations, a general uplift trend is also predicted. In this computation, we assume that the secular change in the gravity field is due to present-day surface mass load changes (Matsuo and Heki, 2010), with no contribution from Glacial Isostatic Adjustment (GIA) or tectonic processes like crustal thickening (see section 3.5.2).

In Figure 3.3, we compare the 10-day averaged detrended GPS height timeseries and GRACE-derived seasonal (detrended) vertical deformation due to the load change. GRACE solutions from GRGS, CSR, GFZ, JPL are all shown together. Results for nine example stations are plotted in Figure 3.3, in which "SIMC" is a composite time series combining two sites SIMR and SIM4 located 136.84 meters apart. In all cases, there is a very close correspondence between the observed GPS and GRACE variations. To emphasize this, we choose a group of GPS stations based on the criteria that the observation span is longer than 3 years, and plot the stacked 10-day averaged GPS and GRACE-derived seasonal (detrended) vertical timeseries for these stations (Figure 3.4). The GPS and GRACE data clearly display very similar and consistent seasonal patterns for both magnitude and phase. For the remainder of this paper, we will use the average seasonal variations measured by GRACE, computed by fitting a model with a linear trend and annual and semi-annual periodic terms, for comparison to the seasonal variations observed by GPS. The seasonal variations should come from the same

physical cause (seasonal mass transport) for both height and gravity change, whereas the long-term trends of the two measurements are expected to differ because the trends from tectonics and GIA will in general be different for these two observables.

We adopted two measures to quantitatively compare the consistence between GPS and GRACE measurements. First, we remove GRACE-derived seasonal deformation from GPS observed detrended height timeseries, and compute the reductions of WRMS (weighted root mean squares) bases on the following equation (van Dam et al., 2007, Tregoning et al., 2009; Tesmer et al., 2011).

$$WRMS_{reduction} = \frac{WRMS_{GPS} - WRMS_{GPS-GRACE}}{WRMS_{GPS}} \quad (2)$$

We use this measure to quantitatively evaluate whether different GRACE solutions can be distinguished, and to identify which GRACE solution to employ for further discussion. We exclude the GFZ solution because of its clear outliers in 2004. For the GPS stations whose observation time is longer than 3 years, the average WRMS reductions for GRACE solutions from GRGS, CSR and JPL are 46.2%, 45.4%, 45.5%, respectively, which indicates that GRGS's GRACE solution is slightly more consistent with the GPS measurements; the difference between CSR and JPL is very small. WRMS reductions are substantial regardless of the GRACE solution used, reflecting nearly a factor of 2 reductions in WRMS. So we adopt the GRACE solution from GRGS in this paper because of its better agreements with GPS and also its better temporal resolution (10 days).

WRMS reductions are plotted for each station in Figure 3.5. All stations show significant and consistent WRMS reduction. The WRMS reduction is significantly larger than that observed for Europe by van Dam et al. (2007), because of the improved GPS processing strategies adopted in this study, and also because the seasonal variations in Nepal are much larger than those for western Europe.

The corrected time series include random measurement noise in addition to possible remaining systematic errors. We assess how much variation remains in the time series by

comparing the WRMS of the whole time series to the short-term WRMS based on days or weeks of data. Because the time series are also expected to include colored noise (Mao et al., 1999; Williams et al., 2004), this provides a conservative assessment of how close to the noise floor the corrected time series are. We quantify the short-term WRMS based on a short time period (1 week, or 2 weeks). Seasonal (annual and semiannual) effects are very small during such short period, so the expected WRMS mainly reflects the basic noise level without residual seasonal effects. A typical example, site CHLM, is shown in Figure 3.6. The WRMS of the whole timeseries (shown in Figure 3.1) for CHLM is 8.63 mm; the WRMS of the first week and first two weeks in 2010 are 2.91 mm and 3.10 mm, respectively; so for CHLM, the WRMS from short-term noise amounts to ~33% of the WRMS for the full timeseries. All other stations exhibit similar results. The average percentage for the selected group (observation time span longer than 3 years) is 29.56% for one-week period, and 31.55% for two-week period. After removing the GRACE seasonal model, the WRMS of the whole time series is reduced to ~53.8% of the original time series, which is only ~1.75 times larger than the short-term WRMS. On other words, after correcting the seasonal effects with GRACE data, the WRMS of GPS timeseries is reduced from ~3 times the short-term noise level to ~1.75 times the short-term noise level. The remaining noise in the corrected time series arises from a combination of longer-term correlated noise, errors in the seasonal hydrological corrections, and interannual variations in the load. Past studies on GPS coordinate noise (Mao et al., 1999; Williams et al., 2004) suggest that the GPS noise is a combination of white noise plus either flicker noise or a more general power law noise, and the coordinate uncertainty can be underestimated if the time-correlated noise is neglected.

Secondly, we also compare the annual amplitudes for both GPS and GRACE-derived seasonal displacements (Figure 3.7). For this comparison, we fit both the GPS and GRACE-derived deformation timeseries with linear, annual and semi-annual components, and then extract and compare the amplitudes of their annual components. If the measurements of GPS and GRACE perfectly match each other, then all the dots in Figure 3.7 should lie in the “slope = 1” line (blue dashed line in Figure

3.7). With the actual observed data and their uncertainties, we use the weighted total least squares method (Krystek and Anton, 2007) to derive the best fit line and its uncertainty (red dash-dot line in Figure 3.7), whose slope is $\sim 0.90 \pm 0.11$. Our best fit slope does not exclude a linear 1:1 relationship

3.4 Long-term uplift due to the mass loss

Besides the significant seasonal variations discussed above, there is also a long-term uplift contained in GRACE-derived vertical displacement (Figure 3.2), which is primarily due to the mass loss in the Himalaya (Matsuo and Heki, 2010), and potential GIA effects. Under the influence of climate change, snow and ice in the high mountains of the Himalaya is melting rapidly. Observations from both field records (Dyurgerov and Meier, 2005) and satellite gravimetry (GRACE) (Matsuo and Heki, 2010) have confirmed this rapid ice loss. Matsuo and Heki (2010) reported the average ice loss rate can reach $\sim 47\text{Gt/yr}$, equivalent to $\sim 0.13\text{mm/yr}$ global sea level rise.

The earth, behaving like an elastic body, uplifts in a response to the load loss. We compute the GRACE-derived long-term uplift using the trend from the GRGS solutions for all continuous GPS sites used in this paper (Figure 3.8, top). The results indicate an overall uplift for the whole region, at the $\sim 1\text{ mm/year}$ level. Then we remove this cryospheric-induced uplift from GPS actual observed vertical rates to derive the corrected vertical velocities (Figure 3.8, bottom), which can be compared to the predictions of models that were fit to the horizontal GPS velocities. Here we assume that GIA is negligible (see section 5.2). We use CATS, a timeseries analysis software package (Williams, 2008), to estimate the velocities and their uncertainties assuming a power-law noise model, and the results are included in Table 3.1 (column 6). The average spectral index for continuous GPS sites in Nepal is -0.42 , very similar to results from other regions. Zhang et al. (1997) found that the mean spectral index for GPS stations in southern California is about -0.4 .

3.5 Discussion

3.5.1 Tectonic interpretation for the corrected vertical rates, assuming no GIA effect

The tectonic process in Nepal Himalaya is dynamic and dominated by the strong convergence between the Indian and Eurasian plates. The underthrusting Indian lithosphere slides on the Main Himalayan Thrust (MHT) fault, which extends from a shallow depth under Nepal to the mid-crust under southern Tibet (Avouac 2003; Nábělek et al., 2009). During the interseismic period, the upper part of MHT is locked, and the lower part is creeping (Bettinelli et al., 2006). So the current observed GPS vertical rates (seasonal components removed) should be composed of both tectonic impact and the response of mass loss.

We model the vertical rates for continuous GPS stations based on previous studies of interseismic slip of the MHT (Jouanne et al., 1999; Jouanne et al., 2004; Bettinelli et al., 2006), using a 2-dimensional dislocation model (Singh and Rani, 1993). The parameters of the MHT and the comparison between modeled and observed vertical rates are given in Table 3.2 and in Figure 3.9. GPS stations in Nepal with long enough observation and uncertainty of vertical rate smaller than 0.85 mm/year are selected for this comparison. Most of the corrected vertical velocities, especially in the central part of Nepal, agree with the model predictions for interseismic strain from the MHT. However, there are several discrepancies in the western and eastern Nepal, which may reflect the lateral variation of the MHT and some local effects, such as groundwater extraction. Rodell et al. (2009) reports rapid groundwater extraction in India, and Nepal is also dependent on groundwater for irrigation (Shah et al., 2006). Studies indicate that withdrawal of groundwater produces localized subsidence, in which can be large relative to tectonic deformation (Bawden et al., 2001, Watson et al., 2002). Besides, the lateral variations of large earthquake occurred along the Himalayan arc (Bilham et al., 2001) may indicate different part of the arc is experiencing varied interseismic status.

In order to verify whether the goodness of fit of the interseismic slip model is improved after correction for the uplifts due to load decrease, we compare the theoretical results from interseismic slip model of Bettinelli et al. (2006) and vertical rates of continuous GPS, both before and after correction. We find that the overall weighted misfit decreases by 25.0% for all the stations in Figure 3.9; for western and central Nepal, the model goodness of fit is improved and the misfit decreases by 11.2% and 35.1%, respectively. But the misfit in eastern Nepal actually increases by 34.4%, although this is based on only 3 sites. Because of the small number of sites, it is not clear whether the increase in misfit is significant. If it is, it might be attributed to either the inaccuracy of interseismic model, like the lateral slip variation along the arc, or the actual long-term load decrease in eastern Nepal may be not as significant as western and central parts.

3.5.2 GIA and other effects

In this study, we have ignored possible effects of GIA, which can cause both gravity change and vertical motion. Whether there was a large ice sheet in the Himalaya and Tibet during the last glacier period is still debated (e.g., Derbyshire et al. (1991) and Kuhle (1998)). Kaufmann and Lambeck (1997), based on a maximum large ice sheet model, predicted that present vertical and horizontal extension rates in Tibet due to GIA could reach 7 mm/year and 2 mm/year. Kaufmann (2005) presented a similar model. However, even for these models with extremely large past ice masses, the predicted effects in Nepal are small, no more than 2 mm/yr uplift rate. GIA effects are most likely smaller than predicted by these models. Field study of glacier geology (Derbyshire et al., 1991) also indicates a smaller ice sheet model at the last glacier cycle, which would not produce significant present vertical displacement (Kaufmann and Lambeck, 1997). In addition, GPS and absolute gravity surveys in southern and southeast Tibet (Sun et al., 2009) also do not observe the uplift and gravity changes that the GIA model (Kaufmann, 2005) predicts. Regardless of the ice model, GIA effects on the present gravity change should not be significant in Nepal, so we neglect them for our study here.

Matsuo and Heki (2010) argued that the tectonic uplift of Tibetan Plateau is too slow to seriously interrupt the isostatic equilibrium process, and thus would have only a small effect for the gravity change. The GRACE-derived negative gravity change (Fig. 3 of Matsuo and Heki 2010, in terms of equivalent water height) is clearly located in the high mountain areas, and there is no obvious isostatic effect over the entire plateau. So the long-term gravity change related to tectonic isostatic equilibrium should be small relative to cryospheric effect, and probably contributes negligibly to the current GRACE observations. Therefore we assume the long-term gravity change revealed by GRACE data is mainly because the mass loss in the study area, and ignore the tectonic impacts on gravity change. This assumption is realistic because the cryosphere-induced gravity change in the Himalaya is much more rapid and significant.

3.5.3 Seasonal variations in horizontal displacements

Bettinelli et al. (2008) found seasonal variations in GPS north displacement in Nepal Himalaya, and interpreted it as due to the lithospheric response to hydrological load variation. They also demonstrated a correlation between seasonal seismicity variation and seasonal strain change produced by surface hydrological load.

Here we also calculate GRACE-derived horizontal deformation, and compare it with the GPS measurements. The GRACE solution from GRGS is used here. Figure 3.10 shows an example (site KKN4) of the comparison between GPS observed and GRACE-derived horizontal displacements (left), and also the stacked detrended horizontal timeseries (right) using the same sites as Figure 3.4. The magnitude of GRACE seasonal variation in north is about 2~3 times of that in east. GPS and GRACE clearly show significant and consistent seasonal variations in the north component, and the average WRMS reduction in north is ~32.6%. The correlation between GPS and GRACE in the east component is weak, with the average WRMS reduction only ~2.3%. This mainly reflects to the lower signal to noise ratio for the east component. The correlation between GPS and GRACE in the north component further confirms that the

seasonal signal in GPS is caused by the hydrological load in Nepal Himalaya, which has been mainly analyzed and discussed in terms of vertical deformation in this paper.

3.5.4 Removing hydrological loading deformation from GPS measurements using GRACE data

In our study, we have tried to model seasonal and long-term deformation due to hydrological effects based on GRACE observations, and compare that with the observed GPS height variation. In addition, we also attempt to remove GRACE-derived hydrological vertical rates from GPS measurements. Using this method, we manage to separate tectonic and hydrological effects, both of which contribute to the vertical velocity field. The good seasonal correlation between GPS and GRACE signals indicates that the long-term uplifts revealed by GRACE measurements are probably true and mixed in the GPS measurements.

Due to a warming climate, the cryosphere is experiencing considerable mass loss globally. Large surface mass movements cause the elastic earth to deform, and this hydrology-induced deformation is superposed with other phenomena, mainly tectonics. In this paper, we present a way to remove this hydrological effect using GRACE measurements. This method can be applied for other similar purposes. For example, seasonal variations for campaign GPS measurements usually can not be well constrained because of their limited observations, mostly once per year. GRACE has continuous measurements since its launch in March 2002, and can provide detailed seasonal variation for gravity field and its resulting seasonal displacement due to load changes. Therefore, in order to achieve better linear velocities for continuous or campaign GPS sites, GRACE-derived seasonal variations for vertical deformation can be used to correct seasonal influences on the GPS time series. We choose the continuous GPS station CHLM for example. In Figure 3.11, we compare the results for all three components: East, North, and Height. In each component, the upper timeseries (blue) is the original observation, and the lower (red) is the corrected timeseries with seasonal effects removed using GRACE-derived seasonal variations. The misfit (χ^2 divided by degrees of freedom)

between data and a linear fit decreases by 32% (from 7.13 to 4.85) in height, by 42% (from 13.24 to 7.63) in north; and there is almost no decrease in east (from 7.77 to 7.66). The north component of the corrected time series shows some residual in-phase variations, which suggests that the GRACE-based load correction was too small. This could happen due to smoothing in the GRACE solution if the wavelength of the load is smaller than the smoothing length scale used in the GRACE solution. Although the example shown here is for a continuous site, the good results in height and north indicate that our method also can be employed for GPS campaign measurements. We have tested this for campaign sites with long measurement histories in the Himalaya and Tibet, and in many cases the WRMS reduction for campaign sites is ~50% in height, for sites where measurements were carried out at different times of year.

3.6 Conclusions

We combine GPS and GRACE measurements to study vertical motions in the Nepal Himalaya. Both GPS and GRACE observe strong seasonal variations. We utilize GRACE data to model the resulting vertical displacements due to the changing hydrological loads. Quantitative comparisons between the observed GPS seasonal vertical deformation and GRACE-derived seasonal deformation demonstrate that a consistent physical mechanism is responsible for the correlation between these two kinds of geodetic measurements. Besides the significant seasonal signal, GRACE also exhibits a long-term mass loss in this region, which is principally due to the melting ice and snow in high mountains of the Himalaya. We calculate the consequent uplift caused by the load decrease, and remove this hydrological effect from observed GPS vertical rates. The residual vertical rates are mainly dominated by tectonic deformation due to the earthquake cycle in the thrusting. We then employ a 2-D dislocation model to compute the tectonic vertical rates based on previous studies; those studies estimated fault models from the GPS horizontal velocities. Comparison between observed and modeled vertical rates suggests that the interseismic slip of MHT is able to explain the most of the vertical motion of most GPS stations, although the whole arc shows some lateral variations.

Correction for the long-term uplift predicted by the GRACE data improves the agreement between GPS vertical rates and the models based on horizontal data. The GPS vertical velocities are still too noisy to discriminate between the different horizontal slip models, but they may contribute to the estimation of models based on 3D velocities once loading effects are removed.

Acknowledgements

The authors gratefully appreciate Jean-Philippe Avouac and his group at Caltech Tectonics Observatory for establishing and maintaining the GPS stations in Nepal, and for making the data available to the public. The two stations in Bhutan were set up and operated by the Geological Survey of Bhutan (Dowchu Dukpa) and the Royal Bhutan Institute of Technology (G. Prasad Babu) in collaboration with Roger Bilham of the University of Colorado. This study could not have been done without their work and their generous sharing of the data with the public. We also thank the GRGS, CSR, GFZ and JPL teams for their online accessible GRACE solutions. Kosuke Heki and an anonymous reviewer provided helpful comments and suggestions that improve the manuscript. Discussions with Anthony Arendt and Ronni Grapenthin (Geophysical Institute, UAF), Lin Liu (Stanford University) and Jin Li (Shanghai Astronomical Observatory) also help this study. This work is supported by NSF grant EAR-0911677.

References

- Avouac, J. P. (2003), Mountain building, erosion, and the seismic cycle in the Nepal Himalaya. *Adv. Geophys.*, 46.
- Bawden, G. W., W. Thatcher, R. S. Stein, C. Wicks, K. Hudnut, and G. Peltzer (2001), Tectonic contraction across Los Angeles after removal of groundwater pumping effects, *Nature*, 412, 812– 815, 2001.
- Bettinelli, P., J.-P. Avouac, M. Flouzat, F. Jouanne, L. Bollinger, P. Wills, G. R. Chitrakar (2006), Plate motion of India and interseismic strain in the Nepal Himalaya from GPS and DORIS measurements, *J Geod*, 80: 567-589, DOI 10.1007/s00190-006-0030-3.
- Bettinelli, P., J.-P. Avouac, M. Flouzat, L. Bollinger, G. Ramillien, S. Rajaure, and S. Sapkota (2008), Seasonal variations of seismicity and geodetic strain in the Himalaya induced by surface hydrology, *Earth Planet. Sci. Lett.*, 266, 332–344.
- Bilham, R., V. K. Gaur and P. Molnar (2001), Himalayan Seismic Hazard, *Science*, 293, 1442- 1444.
- Blewitt, G., D. Lavallée, P. Clarke, and K. Nurudinov (2001), A new global model of Earth deformation: Seasonal cycle detected, *Science*, 294, 2342–2345.
- Boehm J, A. Niell, P. Tregoning, H. Schuh (2006) Global Mapping Function (GMF): A new empirical mapping function based on numerical weather model data. *Geophys Res Lett* 33, L07304, doi:10.1029/2005GL025546.
- Boehm J, R. Heinkelmann, H. Schuh (2007) Short Note: A global model of pressure and temperature for geodetic applications. *J Geod*, doi:10.1007/s00190-007-0135-3.
- Bruinsma, S., J. Lemoine, R. Biancale and N. Vales (2010), CNES/GRGS 10-day gravity field models (release 2) and their evaluation. *Advances in Space Research*, 45, 587-601.
- Chen, J. L., C. R. Wilson, and B. D. Tapley (2006), Satellite gravity measurements confirm accelerated melting of Greenland Ice Sheet, *Science*, 313, 1958–1960 doi:10.1126/science.1129007.

- Cheng, M., and B. D. Tapley (2004), Variations in the Earth's oblateness during the past 28 years, *J. Geophys. Res.*, 109, B09402, doi:10.1029/2004JB003028.
- Derbyshire, E., Y. Shi, J. Li, B. Zheng, S. Li, J. Wang (1991), Quaternary glaciation of Tibet: the geological evidence, *Quat. Sci. Rev.* 10, 485-510.
- Dong, D., P. Fang, Y. Bock, M. K. Cheng, and S. Miyazaki (2002), Anatomy of apparent seasonal variations from GPS-derived site position time series, *J. Geophys. Res.*, 107(B4), 2075, doi:10.1029/2001JB000573.
- Dyrgerov, M. and M. F. Meier (2005), *Glaciers and the Changing Earth System: A 2004 Snapshot. Occasional Paper 58*, Institute of Arctic and Alpine Research, University of Colorado, Boulder, p. 118.
- Farrell W. E. (1972), Deformation of the Earth by surface loads. *Rev Geophys*, 10, 761-797.
- Fu, Y., J. T. Freymueller, and T. van Dam (2012), The effect of using inconsistent ocean tidal loading models on GPS coordinate solutions, *J. Geod.*, 86(6), 409-421, doi:10.1007/s00190-011-0528-1.
- Grapenthin, R., F. Sigmundsson, H. Geirsson, T. Árnadóttir, and V. Pínel (2006), Icelandic rhythmicity: Annual modulation of land elevation and plate spreading by snow load, *Geophys. Res. Lett.*, 33, L24305, doi:10.1029/2006GL028081.
- Heki, K. (2001), Seasonal modulation of interseismic strain buildup in north-eastern Japan driven by snow loads, *Science*, 293(5527), 89-92.
- Jouanne F, J. L. Mugnier, M. R. Pandey, J. F. Gamond, P. Le Fort, L. Serrurier, C. Vigny, J. P. Avouac, IDYL-HIM members. (1999) Oblique convergence in Himalaya of western Nepal deduced from preliminary results of GPS measurements. *Geophys Res Lett* 26(13):1933-1936.
- Jouanne F, J. L. Mugnier, J. F. Gamond, P. Le Fort, M. R. Pandey, L. Bollinger, M. Flouzat, J. P. Avouac (2004) Current shortening across the Himalayas of Nepal. *Geophys J Int* 157(1):1-14, DOI: 10.1111/j.1365-246X.2004.02180.x.

- Kaufmann, G. and K. Lambeck (1997), Implications of Late Pleistocene glaciation of the Tibetan Plateau for present-day uplift rates and gravity anomalies, *Quaternary Research*, 48 (3) (1997), 267–279.
- Kaufmann, G. (2005), Geodetic signatures of a Late Pleistocene Tibetan ice sheet. *J. Geodyn.* 39, 111C125.
- Khan, S. A., J. Wahr, M. Bevis, I. Velicogna, and E. Kendrick (2010), Spread of ice mass loss into northwest Greenland observed by GRACE and GPS, *Geophys. Res. Lett.*, 37, L06501, doi:10.1029/2010GL042460.
- Krystek, M. and M. Anton (2007), A weighted total least-squares algorithm for fitting a straight line, *Meas. Sci. Technol.*, 18, 3438-3442.
- Kuhle, M. (1998), Reconstruction of the 2.4 million km² late Pleistocene ice sheet on the Tibetan Plateau and its impact on the global climate, *Quaternary International*, 45/46, 71-108.
- Kusche, J., and E. J. O. Schrama (2005), Surface mass redistribution inversion from global GPS deformation and Gravity Recovery and Climate Experiment (GRACE) gravity data, *J. Geophys. Res.*, 110, B09409, doi:10.1029/2004JB003556.
- Lavé, J. and J. P. Avouac (2001), Fluvial incision and tectonic uplift across the Himalayas of central Nepal, *J. Geophys. Res.*, 106, B11, 26,561-26,591.
- Luthcke S. B., A. A. Arendt, D. D. Rowlands, J. J. McCarthy, C. F. Larsen (2008), Recent glacier mass changes in the Gulf of Alaska region from GRACE mascon solutions, *Journal of Glaciology*, 54(188), 767-777.
- Mao, A., C. G. A. Harrison, and T. H. Dixon (1999), Noise in GPS coordinate time series, *J. Geophys. Res.*, 104, 2797– 2816.
- Matsuo, K. and K. Heki (2010), Time-variable ice loss in Asian high mountains from satellite gravimetry, *Earth Planet. Sci. Lett.*, 290, 30-36.
- Molnar, P., and P. Tapponier (1975), Cenozoic tectonics of Asia: Effects of a continental collision, *Science*, 189, 419-426.

- Nábělek, J., G. Hetényi, J. Vergne, S. Sapkota, B. Kafle, M. Jiang, H. Su, J. Chen, B. Huang and the Hi-CLIMB Team (2009), Underplating in the Himalaya-Tibet Collision Zone Revealed by the Hi-CLIMB Experiment, *Science*, 325 1371-1374.
- Rodell, M., I. Velicogna, J.S. Famiglietti (2009), Satellite-based estimates of groundwater depletion in India. *Nature* 460, 999–1002.
- Schmid R, P. Steigenberger, G. Gendt, M. Ge, M. Rothacher (2007) Generation of a consistent absolute phase center correction model for GPS receiver and satellite antennas. *J Geod* 81(12), 781-798, DOI: 10.1007/s00190-007-0418-y.
- Shah, T., O. P. Singh and A. Mukherji (2006), Some aspects of South Asia's groundwater irrigation economy: analyses from a survey in India, Pakistan, Nepal Terai and Bangladesh, *Hydrogeology Journal*, 14, 286-309.
- Singh S. J, S. Rani (1993) Crustal deformation associated with two dimensional thrust faulting. *J Phys Earth* 41(2) 87–101.
- Steckler, M. S., S. L. Nooner, S. H. Akhter, S. K. Chowdhury, S. Bettadpur, L. Seeber, and M. G. Kogan (2010), Modeling Earth deformation from monsoonal flooding in Bangladesh using hydrographic, GPS, and Gravity Recovery and Climate Experiment (GRACE) data, *J. Geophys. Res.*, 115, B08407, doi:10.1029/2009JB007018.
- Sun, W., Q. Wang, H. Li, Y. Wang, S. Okubo, D. Shao, D. Liu, and G. Fu (2009), Gravity and GPS measurements reveal mass loss beneath the Tibetan Plateau: Geodetic evidence of increasing crustal thickness, *Geophys. Res. Lett.*, 36, L02303, doi:10.1029/2008GL036512.
- Swenson, S., D. Chambers, and J. Wahr (2008), Estimating geocenter variations from a combination of GRACE and ocean model output, *J. Geophys. Res.*, 113, B08410, doi:10.1029/2007JB005338.
- Tesmer V., P. Steigenberger, T. van Dam, T. Mayer-Gürr (2011), Vertical deformations from homogeneously processed GRACE and global GPS long-term series, *J Geod*, DOI 10.1007/s00190-010-0437-8.

- Thomas J., S. C. Rai. (2005), An overview of glaciers, glacier retreat, and subsequent impacts in Nepal, India and China. WWF Nepal Program. March, 2005: 70 pp.
- Tregoning, P., C. Watson, G. Ramillien, H. McQueen, and J. Zhang (2009), Detecting hydrologic deformation using GRACE and GPS, *Geophys. Res. Lett.*, 36, L15401, doi:10.1029/2009GL038718.
- van Dam, T., J. Wahr, and D. Lavallée (2007), A comparison of annual vertical crustal displacements from GPS and Gravity Recovery and Climate Experiment (GRACE) over Europe, *J. Geophys. Res.*, 112, B03404, doi:10.1029/2006JB004335.
- van Dam, T. (2010), NCEP Derived 6-hourly, global surface displacements at 2.5 x 2.5 degree spacing, <http://geophy.uni.lu/ncep-loading.html>.
- Wahr, J., M. Molenaar, and F. Bryan (1998), Time variability of the Earth's gravity field: Hydrological and oceanic effects and their possible detection using GRACE, *J. Geophys. Res.*, 103, 30,205–30,229.
- Watson, K. M., Y. Bock, and D. T. Sandwell (2002), Satellite Interferometric observations of displacements associated with seasonal groundwater in the Los Angeles basin, *J. Geophys. Res.*, 107(B4), 2074, doi:10.1029/2001JB000470.
- Williams, S. D. P., Y. Bock, P. Fang, P. Jamason, R. M. Nikolaidis, L. Prawirodirdjo, M. Miller, and D. J. Johnson (2004), Error analysis of continuous GPS position time series, *J. Geophys. Res.*, 109, B03412, doi:10.1029/2003JB002741.
- Williams, S. D. P. (2008), CATS: GPS coordinate time series analysis software, *GPS Solutions*, 12(2), 147–153, doi:10.1007/s10291-007-0086-4.
- Wu, X., M. B. Heflin, E. R. Ivins, D. F. Argus, and F. H. Webb (2003), Large-scale global surface mass variations inferred from GPS measurements of load-induced deformation, *Geophys. Res. Lett.*, 30(14), 1742, doi:10.1029/2003GL017546.
- Zhang, J., Y. Bock, H. Johnson, P. Fang, S. Williams, J. Genrich, S. Wdowinski, and J. Behr (1997), Southern California Permanent GPS Geodetic Array: Error analysis of daily position estimates and site velocities, *J. Geophys. Res.*, 102(B8), 18,035–18,055.

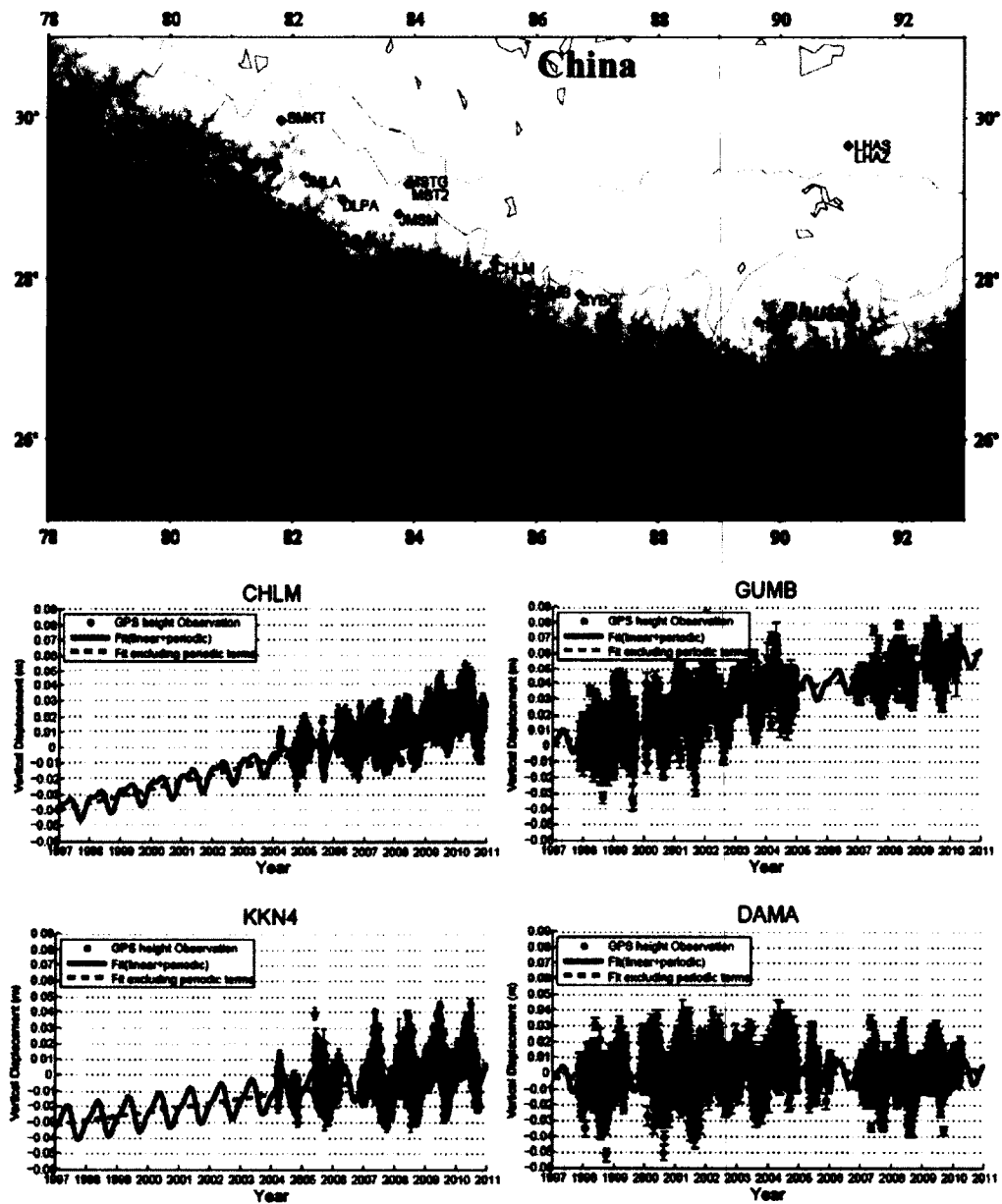


Figure 3.1: Locations of continuous GPS stations in Nepal, and example timeseries for sites CHLM, GUMB, KKN4 and DAMA (red diamonds in the location map). GUMB and DAMA have longer observational time than CHLM and KKN4.

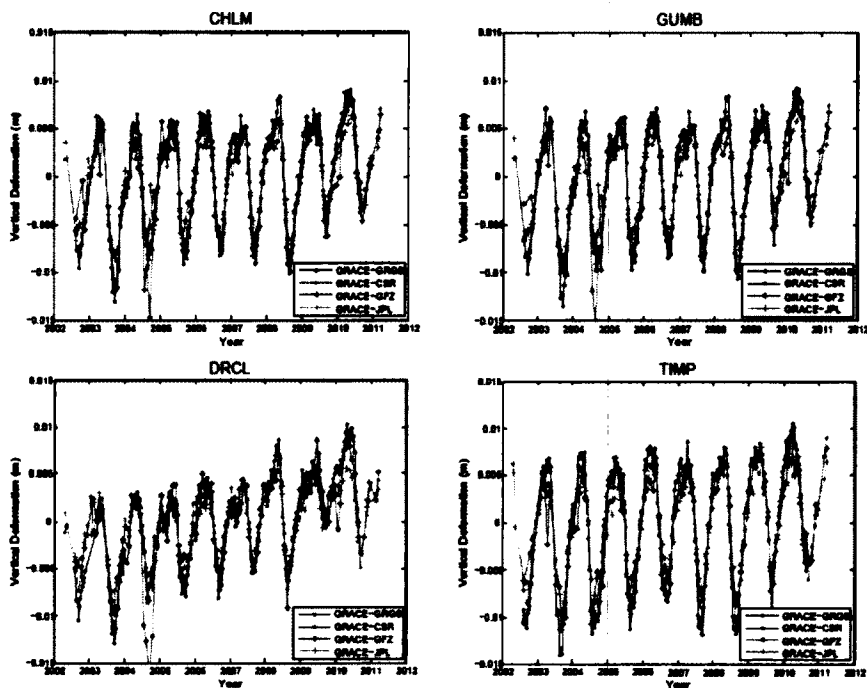


Figure 3.2: GRACE-derived vertical displacement time series due to the changing load calculated for four GPS stations, CHLM, GUMB, DRCL, TIMP. CHLM and GUMB are the same sites as shown in Figure 3.1. DRCL and TIMP are two more distant sites chosen for comparison. Results from different GRACE solution providers (GRGS, CSR, GFZ and JPL) are all presented.

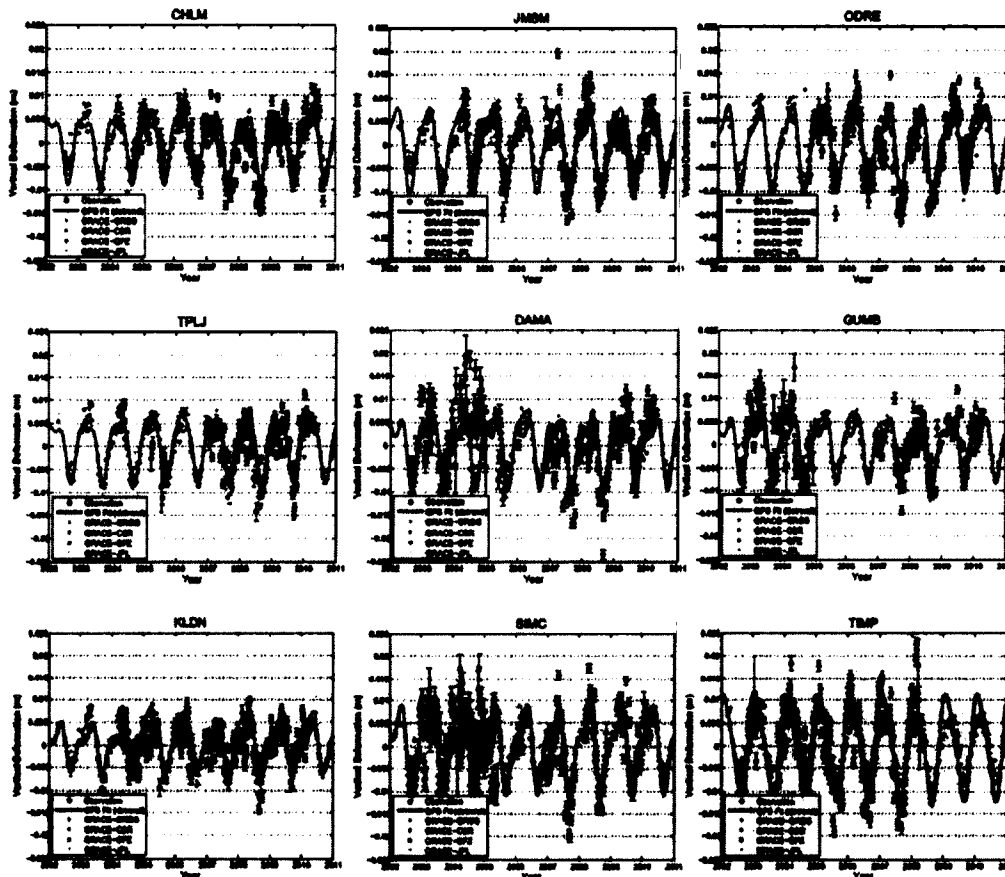


Figure 3.3: Comparison between 10-day averaged GPS detrended heights and GRACE-derived detrended seasonal vertical displacements. Red dots with error bar: 10-day averaged GPS observed detrended vertical deformation. Solid line: best fit (annual plus semi-annual components) for GPS detrended timeseries; GRACE solutions from four data centers are demonstrated with different colors. “SIMC” is a composite timeseries combining SIMR and SIM4.

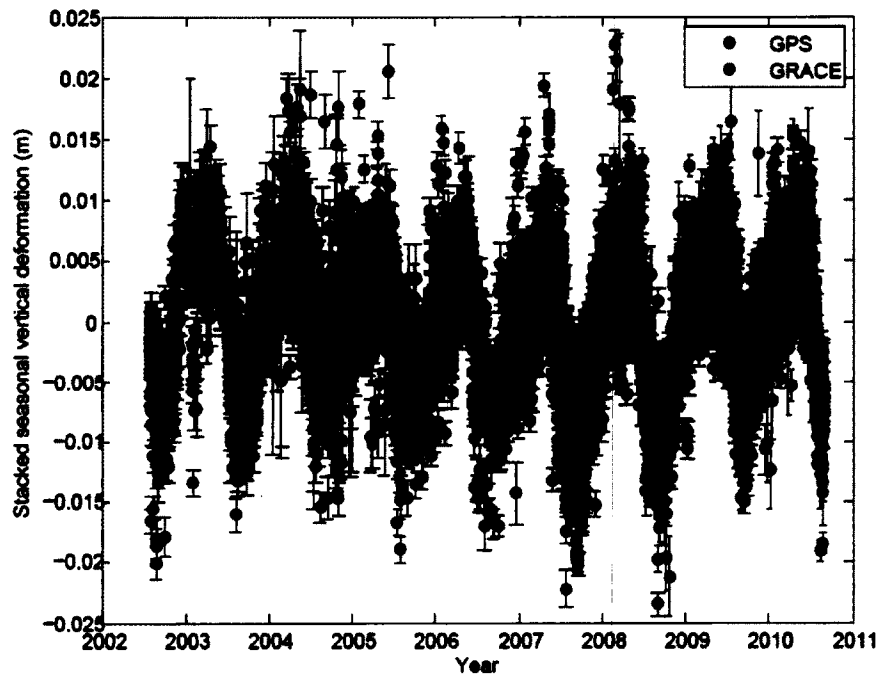


Figure 3.4: Stacked 10-day averaged GPS seasonal (detrended) vertical timeseries and GRACE-derived seasonal vertical timeseries, for the sites with data spans > 3 years (see Table 3.1).

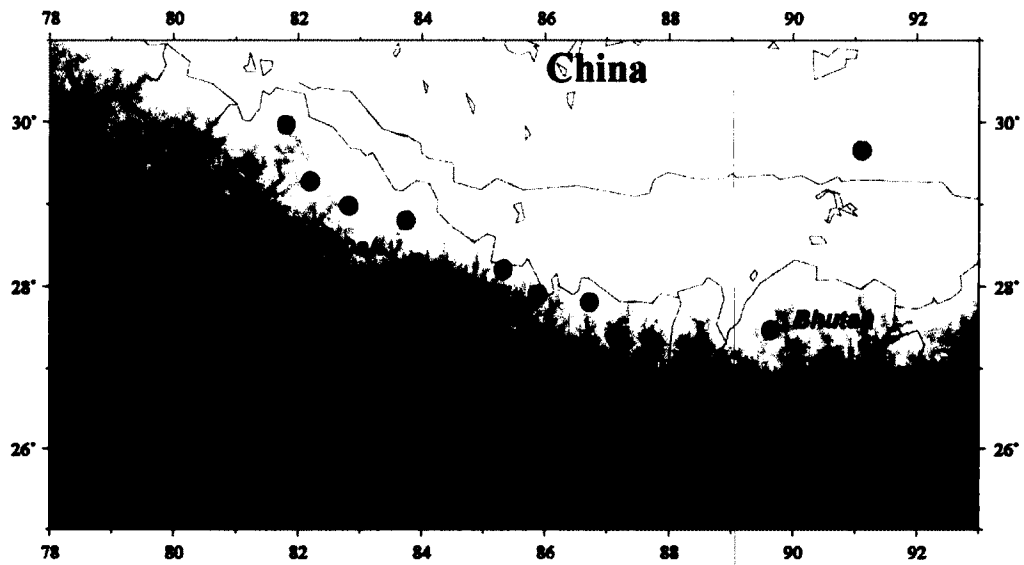


Figure 3.5: WRMS reductions for GPS detrended heights after removing GRACE-derived detrended displacements.

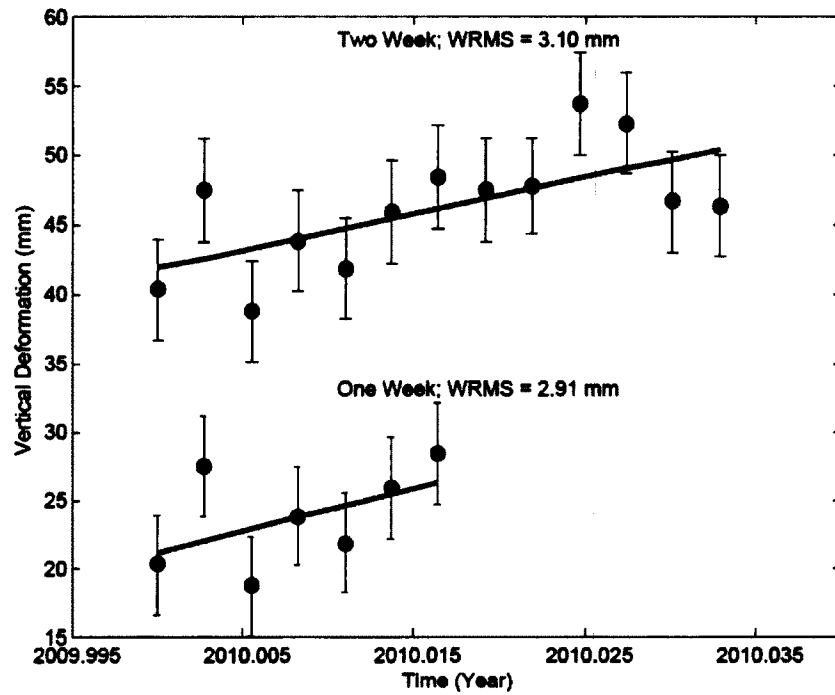


Figure 3.6: Short-term WRMS of station CHLM, computed based on data from the first week of 2010 (blue) and the first two weeks of 2010 (red), respectively.

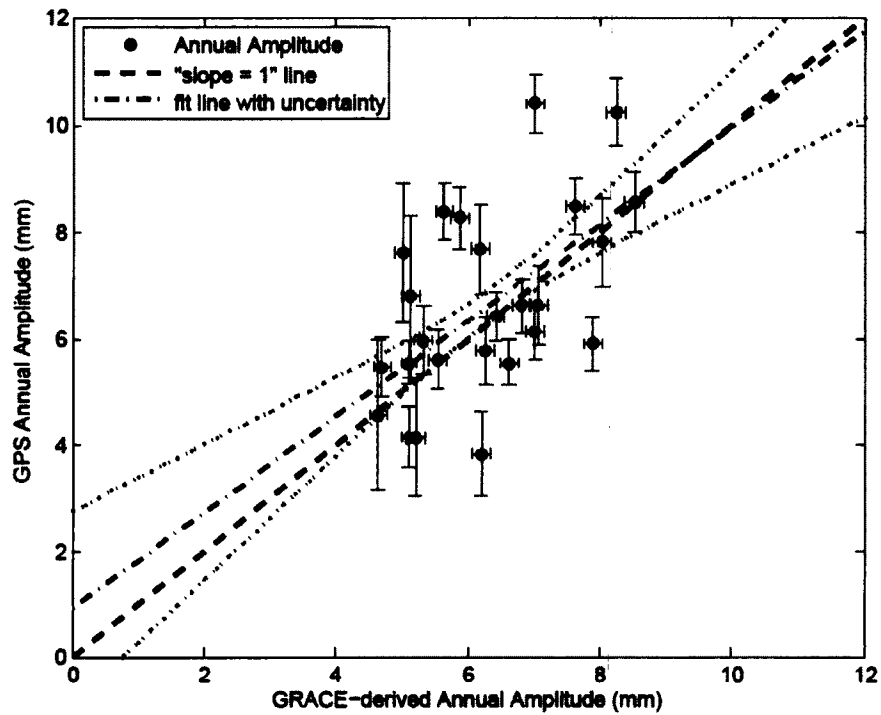


Figure 3.7: Comparison of annual amplitude between GPS observed heights and GRACE-derived vertical displacements. “Slope = 1” line (blue dashed) represents the ideal case in which GPS and GRACE perfectly match each other. The best fit line and its uncertainty (red dash-dot line) is derived using a weighted total least squares method with the actual measurements.

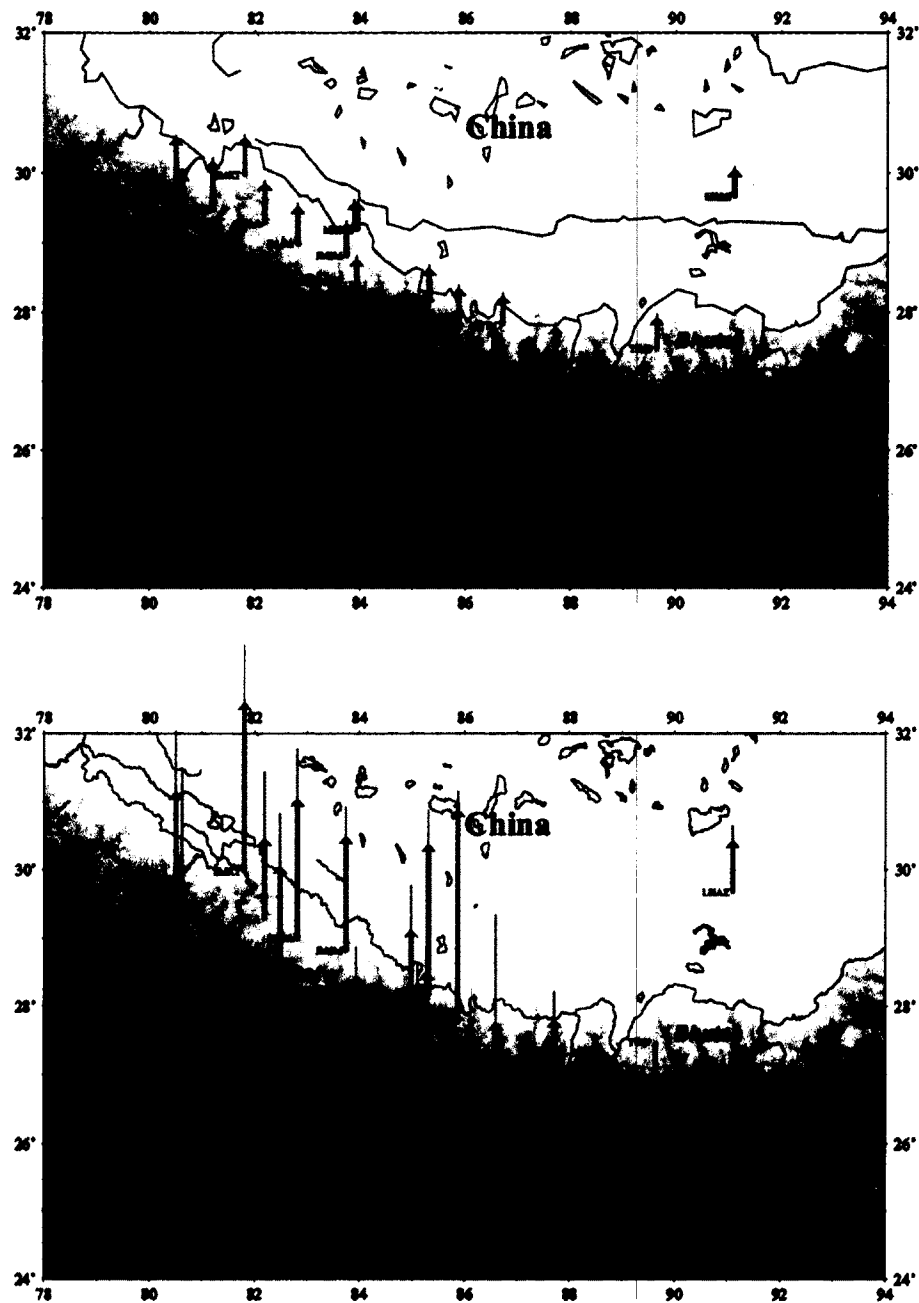


Figure 3.8: Vertical velocity field in Nepal Himalaya. Top: GRACE-derived long-term uplift rates because of the mass loss in the Himalaya area. Bottom: corrected vertical velocities after subtracting the GRACE-derived long-term uplift rate due to load changes; the brown lines indicate the frontal faults of the Main Himalayan Thrust fault system from Lavé and Avouac (2001).

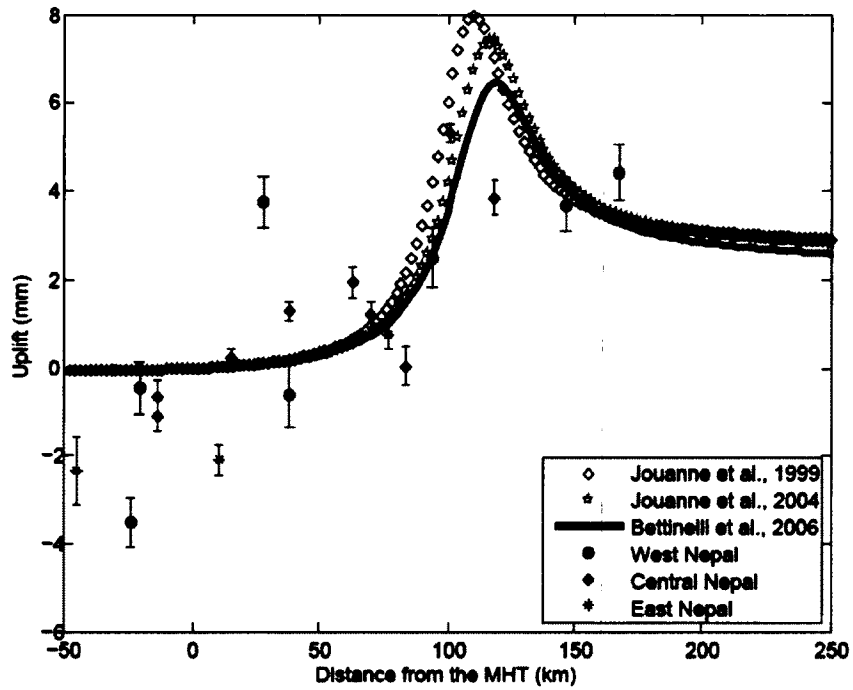


Figure 3.9: Comparison between GPS observed and modeled vertical rates in Nepal. Dots with error bar: corrected GPS height rates with GRACE-derived long-term uplift removed. Continuous line and blue symbols: modeled vertical rates based on previous studies that used horizontal GPS velocities.

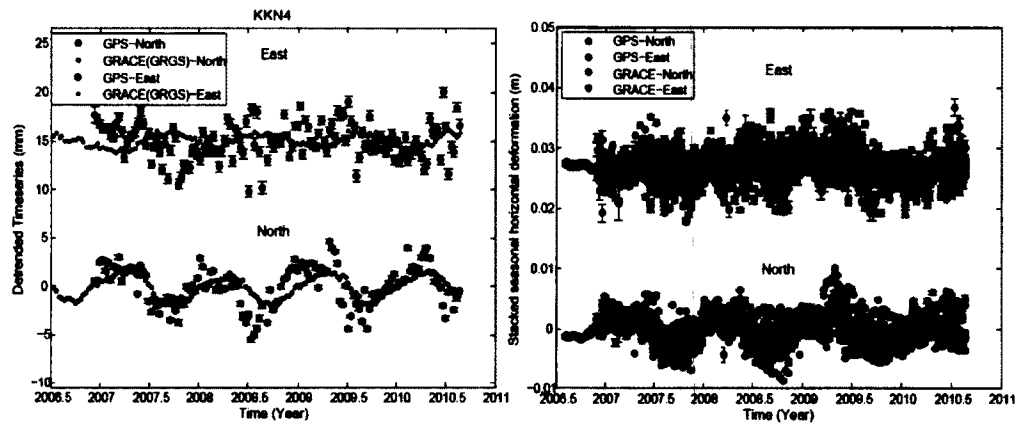


Figure 3.10: Comparison between GPS-observed and GRACE-derived horizontal seasonal displacements. Left: Comparison between GPS observed and GRACE-derived horizontal seasonal (detrended) displacements for site KKN4. Right: Stacked GPS seasonal (detrended) horizontal timeseries and GRACE-derived seasonal horizontal timeseries, for the same sites as Figure 3.4.

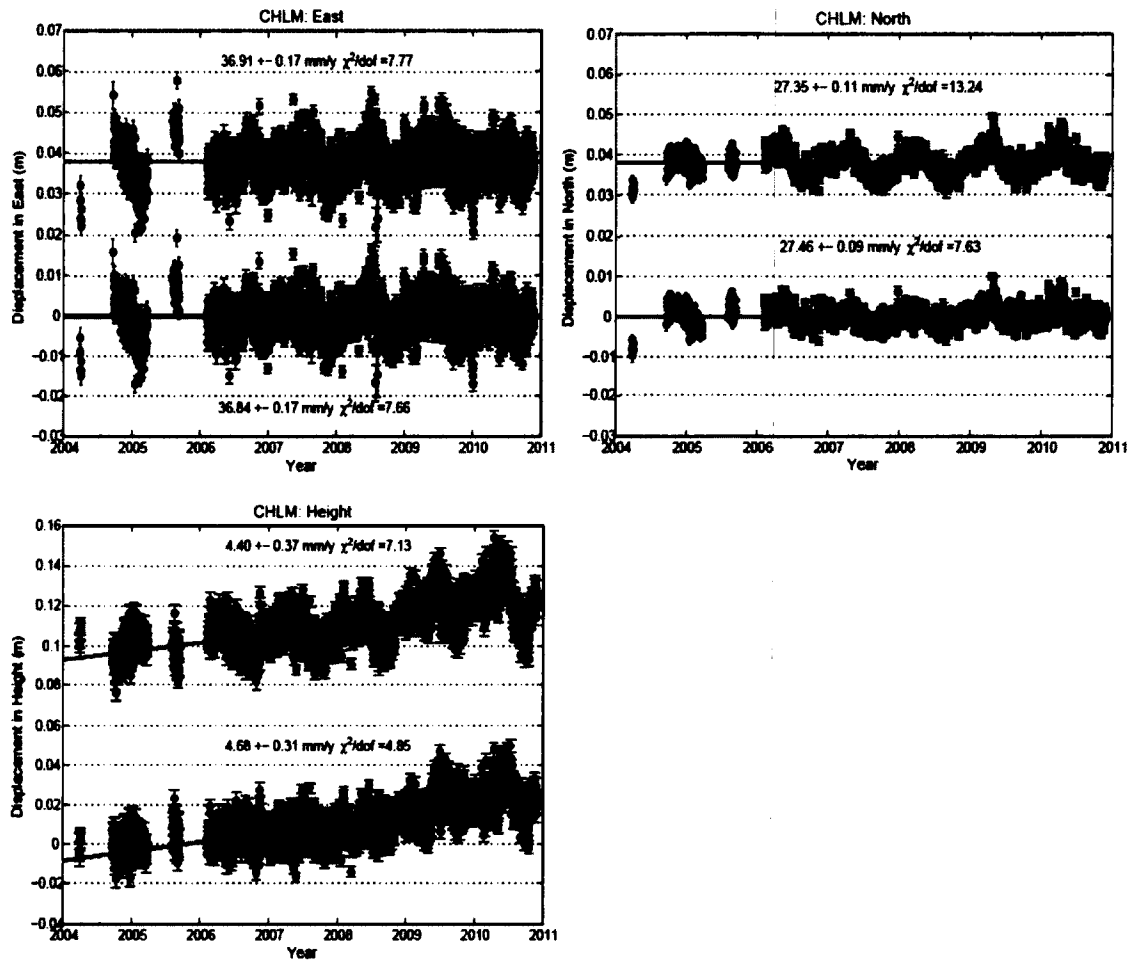


Figure 3.11: Comparison of linear fit between actual GPS observed timeseries (blue) and corrected timeseries (red) with seasonal effects removed, based on GRACE-derived seasonal variations. In order to better show the seasonal variations, we plot the detrended timeseries for the horizontal components; the horizontal velocities in ITRF2008 are given.

Table 3.1: Information of continuous GPS stations in Nepal Himalaya.

| Station | Latitude | Longitude | Observation time | WRMS Reduction in Height/North/East (%) | GPS Vertical Rates (mm/y) | GRACE -derived uplift (mm/y) |
|---------|----------|-----------|------------------|--|---------------------------------|---------------------------------------|
| BMCL* | 28.65 | 81.71 | 2007.21-2010.93 | 35.91/40.38/-4.16 | 0.65 ± 0.73 | 1.26 |
| BRN2 | 26.51 | 87.27 | 2009.38-2009.85 | N/A | N/A | 0.82 |
| BRTG | 26.43 | 87.28 | 2004.20-2008.92 | N/A | -1.50 ± 0.79 | 0.82 |
| BYNA | 29.47 | 81.20 | 2009.29-2010.29 | 42.74/39.40/-1.45 | N/A | 1.23 |
| CHLM* | 28.20 | 85.31 | 2004.24-2010.91 | 52.12/48.00/6.65 | 4.60 ± 0.37 | 0.74 |
| DAMA* | 27.60 | 85.10 | 1997.90-2010.26 | 43.28/41.89/2.66 | 2.16 ± 0.21 | 0.86 |
| DLPA* | 28.98 | 82.81 | 2007.35-2010.90 | 50.75/23.29/-5.71 | 4.61 ± 0.55 | 0.94 |
| DNGD | 28.75 | 80.58 | 2008.34-2010.73 | 36.69/14.10/5.56 | 1.08 ± 0.62 | 1.54 |
| DRCL | 29.73 | 80.50 | 2008.20-2010.94 | 47.56/24.96/-1.50 | 3.87 ± 0.68 | 1.37 |
| GNTW | 29.17 | 80.62 | 2008.32-2010.94 | 22.98/11.91/2.17 | 2.61 ± 1.23 | 1.45 |
| GRHI* | 27.95 | 82.49 | 2007.34-2010.90 | 43.63/-14.83/-1.43 | 4.95 ± 0.58 | 1.20 |
| GUMB* | 27.90 | 85.87 | 1997.90-2010.26 | 48.05/33.91/7.97 | 6.07 ± 0.21 | 0.76 |
| JMLA* | 29.27 | 82.19 | 2007.37-2010.89 | 44.24/26.13/-0.57 | 3.10 ± 0.73 | 1.02 |
| JMSM* | 28.80 | 83.74 | 2004.33-2010.90 | 50.23/24.16/12.51 | 3.79 ± 0.33 | 0.81 |
| KKN4* | 27.80 | 85.27 | 2004.22-2010.74 | 49.33/37.04/-6.71 | 2.05 ± 0.29 | 0.82 |
| KLDN* | 27.76 | 83.60 | 2004.28-2010.15 | 33.43/38.78/10.15 | 1.25 ± 0.21 | 1.03 |
| LHAS | 29.65 | 91.10 | 1995.38-2007.07 | 31.36/26.19/8.79 | 0.62 ± 0.27 | 0.69 |
| LHAZ* | 29.65 | 91.10 | 1999.92-2011.23 | 38.40/42.40/3.69 | 2.04 ± 0.17 | 0.69 |
| MST2 | 29.17 | 83.95 | 2009.81-2009.82 | N/A | N/A | 0.69 |
| MSTG | 29.17 | 83.89 | 2004.32-2009.80 | N/A | N/A | 0.70 |
| NPGJ* | 28.11 | 81.59 | 2007.38-2010.88 | 47.71/33.01/6.62 | -2.14 ± 0.58 | 1.37 |
| ODRE* | 26.86 | 87.39 | 2004.86-2010.16 | 54.43/24.51/7.14 | -1.29 ± 0.35 | 0.81 |
| RBIT | 26.84 | 89.39 | 2003.81-2005.99 | 37.42/8.28/4.08 | N/A | 0.78 |
| RMJT | 27.30 | 86.55 | 2009.84-2009.84 | N/A | N/A | 0.80 |
| RMTE | 26.99 | 86.59 | 2008.73-2010.15 | 55.36/25.44/20.06 | 2.19 ± 1.16 | 0.83 |
| SIM4* | 27.16 | 84.98 | 2004.23-2010.26 | 51.92/32.06/0.64 | -0.16 ± 0.33 | 0.93 |
| SIMR* | 27.16 | 84.98 | 1997.91-2005.37 | 24.09/15.96/7.69 | 3.90 ± 0.48 | 0.93 |
| SMKT | 29.96 | 81.80 | 2008.37-2010.89 | 45.76/12.16/10.41 | 5.38 ± 0.64 | 0.95 |
| SRNK | 28.26 | 83.93 | 2005.28-2010.83 | 27.64/15.05/6.82 | 0.94 ± 0.42 | 0.89 |
| SYBC | 27.81 | 86.71 | 2008.76-2009.89 | 54.20/48.96/-2.54 | N/A | 0.74 |
| TIMP* | 27.47 | 89.63 | 2002.38-2008.26 | 45.60/41.69/-4.84 | -1.92 ± 0.45 | 0.78 |
| TPLJ* | 27.35 | 87.70 | 2004.19-2010.17 | 46.14/49.37/3.19 | 1.55 ± 0.32 | 0.77 |

N/A: the observation time span is too short or signals are too noisy.

Stations marked with an asterisk (*) are the sites used for the stack in Figures 3.4 and 3.10.

Table 3.2: Parameters of the Main Himalayan Thrust fault model adopted based on previous studies.

| Model | Fault Geometry of the creeping zone | | Velocity of Dip slip (mm/year) |
|-------------------------|-------------------------------------|--------|--------------------------------|
| | Depth (km) | Dip(°) | |
| Jouanne et al., 1999 | 17 | 9 | 20.5 |
| Jouanne et al., 2004 | 19 | 9.5 | 19 |
| Bettinelli et al., 2006 | 20.9 | 10.3 | 16.3 |

Chapter 4 Seasonal Hydrological Loading in Southern Alaska Observed by GPS and GRACE¹

Abstract

We compare vertical seasonal loading deformation observed by continuous GPS stations in southern Alaska and modeled vertical displacements due to seasonal hydrological loading inferred from GRACE. Seasonal displacements are significant, and GPS-observed and GRACE-modeled seasonal displacements are highly correlated. We define a measure called the WRMS Reduction Ratio to measure the fraction of the position variations at seasonal periods removed by correcting the GPS time series using a seasonal model based on GRACE. The median WRMS Reduction Ratio is 0.82 and the mean is 0.73 ± 0.26 , with a value of 1.0 indicating perfect agreement of GPS and GRACE. The effects of atmosphere and non-tidal ocean loading are important; we add the AOD1B de-aliasing model to the GRACE solutions because the displacements due to these loads are present in the GPS data, and this improves the correlations between these two geodetic measurements. We find weak correlations for some stations located in areas where the magnitude of the load changes over a short distance, due to GRACE's limited spatial resolution. GRACE models can correct seasonal displacements for campaign GPS measurements as well.

4.1 Introduction

Geodetic observations have been used to study the seasonal hydrological mass cycle and its loading effects, such as the Global Positioning System (GPS) seasonal position variations in Japan (Heki, 2004), Amazon basin (Bevis et al., 2005) and Iceland (Grapenthin et al., 2006). The NASA/DLR Gravity Recovery and Climate Experiment (GRACE) has been used to study the ground seasonal deformation together with GPS (e.g. Davis et al. (2004)). Although van Dam et al. (2007) reported poor correlation

¹Fu, Y., J. T. Freymueller, and T. Jensen (2012), Seasonal hydrological loading in southern Alaska observed by GPS and GRACE, *Geophys. Res. Lett.*, 39, L15310, doi:10.1029/2012GL052453.

between GPS and GRACE over Europe and attributed it to GPS processing flaws, more recent studies have shown consistent seasonal displacements between GPS and GRACE in West Africa (Nahmani et al., 2012), and the Nepal Himalaya (Fu and Freymueller, 2012), because of strong seasonal hydrological loading and improved GPS processing.

Mountainous and located at high latitude, southern Alaska has a long winter season for snow and ice accumulation and a warm summer season for melting, an ideal situation for strong seasonal hydrologic mass variation. Seasonal vertical deformation of GPS timeseries in southern Alaska was reported by Freymueller et al. (2008). Previous GRACE studies indicate clear seasonal gravity changes in southeast Alaska caused by seasonal hydrologic mass variations (Tamisiea et al., 2005, Chen et al., 2006, Luthcke et al., 2008, Davis et al., 2012). In this paper, we investigate the seasonal variation observed by GPS and GRACE across southern Alaska, and analyze the correlation between these two geodetic observations using an elastic loading model.

4.2 Data

4.2.1 GPS data

Sixty-four former and current continuous GPS stations in southern Alaska (Figure 4.1) are analyzed in this study. Thirty of them are Plate Boundary Observatory (PBO) GPS stations, and others are installed and maintained by a variety of other organizations (see Table 4.1). We used GPS data between July 2002 and December 2011. We employ the GIPSY/OASIS-II (Version 5.0) software in point positioning mode to obtain daily coordinates and covariances, and then transform the daily free network solutions into ITRF2008 (Altamimi et al., 2011). We estimate this daily frame alignment transformation ourselves, using a set of reliable ITRF stations (~30 stations each day). The complete analysis procedure is as described in Fu and Freymueller (2012). We correct for solid earth tides and ocean tidal loading (Fu et al., 2012) in the GPS processing, but not atmospheric pressure loading or any other loading variations with

periods >1 day. We average the GPS daily solutions to weighted 10-day averages (using GIPSY's utility `stamrg`) to compare with the GRACE solutions.

4.2.2 GRACE data

We use spherical harmonic coefficients of the Earth's gravity field estimated from GRACE data (Bruinsma et al., 2010) and load Love numbers (Farrell, 1972) to model the elastic displacements due to the changing load (Wahr et al., 1998; Kusche and Schrama, 2005). In order to maintain consistency with the loading effects present in the GPS solutions, we add GRACE's Atmosphere and Ocean De-aliasing Level-1B (AOD1B) solution (GAC solution) to the GRACE spherical harmonic solutions. By doing this, both atmospheric and non-tidal ocean loads are present in both GPS and GRACE solutions.

We use the second release of 10-day gravity fields models (RL02) provided by the Space Geodesy Research Group (GRGS), a scientific consortium of 10 French research teams. Spherical harmonic coefficients up to degree and order 50 for the gravity field are provided every 10 days. The North-South striping noise is reduced with an improved data editing and solution regularization, and no further smoothing is required since it has been stabilized during the data process. Bruinsma et al. (2010) described the GRACE data processing strategies. We replace the degree-1 components with results obtained by Swenson et al. (2008). All the analyses in this paper use the GRACE solutions from GRGS for its better temporal resolution. Our previous study of the Himalaya (Fu and Freymueller, 2012) found that this GRACE solution showed slightly better agreement with GPS than other solutions. We also show GRACE Level-2 RL-04 solutions from CSR (Center for Space Research, Austin, USA) for comparison (Figure 4.1). For its monthly products, we replace C20 terms with the results from observations of Satellite Laser Ranging (Cheng and Tapley, 2004), and Degree-1 components using Stokes coefficients derived by Swenson et al. (2008). We adopted 350 km as the averaging radius for Gaussian smoothing for the CSR solution (Wahr et al., 1998). Example timeseries for GRACE-modeled vertical seasonal displacements are given in Figure 4.2.

4.3 Results

We compare the GPS observed and GRACE modeled vertical seasonal (detrended) displacements, and find that both show significant and consistent seasonal variations (Figure 4.1). We fit annual and semiannual variations to the GRACE displacement predictions, and use this seasonal correction for analysis rather than the raw timeseries. In order to quantitatively evaluate the consistency between GPS-observed and GRACE-modeled seasonal height variations, we define a measure termed the “WRMS (Weighted Root-Mean-Squares) Reduction Ratio”, expressed as follows:

$$Ratio_{WRMS_reduction} = \frac{WRMS_{GPS} - WRMS_{GPS-GRACE}}{WRMS_{GPS} - WRMS_{GPS-GPS_{fit}}} \quad (1)$$

$WRMS_{GPS}$ is the WRMS of the GPS detrended timeseries, including its seasonal variations; $WRMS_{GPS-GRACE}$ is the WRMS of the GPS timeseries with seasonal effects corrected by seasonal GRACE-modeled detrended displacements; $WRMS_{GPS-GPS_{fit}}$ is the WRMS of the GPS timeseries with seasonal signals removed by fitting annual plus semiannual terms to the GPS timeseries. The WRMS Reduction Ratio reflects the agreement of the GPS and GRACE timeseries in both amplitude and phase, and scales the improvement relative to the amplitude of seasonal variations actually present. A value of 1.0 would indicate perfect agreement between GPS-observed and GRACE-modeled annual plus semi-annual seasonal displacements. Theoretically, the WRMS Reduction Ratio can not exceed 1, because the fit of GPS timeseries with annual and semiannual terms can not be worse than any other model of annual and semiannual terms.

Figure 4.3 shows examples of the WRMS reductions for 14 GPS stations. The top of each bar indicates $WRMS_{GPS}$; the dots demonstrate $WRMS_{GPS-GRACE}$; the bottom of each bar denotes $WRMS_{GPS-GPS_{fit}}$, which is not zero because of noise remaining in the GPS timeseries and also interannual variations. When the dot is close to the bottom of the bar, it indicates that the seasonal variation in the GPS and GRACE are very similar.

Figure 4.4 depicts the WRMS Reduction Ratios for all the continuous GPS sites analyzed in this study; values are provided in Table 4.1. The WRMS decreases for 62 out of 64 stations when corrections based on GRACE are applied, with a median WRMS Reduction Ratio of 0.82 and a mean WRMS Reduction Ratio of 0.73 ± 0.26 . The only two sites with negative WRMS Reduction Ratios are AC03 and SELD (at the SW tip of the Kenai Peninsula, Figure 4.4), with -0.03 and -0.02, respectively. The consistency of seasonal signals between GPS and GRACE demonstrates that the seasonal position oscillations in southern Alaska are mainly caused by long-wavelength hydrological mass loading, which is due to snow and ice accumulation during the winter season and melt during the spring and summer seasons. This seasonal cycle is also accompanied by massive long-term mass losses (Arendt et al., 2002; Chen et al., 2006; Larsen et al., 2007; Luthcke et al., 2008; Berthier et al., 2010).

Figure 4.4 indicates that stations close to high mountains and heavily glaciated areas show better agreements between GPS and GRACE; and distant stations show weaker correlation. This is due to the discrepancy of spatial resolutions for two geodetic tools. Within the mountainous coastal areas, the long-wavelength seasonal hydrological loading (snow and ice) is uniform for most places, so the GRACE solutions, which are averaged over a larger spatial area, accurately represent the loads at any specific point measured by GPS. However, in areas where the magnitude of the load changes over a short distance, the spatial averaging of GRACE can result in inaccurate predicted displacements. The sites AC03 and SELD are good examples of this problem. These sites are located at low elevation along the coast, so snow accumulation is relatively low within 30-40 km of the sites. However, coastal mountains that accumulate very large snow loads extend from ~60 to 200 km to the east of these sites. Because GRACE cannot resolve such short-wavelength variations in the loads, the displacements predicted from GRACE overestimate the amplitude of the seasonal variations at these sites. The same is true for all other low-elevation stations in the Cook Inlet area (ellipse in Figure 4.4). This low-lying area is surrounded by mountains with large accumulations of snow, and

GRACE over-predicts the amplitudes of seasonal displacements across the entire region by varying amounts.

Interannual variations of seasonal oscillations are also apparent (Figure 4.1). One example is the low “peak” in 2008 for station ELDC, and the low “trough” in early 2009 (see figure 4.1); it is clear that both GPS and GRACE show the same interannual variations. The summer of 2008 was wet and cold over most of southern Alaska, so there was less melting than usual in summer 2008 and a resulting heavier-than-average snow load throughout the next year. The period from 2002-2005 also showed more rapid uplift than the period since 2005 for many sites (see LEVC in Figure 4.1). A correction based the time series may produce even better results.

In this study, we do not correct for atmospheric and non-tidal ocean loading effects during GPS data processing. Instead, we combine the GRACE and AOD1B solutions (Flechtner, 2007) so that atmospheric and non-tidal ocean loading effects are included in both the GPS and GRACE solutions. Figure 4.5 shows three example GPS sites (AC57, AB42 and GUS2) comparing the GRACE-modeled height displacements with and without the AOD1B model. It is clear that the seasonal fit of the GRACE solutions with AOD1B (blue dashed lines) agrees with the GPS seasonal variations (black dashed lines) better than the solutions without AOD1B (cyan dashed lines), for both amplitude and phase. The WRMS Reduction Ratio also improves for AC57 from 0.75 using GRACE solutions without AOD1B to 0.96 with AOD1B included; the improvements are from 0.81 to 0.95 for AB42; and from 0.73 to 0.96 for ATW2. The mean WRMS Reduction Ratio improves from 0.67 to 0.73 for all continuous stations analyzed in this paper. Consistent treatment of atmospheric and non-tidal ocean loading is essential for comparing or combining GPS and GRACE solutions.

4.4 Discussion

GPS campaign measurements, or GPS episodic measurements, usually re-survey the bench marks once per year at most. When estimating the velocity for a campaign GPS site, seasonal effects are ignored due to limited observations. However, for the GPS

campaign stations located where seasonal hydrologic loading is significant, and if the sites were surveyed at different times of year, the estimated linear velocities can be biased by neglecting the seasonal impacts.

We can use GRACE continuous measurements to model the seasonal ground displacements, and use them to correct the seasonal effects for campaign GPS data. Figure 4.6 shows an example for GPS campaign site FS32 located near the Juneau Icefield (see Figure 4.1). The upper GPS timeseries (blue) show the original observed data. With seasonal impacts corrected based on GRACE measurements, the misfit (χ^2 per degree of freedom) decreases by 64% (from 8.89 to 3.23) in the seasonally corrected timeseries (red). The most evident improvement occurs in 2009 (see highlight box in Figure 4.6); the GPS site was measured at a different time of year in 2009, and its seasonal effect can be corrected well with GRACE data.

4.5 Conclusions.

GRACE-modeled vertical displacements due to seasonal hydrologic loading show high correlation with GPS observed seasonal position variations, which confirms that the hydrological mass cycle is the main cause of seasonal ground deformation in southern Alaska. Loading models based on GRACE data can effectively remove seasonal effects in both continuous and campaign GPS measurements in this region of very large seasonal hydrological load variations. Loading models based on GRACE perform well except in areas where the magnitude of the seasonal load changes over short spatial distances; this limitation is a consequence of the lack of spatial resolution in GRACE. Because the seasonal deformations can be so large, periodic seasonal displacements should be considered in regional reference frame realization (Freymueller, 2009).

Acknowledgments

The authors gratefully appreciate all the colleagues who had attended the GPS field work in southern Alaska. We also thank UNAVCO and the NSF EarthScope program for maintaining the PBO continuous GPS measurements in Alaska. Discussions with

Anthony Arendt and Christopher Larsen greatly improve this study, and we thank two anonymous reviewers for comments that helped us improve the manuscript. This work was supported by NSF grant EAR-0911764 to JTF, and a Global Change Student Grant to YF. The loading timeseries for both GPS and GRACE are available from the authors.

References

- Altamimi, X., X. Collilieux, and L. Metivier (2011), ITRF2008: An improved solution of the International Terrestrial Reference Frame, *J. Geod.*, 85(8), 457-473, doi:10.1007/s00190-011-0444-4.
- Arendt, A. A., K. A. Echelmeyer, W. D. Harrison, C. S. Lingle, and V. B. Valentine (2002), Rapid wastage of Alaska glaciers and their contribution to rising sea level, *Science*, 297, 382–386, doi:10.1126/science.1072497.
- Berthier, E., E. Schiefer, G. K. C. Clarke, B. Menounos, and F. Rémy (2010), Contribution of Alaskan glaciers to sea-level rise derived from satellite imagery, *Nat. Geosci.*, 3, 92–95, doi:10.1038/ngeo737.
- Bevis, M., D. Alsdorf, E. Kendrick, L. P. Fortes, B. Forsberg, R. Smalley Jr., and J. Becker (2005), Seasonal fluctuations in the mass of the Amazon River system and Earth's elastic response, *Geophys. Res. Lett.*, 32, L16308, doi:10.1029/2005GL023491.
- Bruinsma, S., J. Lemoine, R. Biancale, and N. Vales (2010), CNES/GRGS 10-day gravity field models (release 2) and their evaluation, *Adv. Space Res.*, 45, 587–601, doi:10.1016/j.asr.2009.10.012.
- Chen, J. L., B. D. Tapley, and C. R. Wilson (2006), Alaskan mountain glacial melting observed by satellite gravimetry, *Earth Planet. Sci. Lett.*, 248, 353–363.
- Cheng, M., and B. D. Tapley (2004), Variations in the Earth's oblateness during the past 28 years, *J. Geophys. Res.*, 109, B09402, doi:10.1029/2004JB003028.
- Davis, J. L., P. Elósegui, J. X. Mitrovica, and M. E. Tamisiea (2004), Climate-driven deformation of the solid Earth from GRACE and GPS, *Geophys. Res. Lett.*, 31, L24605, doi:10.1029/2004GL021435.
- Davis, J. L., B. P. Wernicke, and M. E. Tamisiea (2012), On seasonal signals in geodetic time series, *J. Geophys. Res.*, 117, B01403, doi:10.1029/2011JB008690.
- Farrell, W. E. (1972), Deformation of the Earth by surface loads, *Rev. Geophys.*, 10, 761–797, doi:10.1029/RG010i003p00761.

- Flechtner, F. (2007), AOD1B product description document for product releases 01 to 04, GR-GFZ-AOD-0001 Rev. 3.1, 43 pp., Univ. of Tex. at Austin, Austin.
- Freymueller, J. T., H. Woodard, S. Cohen, R. Cross, J. Elliott, C. Larsen, S. Hreinsdottir, and C. Zweck (2008), Active deformation processes in Alaska, based on 15 years of GPS measurements, in *Active Tectonics and Seismic Potential of Alaska*, Geophys. Monogr. Ser., vol. 179, edited by J. T. Freymueller et al., pp. 1–42, AGU, Washington, D.C.
- Freymueller J. T. (2009) Seasonal Position variations and regional reference frame realization. In: Drewes H (ed) *Geodetic reference frames*, IAG Symposium Munich, Germany, 9–14 October 2006, International Association of Geodesy Symposia, vol 134, Springer, pp 191–196. doi:10.1007/978-3-642-00860-3_30
- Fu, Y., J. T. Freymueller, and T. van Dam (2012), The effect of using inconsistent ocean tidal loading models on GPS coordinate solutions, *J. Geod.*, 86(6), 409-421, doi:10.1007/s00190-011-0528-1.
- Fu, Y., and J. T. Freymueller (2012), Seasonal and long-term vertical deformation in the Nepal Himalaya constrained by GPS and GRACE measurements, *J. Geophys. Res.*, 117, B03407, doi:10.1029/2011JB008925.
- Grapenthin, R., F. Sigmundsson, H. Geirsson, T. Árnadóttir, and V. Pinel (2006), Icelandic rhythmicity: Annual modulation of land elevation and plate spreading by snow load, *Geophys. Res. Lett.*, 33, L24305, doi:10.1029/2006GL028081.
- Heki, K. (2004), Dense GPS array as a new sensor of seasonal changes of surface loads, in *The State of the Planet: Frontiers and Challenges in Geophysics*, Geophys. Monogr. Ser., vol. 150, edited by R. S. J. Sparks and C. J. Hawkesworth, pp. 177–196, AGU, Washington, D. C.
- Kusche, J., and E. J. O. Schrama (2005), Surface mass redistribution inversion from global GPS deformation and Gravity Recovery and Climate Experiment (GRACE) gravity data, *J. Geophys. Res.*, 110, B09409, doi:10.1029/2004JB003556.

- Larsen, C. F., R. J. Motyka, A. A. Arendt, K. A. Echelmeyer, and P. E. Geissler (2007), Glacier changes in southeast Alaska and northwest British Columbia and contribution to sea level rise, *J. Geophys. Res.*, 112, F01007, doi:10.1029/2006JF000586.
- Luthcke, S. B., A. A. Arendt, D. D. Rowlands, J. J. McCarthy, and C. F. Larsen (2008), Recent glacier mass changes in the Gulf of Alaska region from GRACE mascon solutions, *J. Glaciol.*, 54, 767–777, doi:10.3189/002214308787779933.
- Nahmani, S., O. Bock, M. Bouin, A. Santamaría-Gómez, J. Boy, X. Collilieux, L. Métivier, I. Panet, P. Genthon, C. Linage, and G. Wöppelmann (2012), Hydrological deformation induced by the West African Monsoon: Comparison of GPS, GRACE and loading models, *J. Geophys. Res.*, 117, B05409, doi:10.1029/2011JB009102.
- Swenson, S., D. Chambers, and J. Wahr (2008), Estimating geocenter variations from a combination of GRACE and ocean model output, *J. Geophys. Res.*, 113, B08410, doi:10.1029/2007JB005338.
- Tamisiea, M. E., E. W. Leuliette, J. L. Davis, and J. X. Mitrovica (2005), Constraining hydrological and cryospheric mass flux in southeastern Alaska using space-based gravity measurements, *Geophys. Res. Lett.*, 32, L20501, doi:10.1029/2005GL023961.
- van Dam, T., J. Wahr, and D. Lavallée (2007), A comparison of annual vertical crustal displacements from GPS and Gravity Recovery and Climate Experiment (GRACE) over Europe, *J. Geophys. Res.*, 112, B03404, doi:10.1029/2006JB004335.
- Wahr, J., M. Molenaar, and F. Bryan (1998), Time variability of the Earth's gravity field: Hydrological and oceanic effects and their possible detection using GRACE, *J. Geophys. Res.*, 103, 30,205–30,229, doi:10.1029/98JB02844.

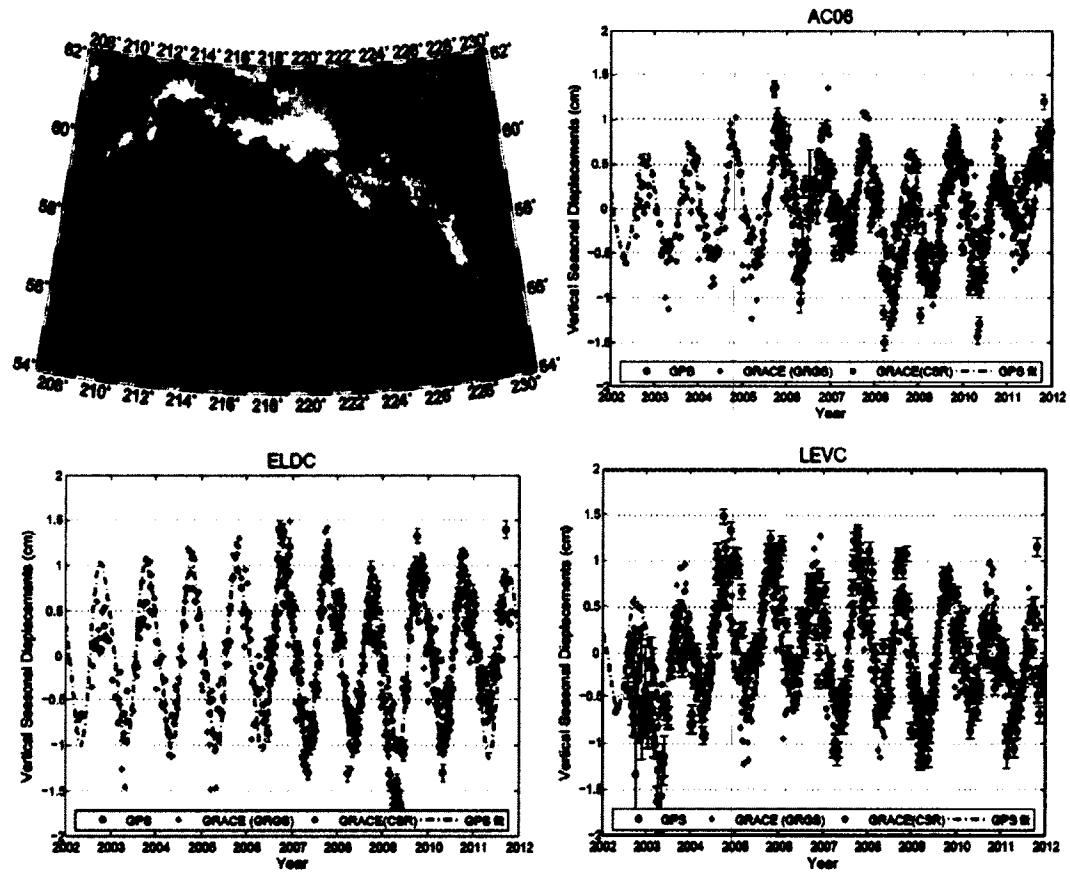


Figure 4.1: Distribution of Continuous GPS station and example timeseries. Top left: distribution of continuous GPS stations (blue diamonds) in southern Alaska; white-color regions denote glaciated areas. Brown circles are sites used for the AOD1B study (Figure 4.5). Black star is the campaign site used for Figure 4.6. Three examples (AC06, ELDC and LEVC) of GPS vertical seasonal (detrended) timeseries and their GRACE-modeled seasonal vertical displacements are shown. GRACE solutions from GRGS and CSR are used.

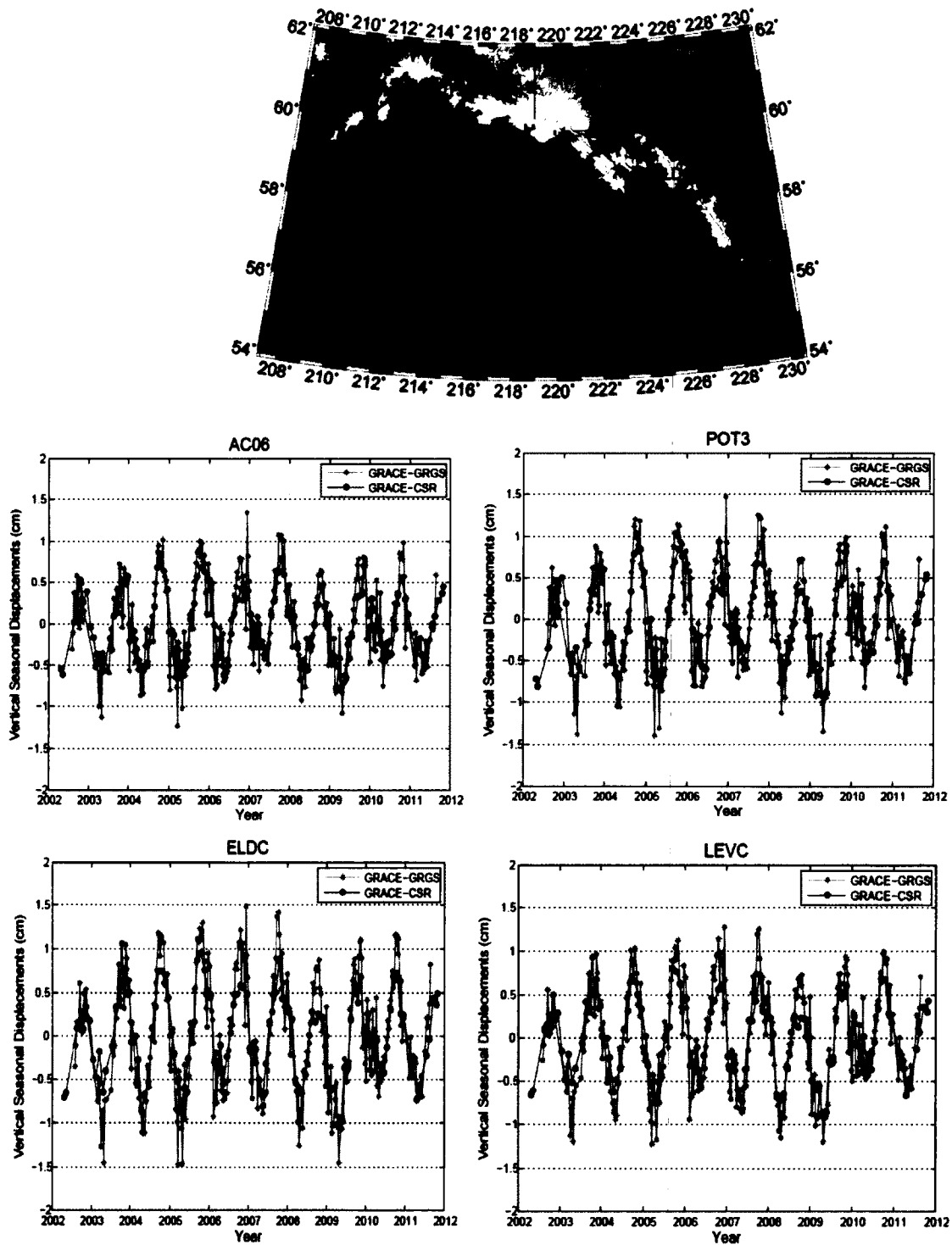


Figure 4.2: Four examples (AC06, POT3, ELDC and LEVC) for GRACE-modeled vertical seasonal displacements. Their locations are also given in the upper figure.

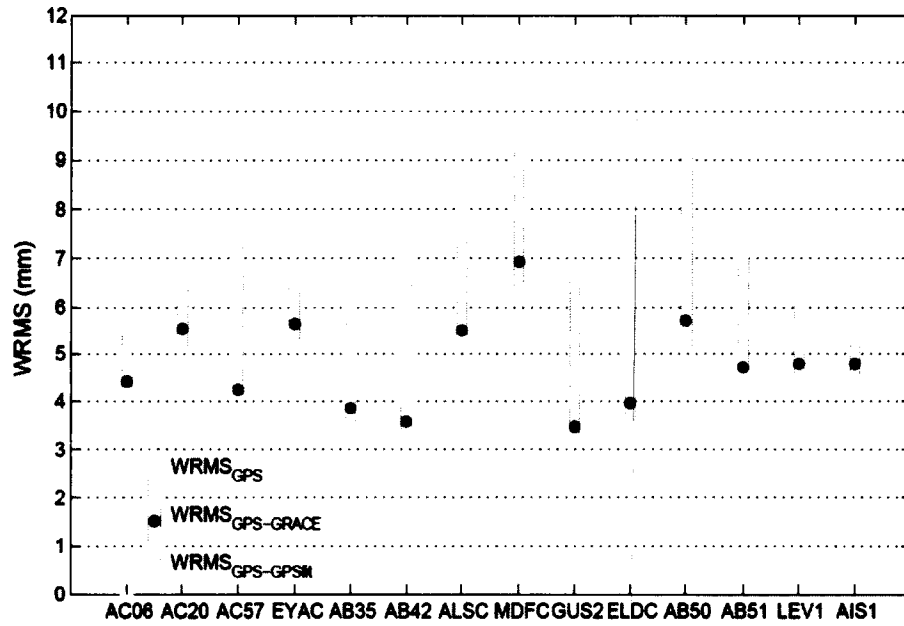


Figure 4.3: Selected examples of the WRMS reduction when removing GPS seasonal variation using GRACE-modeled seasonal displacements. Selected stations are distributed from west to east (southeast).

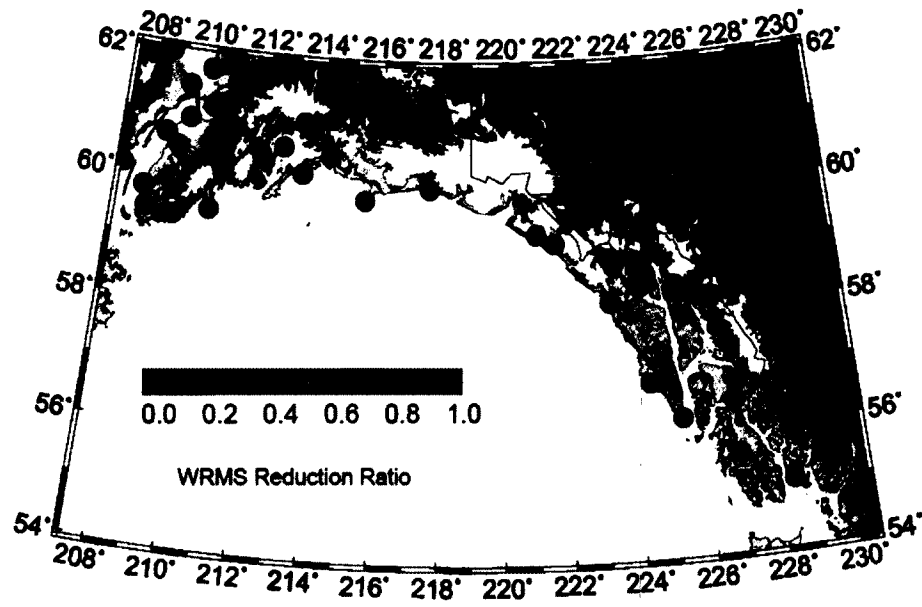


Figure 4.4: The WRMS Reduction Ratios for all continuous GPS stations in southern Alaska. The Ellipse (northwest) highlights low-elevation coastal stations of Cook Inlet, where GRACE consistently overestimates the amplitude of the seasonal variations.

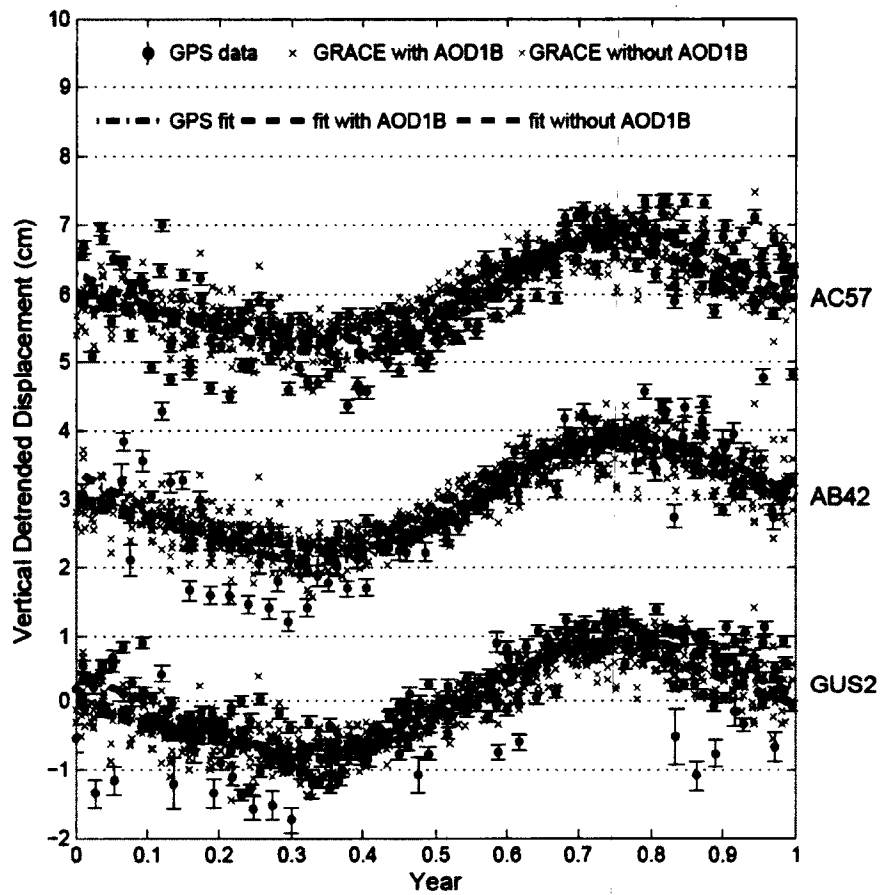


Figure 4.5: Seasonal variations for three example stations (AC57, AB42 and GUS2, see Figure 4.1 for their locations), plotted by fractional year. GRACE-modeled vertical displacements (and their best-fit lines) using solutions with AOD1B and without AOD1B are plotted together for comparison.

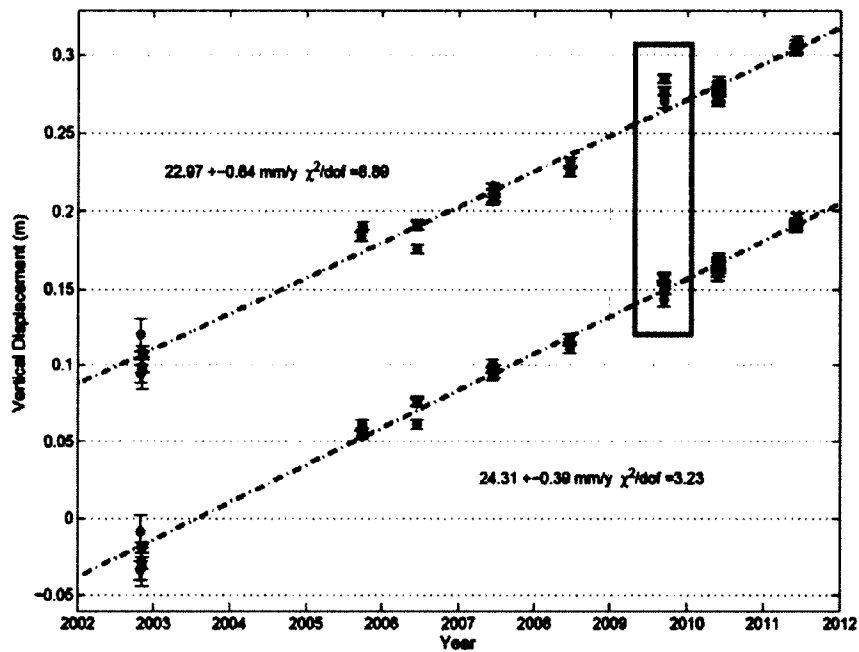


Figure 4.6: Timeseries of campaign GPS site FS32, see Figure 4.1 for its location. Top: (blue) original observed GPS timeseries. Bottom: (red) corrected timeseries with seasonal loading deformation removed based on GRACE data. An obvious improvement for the measurements in 2009 is highlighted.

Table 4.1: Information of continuous GPS stations analyzed in this study for southern Alaska. Site locations, observational time, and their WRMS Reduction Ratios when seasonal vertical deformations are removed using GRACE-modeled seasonal displacements are provided. Stations with antenna covered by snow during winter are not used in this study. "LEVC" is a composite time series combining two sites LEV1 and LEV5.

| Station | Latitude | Longitude | Elevation (m) | Observation Time | WRMS Reduction Ratio | Agency ^a |
|---------|----------|-----------|------------------|------------------|-------------------------|---------------------|
| AB35 | 60.079 | -142.389 | 536.72 | 2007.65-2011.43 | 0.8712 | PBO |
| AB42 | 59.340 | -138.898 | 773.25 | 2006.58-2011.98 | 0.9569 | PBO |
| AB43 | 58.198 | -136.640 | 26.93 | 2007.38-2011.98 | 0.9630 | PBO |
| AB44 | 59.528 | -135.228 | 304.12 | 2005.62-2011.98 | 0.8968 | PBO |
| AB48 | 56.245 | -134.646 | 5.26 | 2005.76-2010.99 | 0.2500 | PBO |
| AB49 | 55.580 | -133.068 | 17.54 | 2006.33-2011.98 | 0.4980 | PBO |
| AB50 | 58.416 | -134.545 | 51.49 | 2005.62-2011.98 | 0.8738 | PBO |
| AB51 | 56.797 | -132.913 | 75.81 | 2005.76-2011.98 | 0.9715 | PBO |
| AC03 | 59.770 | -151.864 | 19.59 | 2007.92-2011.65 | -0.0384 | PBO |
| AC06 | 59.763 | -150.890 | 631.40 | 2005.70-2011.98 | 0.9425 | PBO |
| AC09 | 59.868 | -144.523 | 368.87 | 2007.65-2011.98 | 0.3763 | PBO |
| AC11 | 61.807 | -148.331 | 790.83 | 2005.57-2011.98 | 0.8853 | PBO |
| AC15 | 60.481 | -149.724 | 151.41 | 2005.79-2011.98 | 0.8991 | PBO |
| AC16 | 60.518 | -148.093 | 34.05 | 2007.54-2011.98 | 0.7315 | PBO |
| AC20 | 60.929 | -149.352 | 43.64 | 2005.54-2011.98 | 0.7513 | PBO |
| AC23 | 60.475 | -150.877 | 80.76 | 2007.46-2011.98 | 0.2094 | PBO |
| AC32 | 61.473 | -150.736 | 1347.74 | 2006.86-2011.98 | 0.8003 | PBO |
| AC35 | 59.375 | -150.793 | 408.40 | 2006.53-2011.98 | 0.9172 | PBO |
| AC36 | 60.955 | -150.608 | 46.45 | 2008.12-2011.98 | 0.3019 | PBO |
| AC43 | 59.521 | -149.628 | 69.52 | 2007.65-2011.98 | 0.8179 | PBO |
| AC44 | 61.242 | -149.567 | 832.13 | 2008.61-2011.98 | 0.7618 | PBO |
| AC46 | 61.986 | -151.524 | 619.73 | 2006.66-2011.98 | 0.5895 | PBO |
| AC47 | 60.081 | -152.623 | 922.24 | 2007.73-2011.98 | 0.7804 | PBO |
| AC48 | 60.645 | -147.343 | 379.52 | 2007.65-2011.98 | 0.9043 | PBO |
| AC51 | 61.498 | -151.835 | 957.38 | 2007.70-2011.98 | 0.8229 | PBO |
| AC53 | 61.768 | -150.068 | 57.47 | 2006.69-2011.98 | 0.0699 | PBO |
| AC57 | 61.138 | -145.742 | 826.34 | 2006.47-2011.98 | 0.9695 | PBO |
| AIS1 | 55.069 | -131.599 | 32.16 | 2002.58-2008.09 | 0.7365 | USCG |
| AIS5 | 55.069 | -131.599 | 32.36 | 2008.09-2011.98 | 0.8559 | USCG |
| ALSC | 59.186 | -138.318 | 28.32 | 2007.43-2011.65 | 0.9744 | GI-UAF |
| ATW2 | 61.597 | -149.132 | 97.06 | 2002.58-2011.98 | 0.9635 | PBO |
| BCDL | 58.425 | -130.025 | 802.09 | 2004.89-2011.92 | 0.8090 | PBC-GSC |
| BIS1 | 56.854 | -135.539 | 66.58 | 2002.58-2008.47 | 0.2287 | USCG |
| BIS5 | 56.854 | -135.539 | 66.77 | 2008.47-2011.98 | 0.1672 | USCG |
| BMCP | 58.782 | -136.479 | 20.18 | 2006.42-2011.43 | 0.5907 | GI-UAF |
| CHI3 | 60.237 | -146.646 | 94.55 | 2002.58-2007.70 | 0.7457 | USCG |
| CHI4 | 60.237 | -146.646 | 91.19 | 2002.58-2007.70 | 0.8256 | USCG |
| CMJV | 61.165 | -149.844 | 57.90 | 2002.58-2009.13 | 0.7090 | C-CORS |
| ELDC | 58.971 | -135.222 | 13.37 | 2006.44-2011.73 | 0.9196 | GI-UAF |
| EYAC | 60.548 | -145.749 | 146.02 | 2005.40-2011.98 | 0.7028 | PBO |

Table 4.1 continued ...

| | | | | | | |
|------|--------|----------|---------|-----------------|---------|--------|
| GUS1 | 58.417 | -135.697 | 19.67 | 2002.83-2008.47 | 0.9239 | USCG |
| GUS2 | 58.417 | -135.697 | 19.88 | 2002.58-2008.47 | 0.9547 | USCG |
| GUS5 | 58.417 | -135.697 | 19.98 | 2008.47-2011.98 | 0.8463 | USCG |
| GUS6 | 58.417 | -135.697 | 20.19 | 2008.47-2011.98 | 0.8539 | USCG |
| JNU1 | 58.362 | -134.585 | 15.48 | 2003.10-2011.98 | 0.9231 | FAA |
| KEN1 | 60.675 | -151.350 | 56.03 | 2002.58-2007.68 | 0.6365 | USCG |
| KEN5 | 60.675 | -151.350 | 56.31 | 2007.68-2011.98 | 0.8484 | USCG |
| KEN6 | 60.674 | -151.350 | 56.69 | 2007.68-2011.98 | 0.8439 | USCG |
| LEV6 | 56.465 | -133.092 | 25.37 | 2002.58-2011.98 | 0.7993 | USCG |
| LEV2 | 56.465 | -133.092 | 25.19 | 2002.75-2007.62 | 0.7013 | USCG |
| MDFC | 60.121 | -136.958 | 896.98 | 2006.75-2011.73 | 0.7961 | GI-UAF |
| PALM | 61.585 | -149.119 | 81.23 | 2006.20-2011.02 | 0.8989 | C-CORS |
| POT3 | 61.056 | -146.696 | 35.74 | 2002.58-2007.68 | 0.8930 | USCG |
| POT4 | 61.056 | -146.697 | 37.04 | 2002.75-2007.68 | 0.9383 | USCG |
| POT5 | 61.056 | -146.696 | 35.98 | 2007.70-2011.98 | 0.9457 | USCG |
| POT6 | 61.056 | -146.697 | 37.25 | 2007.70-2011.98 | 0.7187 | USCG |
| QUIC | 58.908 | -136.586 | 23.74 | 2006.44-2011.40 | 0.9038 | GI-UAF |
| SELD | 59.445 | -151.706 | 20.37 | 2008.01-2010.88 | -0.0265 | PBO |
| SPCG | 61.291 | -152.022 | 1342.73 | 2004.69-2011.98 | 0.9068 | AVO |
| SPCR | 61.200 | -152.209 | 1004.32 | 2004.69-2011.98 | 0.8890 | AVO |
| TBON | 61.179 | -149.785 | 93.14 | 2006.20-2011.95 | 0.7948 | C-CORS |
| TSEA | 61.187 | -149.894 | 42.94 | 2002.58-2011.98 | 0.6628 | C-CORS |
| WHIT | 60.750 | -135.222 | 1427.38 | 2002.64-2011.76 | 0.3827 | GSC |
| ZANI | 61.229 | -149.780 | 80.19 | 2002.97-2011.98 | 0.5364 | FAA |

^aPBO, Plate Boundary Observatory;

USCG, US Coast Guard/NGS(CORS);

GI-UAF, Geophysical Institute, University of Alaska Fairbanks;

PBC-GSC, Province of British Columbia, and Pacific Geoscience Center, Geological Survey of Canada;

C-CORS, Cooperative CORS (CMJV: Crazy Mountains Joint Venture; TSEA: The Surveyor's Exchange; PALM, TBON: Alaska Dept. of Transportation);

FAA, Federal Aviation Administration;

AVO, Alaska Volcano Observatory;

GSC, Geological Survey of Canada.

Chapter 5 Conclusions

I have identified a potential spurious noise source of GPS coordinate solutions. Aliased periodic errors at periods of ~14-day, semiannual and annual can be propagated into GPS daily timeseries if orbit/clock users adopt an inappropriate reference frame to model Ocean Tidal Loading (OTL). With improved data processing strategies, GPS and GRACE observations have been shown to measure highly correlated seasonal hydrological loadings, in both Nepal Himalaya and southern Alaska.

Chapter 2 showed that significant biases can be introduced into GPS solutions when a user solution uses OTL coefficients computed in a different reference frame to those used by the analysis center in their product generation solution. The choice of frame for the OTL model computations has a substantial effect on estimated satellite clock parameters, and a smaller effect on the estimated satellite orbits.

Solutions in which inconsistent OTL coefficients are used display significant differences at several periodic components that are characteristic of aliasing of OTL errors. Power spectrum analysis for our 6-year detrended timeseries of continuous GPS positions shows that the most distinguishable difference occurs at a period of about ~14 days. Using JPL's current and reanalysis orbits products, which use OTL coefficients computed in the CM frame in accordance with IERS Conventions, we find a significant spectral peak at ~14-day period in the solution with OTL coefficients computed in the CE frame, but no peak at this period in the solutions using OTL computed in the CM frame. This result stands true for both ambiguity-free and ambiguity-fixed solutions. In addition, there are small differences at ~annual and ~semiannual periods.

Therefore, in any solution that uses fixed orbits or fixed orbits and satellite clocks, it is the analyst's responsibility to maintain consistency with the analysis center that generated the products. The need for consistency makes it critical both for analysis centers that generate orbit and clock products and researchers using these products to report which frame was used to compute the OTL coefficients in their analysis. Authors should also make clear which frame they used.

This finding limits the degree to which PPP solutions can be used to assess other small changes or improvements in observation models. PPP solutions can be used for this purpose only when the orbit and clock parameters are not affected by the differences in models. The errors of using inconsistent reference frame to model OTL may be misinterpreted by other sources. For example, the correction for 2nd or higher order ionospheric effects (e.g. Fritsche et al., 2005) may need to be re-evaluated.

Chapter 3 combines GPS and GRACE measurements to study vertical motions in the Nepal Himalaya. Both GPS and GRACE observe strong seasonal variations. I adopt a load model based on GRACE data to model the resulting vertical displacements due to the changing hydrological loads. Quantitative comparisons between the observed GPS seasonal vertical deformation and GRACE-derived seasonal deformation demonstrate that a consistent physical mechanism is responsible for the correlation between these two kinds of geodetic measurements. Besides the significant seasonal signal, GRACE also exhibits a long-term mass loss in this region, which is due to the melting ice and snow in the high mountains of the Himalaya. We calculate the consequent uplift caused by the load decrease, and remove this hydrological effect from observed GPS vertical rates. The residual vertical rates are mainly dominated by tectonic deformation due to the earthquake cycle on the Main Himalayan Thrust. We then use a 2-D dislocation model to compute the tectonic vertical rates based on previous studies; those studies estimated fault models from the GPS horizontal velocities. Comparison between observed and modeled vertical rates suggests that interseismic strain from the MHT is able to explain most of the vertical motion of most GPS stations, although the whole arc shows some lateral variations. Correction for the long-term uplift predicted by the GRACE data improves the agreement between GPS vertical rates and the models based on horizontal data. The GPS vertical velocities are still too noisy to discriminate between the different horizontal slip models, but they may contribute to the estimation of models based on 3D velocities once loading effects are removed.

In Chapter 4, GRACE-modeled vertical displacements due to seasonal hydrologic loading show high correlation with GPS observed seasonal height variations, which

confirms that the hydrological mass cycle is the main cause of seasonal ground deformation in southern Alaska. Loading models based on GRACE data can effectively remove seasonal effects in both continuous and campaign GPS measurements in this region of very large seasonal hydrological load variations. Loading models based on GRACE perform well except in areas where the magnitude of the seasonal load changes over short spatial distances; this limitation is a consequence of the lack of spatial resolution in GRACE.

Because the seasonal deformations in specific regions, such as the Nepal Himalaya (Chapter 3), southern Alaska (Chapter 4), the Amazon River area (Bevis et al., 2005) and western Africa (Nahmani et al., 2012), can be so large, periodic seasonal displacements should be considered in regional reference frame realization (Freymueller, 2009). GRACE data (and potentially hydrology models) provide measurements to quantify the seasonal surface mass variations, which can be used to model its resulting seasonal crustal displacements. Hence, further study of incorporating seasonal variations in Regional and Global Terrestrial Reference Frame based on GRACE data (and hydrology models) seems promising.

How to use GPS and GRACE data to separate the effects of Glacial Isostatic Adjustment (GIA), current mass transport and tectonics globally and regionally is an essential task for geodesy community (Wu et al., 2010), but still challenging. In southeast Alaska, the Geophysical Institute of UAF is maintaining dense GPS (continuous and campaign mode) measurements (Elliott et al., 2010), and it should be an ideal study area to perform such research, especially because Chapter 4 has shown that GPS and GRACE can be successfully correlated in terms of seasonal hydrological loading.

References

- Bevis, M., D. Alsdorf, E. Kendrick, L. P. Fortes, B. Forsberg, R. Smalley Jr., and J. Becker (2005), Seasonal fluctuations in the mass of the Amazon River system and Earth's elastic response, *Geophys. Res. Lett.*, 32, L16308, doi:10.1029/2005GL023491.
- Elliott, J. L., C. F. Larsen, J. T. Freymueller, and R. J. Motyka (2010), Tectonic block motion and glacial isostatic adjustment in southeast Alaska and adjacent Canada constrained by GPS measurements, *J. Geophys. Res.*, 115, B09407.
- Freymueller J. T. (2009) Seasonal Position variations and regional reference frame realization. In: Drewes H (ed) Geodetic reference frames, IAG Symposium Munich, Germany, 9–14 October 2006, International Association of Geodesy Symposia, vol 134, Springer, pp 191–196. doi:10.1007/978-3-642-00860-3_30.
- Fritsche, M., R Dietrich, C Knöfel, A Rülke, S Vey, M Rothacher, and P Steigenberger (2005), Impact of higher-order ionospheric terms on GPS estimates, *Geophys. Res. Lett* 32, L23311, doi:10.1029/2005GL024342.
- Nahmani, S., O. Bock, M. Bouin, A. Santamaría-Gómez, J. Boy, X. Collilieux, L. Métivier, I. Panet, P. Genthon, C. Linage, and G. Wöppelmann (2012), Hydrological deformation induced by the West African Monsoon: Comparison of GPS, GRACE and loading models, *J. Geophys. Res.*, 117, B05409, doi:10.1029/2011JB009102.
- Wu, X., M. B. Heflin, H. Schotman, B. L. A. Vermeersen, D. Dong, R. S. Gross, E. R. Ivins, A. W. Moore, and S. E. Owen (2010), Simultaneous estimation of global present - day water transport and glacial isostatic adjustment, *Nat. Geosci.*, 3(9), 642–646.